Title

Single-Cell Analyses Of Transcriptional Heterogeneity During Drug Tolerance Transition In Cancer Cells By Rna Sequencing

Author

Lee, Mei-Chong Wendy

Publication Date

2014

UNIVERSITY OF CALIFORNIA
SANTA CRUZ

SINGLE-CELL ANALYSES OF TRANSCRIPTIONAL HETEROGENEITY DURING DRUG TOLERANCE TRANSITION IN CANCER CELLS BY RNA SEQUENCING

A dissertation submitted in partial satisfaction of the
requirements for the degree of

DOCTOR OF PHILOSOPHY

in

BIOINFORMATICS

by

Mei-Chong Wendy Lee

December 2014

The dissertation of Mei-Chong Wendy Lee is approved by:

Professor Nader Pourmand, Chair

Professor Kevin Karplus

Professor Rohinton Kamakaka

Dietlind L Gerloff, PhD

Dean Tyrus Miller
Vice Provost and Dean of Graduate Studies

Table of Contents

List of Figures

List of Tables

Abstract

Single-cell analyses of transcriptional heterogeneity during drug tolerance transition in cancer cells by RNA sequencing

by

Mei-Chong Wendy Lee

The acute cellular response to stress generates a subpopulation of reversibly stress-tolerant cells under conditions that are lethal to the majority of the cell population. Stress tolerance is attributed to heterogeneity of gene expression within the cell population to ensure the survival of a minority cell population. I performed whole-transcriptome sequencing analyses of metastatic human breast cancer cells, MDA-MB-231, subjected to the chemotherapeutic agent Paclitaxel at the single-cell- and cell-population levels. Here, I show that specific transcriptional programs are enacted within untreated, stressed, and drug-tolerant cell groups, while generating high heterogeneity between single-cells within and between groups. I further demonstrate that drug-tolerant cells contain specific expressed single nucleotide variants (RNA variants) residing in genes involved in microtubule organization and stabilization as well as cell adhesion and cell surface signaling. Unexpectedly, drug-tolerant cells rapidly reacquire Paclitaxel-sensitivity, high cell-to-cell transcript variability, and a gene expression profile similar to that of the untreated cells within a few rounds of cell division. Thus, single-cell analyses reveal the dynamics of the stress response in terms of cell-specific RNA variants driving heterogeneity, the survival of a minority cell population through generation of specific RNA variants, and the efficient reconversion of stress-tolerant cells back to normalcy.

I dedicate this thesis to my husband,

Dominic Abucejo,

who made all of this possible,

❄

And also to my parents,

Mabel and Howard Lee,

for their unconditional love.

Acknowledgments

It is with immense gratitude that I acknowledge the support and encouragement of my advisor, Dr. Nader Pourmand. Much appreciation also goes to my thesis committee: Dr. Kevin Karplus, Dr. Dietlind Gerloff, and Dr. Rohinton Kamakaka, for guiding my research in the past four years. I am indebted to my colleagues in the Pourmand Lab who are always kind and supportive, especially to Kikuye Koyano, Hana Hadiprodjo, James Perrott, and John Collins for their technical assistance. I am very grateful to Dr. Robert Fowler, Dr. Sami Khuri, Amie Radenbaugh, Hyunsung John Kim, and Ricardo Leitão for their continued support and help in all situations. Last but not least, I would like to express my deepest gratitude to my family, especially to Gregory and Martin, for bringing so much joy and love to my life.

Chapter 1

Introduction

A major barrier to successful cancer treatment is the recurrence of cancer cells with acquired resistance to chemotherapy [10, 28, 94]. However, the molecular events underlying cancer cell evolution towards a drug-resistant phenotype are largely unknown. Recent studies using next generation sequencing (NGS) systems have attempted to identify the genetic changes that drive tumorigenesis and resistance to treatments [37, 61]. These studies have revealed that many of the resistance-imparting mutations identified are different from tumor to tumor. In addition to heterogeneity across tumors from different patients, intratumor heterogeneity adds another level of complexity. Minor subpopulations of cancer cells can harbor aberrations that are associated with resistance to therapy and tumor progression [27, 86, 90]. Thus, treatments may be effective against the majority of the tumor, but a small population of resistant cells can cause the persistence, recrudescence, or recurrence of cancer that is refractory to further treatment. Sequencing-based studies on bulk tumor tissue can only identify mutations present in subpopulations of a heterogeneous tumor in a limited capacity. Rare mutations that are only present in a small number of cells in a cell-population might not be detectable by the traditional bulk-cell sequencing since the rare mutations can be ”drown out” by the major alleles in the population. By sequencing the transcriptome at the single-cell level, it is more likely to identify low abundance mutations that will allow us to identify the drivers of drug resistance.

Resistance of cancer cells to different chemotherapy drugs has been reported in different types of cancer, especially in metastatic breast cancer [43, 122]. One of the commonly used chemotherapy drug for treating solid breast tumors is Paclitaxel (Taxol$^{\text{TM}}$) [7]. Palitaxel has been clinically shown to improve the overall and disease-free survival of metastatic and early-stage breast cancer patients [9, 83]. This cytotoxic agent targets microtubules to interfere with the mitotic spindle, resulting in cell cycle arrest and, ultimately, in apoptosis. However, Paclitaxel resistance is common [65]. Paclitaxel treatment kills most tumor cells but, for the residual cancer cells, the mechanisms of resistance are unclear [7]. An important question is whether mutations that drive drug resistance are common in a cell population, or arise from unique mutations in individual cells.

Recent DNA sequencing advances have enabled the analysis of DNA and RNA within a single-cell. The coupling of whole genome amplification and DNA sequencing has allowed multiple groups to study the genetics of single-cells, but not without significant amplification biases [49, 51, 124]. Moreover, single-cell exome sequencing has confirmed the clonal heterogeneity of a solid tumor identifying key mutations across much of the genome [119]. DNA sequencing can identify mutations across the genome, but is unable to illuminate expressional differences that can contribute significantly to drug resistance. Multiplexed single-cell qPCR assays allow expression-based analysis of up to 96 targets in a single experiment [18]. Recently, a few groups have demonstrated that mRNA sequencing (RNA-Seq) of single-cells using NGS technology is feasible, reproducible, and usable for gene expression-based classification of cell subpopulations [14, 35, 79]. A major advantage of RNA-Seq in single-cell studies is that the entire transcriptome can be surveyed, rather than a limited number of genes. DNA and RNA methodologies are not mutually exclusive and can be combined to generate more biologically significant information.

Here, I leveraged the power of single-cell RNA-Seq to identify single nucleotide variants (SNVs) and gene expression at the single-cell level in a drug-tolerance experimental paradigm. I evaluated three groups of cells from the human breast carcinoma cell line, MDA-MB-231: untreated cells, stressed cells that had been exposed to Paclitaxel treatment for 5 days plus 1 day drug-free, and drug-tolerant cells from a small (n<64) clonal population of cells that resumed proliferation after Paclitaxel treatment. In addition to sequencing the mRNA of single-cells, DNA sequencing of a population of untreated MDA-MB-231 cells and RNA-Seq of bulk cells from each of the three groups were performed to facilitate the identification of single nucleotide variants (SNVs) and RNA variants. I performed differential gene expression profiling for single-cells and population cells of the three groups to identify the transcriptional stress response and cytotoxic effects of Paclitaxel on gene expression. Using SNV calling methods, I performed SNV detection with two other published single-cell RNA-Seq datasets, comparing the variants' frequencies between the datasets from this study and the others found in normal human single-cells and other cancer cells.

Chapter 2

Background

2.1 Single-cell RNA Sequencing

The classical approach in studying gene expression is to grind up tissue and analyze the contents of large pools of cells. However, tissue is often comprised of heterogeneous populations of cells where much variation occurs at the single-cell level. For example, in tumor tissue, there are heterogeneous populations of multiple clonal expansions [5, 27, 99]. Analyzing a tumor as a whole could mask rare, but important, characteristics of the tumor. Many research groups have developed molecular techniques to overcome the challenges of sequencing minute amounts of messenger RNA (mRNA) inside a single-cell. The amount of total RNA present in a single-cell is estimated to be between 1 to 50 picograms (pg), and only 1-5 percent of this mass is composed of mRNA [58]. Most of the current next generation sequencing (NGS) platforms require input amounts of 50-1000 nanograms (ng) of DNA [76]. In order to generate enough starting material for NGS, amplification of nucleic acid is an :essential step for single-cell sequencing. The most commonly employed amplification method is the polymerase chain reaction (PCR). *In-vitro* transcription techniques are also useful in amplifying a cell's RNA, and microfluidic sample preparation further improves the efficiency of sequencing minute amount of mRNA in single-cells.

Single-cell RNA-Seq is a powerful tool for understanding the gene regulatory network at the single-cell level. It has been applied to single-cell studies including human preimplantation embryos, human embryonic stem cells [121], single-cells from dissected hippocampal tissue of mouse [29], and immune cells from mouse [89]. In this section, single-cell mRNA sequencing utilizing the two amplification methods described above, as well as the microfluidic sample preparation technique will be covered. I will also cover a number of commercially available cDNA library preparation kits that are capable of amplifying total RNA at the picogram level.

2.1.1 Single-cell RNA-Seq techniques using PCR technology

Polymerase chain reaction (PCR) is one of the most widely used methods in amplifying DNA [81], commonly used in cDNA synthesis. Briefly, cDNA is first synthesized from mRNA isolated from a single-cell using reverse transcriptase. A primer site is added to the $3'$ end of the first-strand cDNA by the action of a terminal transferase. After the second-strand cDNA is made, the amplification process utilizes the added primer site in the first-strand cDNA and the poly(A) tail of the second-strand cDNA as priming sites for PCR. In 2010, Azim Surani, Kaiqin Lao and colleagues adapted a single-cell protocol developed for single-cell microarray studies for single-cell RNA-Seq, and performed deep sequencing for single-cells of the early mouse embryo on the SOLiD sequencing platform [102]. This was the first method published for single-cell RNA-Seq. First, single-cells were lysed in a relatively mild lysis buffer. Subsequently, cDNA synthesis was performed with two oligo(dT) primers, both containing a 24-nucleotide poly(dT) tail at the 3′ end and a 24-nucleotide anchor sequence to add a universal tail to the cDNAs that served as a universal priming site for second-strand synthesis. Then, the cDNAs were amplified in the PCR step using a pair of primers with an NH2-modification at their 5′ ends with a C6 linker to suppress the contamination of primer dimers in the sequencing library. At the time this paper was published, this technique could only amplify molecules that were no more than 3 kilobases long, so about 40% of transcripts were missed. Nonetheless, the method detected expression of about 12,300 genes in the early mouse embryo cells, which was 75% more than were detected by microarray techniques. But there are a few drawbacks to this technique: it preferentially amplified the 3′ end of mRNAs, and it did not always generate read coverage across full transcripts. In the following year, a group from Sweden, Islam and colleagues, published another PCR-based single-cell RNA-Seq method for Illumina sequencing [35]. This method combines oligo(dT) priming and a template-switching technology in the cDNA synthesis step, known as single-cell tagged reverse transcription (STRT) (Fig 2.1). The goal of template switching is to obtain first-strand cDNAs that have reached the 5′ ends of the RNA template. Using this technique, Islam *et al*. had reliably detected 1,000-6,000 of the ∼25,000 genes in the mouse embryonic stem cells and 2,000-8,000 genes in the mouse embryonic fibroblast cells. There are a few drawbacks in this technique also. First, the majority of the reads were found near the 5′ end of the transcripts, and endogenous transcripts often were not sequenced to their full lengths. In 2012, another Swedish group introduced a single-cell RNA-Seq protocol, known as Smart-Seq, with improved transcriptome coverage by a combination of oligo(dT) priming and template switching, followed by 12-18 cycles of PCR amplification of cDNAs [79]. The cDNA synthesis and amplification methods developed for this prococol is now commercially available, marketed by Clontech, and is known as the SMARTer Ultra Low RNA Kit for Illumina sequencing. The cDNA synthesis steps, including the template-switching step, are identical to the ones described by Islam *et al*. shown in Fig 2.1). They determined that if the starting total RNA is below 1 ng, the detection rate of the less abundant transcripts decreases by at least 40%. After analyzing 12 cancer line cells with this method (four cells each from the LNCaP, PC3, and T24 cell lines), they detected about 8,000 genes per cell with the sensitivity of gene detection similar to that achieved with ~20 pg of starting total RNA. They suggested that at the levels of about a million uniquely mappable reads per cell, the sequencing depth had little effect on transcript detection. It appeared that the transcript detection sensitivity was mainly affected by limited starting amounts of RNA and random loss of low-abundance transcripts, but the majority of the low-abundance and highly expressed transcripts were reliably detected even at the single-cell level. They also applied this method to determine if the global transcriptome analyses of putative circulating tumor cells (CTCs) could reveal their tumor of origin. They performed single-cell sequencing for six NG2$^+$ putative melanoma CTCs isolated from peripheral blood from a patient with recurrent melanoma, two primary melanocytes, seven melanoma cancer cell line (SKMEL5, n=4 and UACC257, n=3) cells and eight human embryonic stem cells. The global transcriptomes and expression patterns of melanoma-associated transcripts strongly supported a melanoma CTC identity for the NG2$^+$ cells. Last, they investigated if the possibilities that this method could be used to identify single-nucleotide polymorphisms (SNPs) and other genetic variants associated with melanomas and other cancers. They identified 4,312 high-confidence genetic variants that are supported by at least two CTCs, and 92% of the high-confidence variant loci coincided with documented SNPs. The authors concluded that, with only a few cells, Smart-Seq could be utilized to screen for SNPs and mutations in transcribed regions. In 2013, Sasagawa and colleagues published another PCR-based single-cell whole transcript amplification method for single-cell RNA-Seq known as Quartz-Seq [85]. This method introduced improvements in three areas: 1) suppression of byproduct synthesis during the amplification process (Fig 2.2); 2) single-tube reaction utilization of a PCR enzyme; and 3) optimized conditions of reverse transcription and second-strand cDNA synthesis. It appeared that the Quartz-Seq was more robust against a shorter cDNA length, able to amplify more transcript isoforms than Smart-Seq. With Quartz-Seq, it is possible to distinguish different cell types but also different cell-cycle phases of the same cell type.

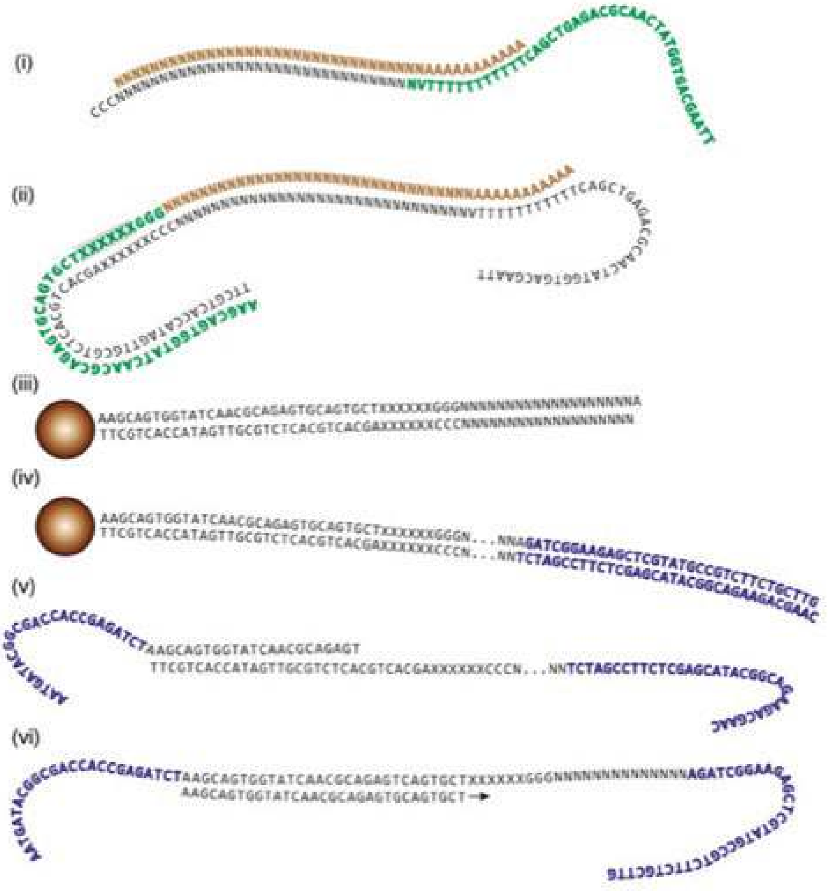
(i)
(ii)
(iii)
AAGCAGTGGTATCAACGCAGAGTGCAGTGCTXXXXXXGGGNNNNNNNNNNNNNNNNNNNA
TTCGTCACCATAGTTGCGTCTCACGTCACGAXXXXXXCCCNNNNNNNNNNNNNNNNNNN
(iv)
AAGCAGTGGTATCAACGCAGAGTGCAGTGCTXXXXXXGGGN...NNAGATCGGAAGAGCTCGTATGCCGTCTTCTGCTTG
TTCGTCACCATAGTTGCGTCTCACGTCACGAXXXXXXCCCN...NNTCTAGCCTTCTCGAGCATACGGCAGAAGACGAAC
(v)
AATGATACGGCGACCACCGAGATCTAAGCAGTGGTATCAACGCAGAGT
TTCGTCACCATAGTTGCGTCTCACGTCACGAXXXXXXCCCN...NNTCTAGCCTTCTCGAGCATACGGCAGAAGACGAAC
(vi)
AATGATACGGCGACCACCGAGATCTAAGCAGTGGTATCAACGCAGAGTCAGTGCTXXXXXXGGGNNNNNNNNNNNNNAGATCGGAAGAGCTCGTATGCCGTCTTCTGCTTG
AAGCAGTGGTATCAACGCAGAGTGCAGTGCT →

Figure 2.1: Overview of the sample preparation steps using single-cell tagged reverse transcription (STRT). (i) First strand cDNA is synthesized from the mRNA (brown) using a tailed oligo-dT primer (green), with 3-6 cytosines added to the 3′ end of the first strand cDNA; (ii) A barcode (shaded XXXXXX) is introduced through a template-switching step initiated by a helper oligo (green); (iii) An amplified product resulted from PCR with single-primer, followed by beads immobilization, fragmentation, and A-tailing; (iv) Ligation of the Illumina P2 adapter (blue) to the free ends; (v) Introducing the P1 adapter in the library PCR step with a primer tailed with the P1 sequence (blue); (vi) Sequencing the final library with a custom primer from the P1 side of template. Each sequencing read begins with the barcode (arrow), followed by three to six Cs and the mRNA insert. Figure copied from Islam et al [35].

2.1.2 Single-cell RNA-Seq techniques with an in-vitro transcription technology

Hashimshony and colleagues published a single-cell RNA-Seq technique in 2012, called CEL-Seq [33]. This method utilizes barcoding and pooling of samples before performing linear amplification of mRNA with only one round of in-vitro transcription [33]. The first-strand cDNA synthesis is enabled by a reverse-transcriptase reaction using a primer designed with an anchored polyT, a unique barcode, the 5′ Illumina sequencing adaptor, and a T7 promoter. After the second-strand cDNA synthesis is performed, the cDNA samples are pooled for an in-vitro transcription reaction. Next, the amplified RNA is fragmented to the appropriate size distribution for sequencing, followed by the addition of the Illumina 3′ adaptor by ligation. The RNA is then reverse transcribed to DNA. The DNA fragments containing both the Illumina adaptors and a barcode are enriched for by PCR. The resulting DNA library is then subjected to paired-end sequencing, where the first read contains the barcode, and the second read contains the mRNA transcript (Fig. 2.3). In terms of robustness, sensitivity, and reproducibility, CEL-Seq may have outperformed the STRT method published by Islam and colleagues (a PCR-based method using single-cell tagged reverse transcription), but is not without its own limitations. CEL-Seq selects for the single fragment of each transcript closest to the 3′ end. Therefore, it has a strong 3′ bias, and is limited in distinguishing alternative splice forms of transcripts. It is also sensitive to small copy numbers of transcripts. By using spike-ins and dilution series, it appears that If the number of copies of a transcript is less than 5, the chance that CEL-Seq will miss it is more than 50%.

2.1.3 Microfluidic Single-cell Preparation for RNA-Seq

Many single-cell RNA-Seq techniques have two main challenges — amplification bias and capture efficiency of the mRNA transcript during cDNA synthesis. On average, the limit of transcript detection is between five to ten mRNA molecules, equivalent to converting between 5% and 10% of RNA molecules in a single-cell to cDNA [33, 35, 79]. All single-cell RNA-Seq methods employ amplification. In 2013, Islam *et al*. in the Karolinska Institute in Sweden, developed a single-cell RNA-Seq preparation system that combined molecular tagging and microfluidics to reduce the amplification bias and increase the efficiency of cDNA synthesis [36]. The molecular tagging method uses unique molecular identifiers (UMIs), essentially the same single-cell tagged reverse transcription (STRT) technique described in Section 2.1.1 that attaches short random sequences to each individual cDNA molecule (Fig. 2.4). UMIs make each molecule in a population distinct, which allows one to measure the absolute number of mRNA molecule in a single-cell prior to the amplification step. By counting the number of UMIs, one can correct for PCR-induced artifacts and amplification bias that are present in the sequencing data. Although, sequences that are not amplified will not be account for. In addition, the use of a microfluidic system, the Fluidigm C1 AutoPrep platform, allows the single-cell cDNA synthesis to take place in an individual enclosed chamber with a reaction volume 200 times smaller than that in

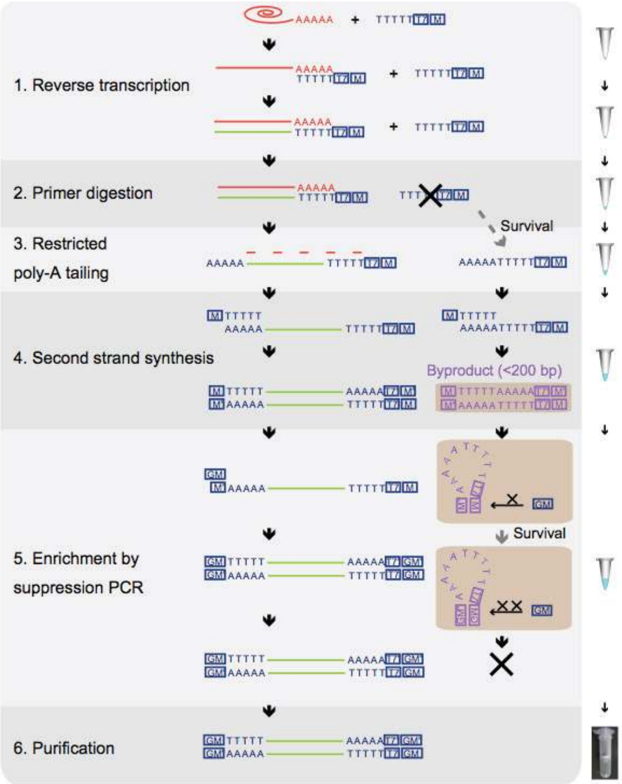

Figure 2.2: Schematic of the single-cell whole transcriptome amplification method used by Quartz-Seq. The entire whole transcriptome amplification process took place in a single PCR tube. Step 1: The reverse-transcription (RT) primer that contains an oligo-dT24, a T7 promoter (T7) sequence, and a PCR target region (M) sequence was used in the first-strand cDNA synthesis. Step 2: Exonuclease I was then used to digest the majority of the RT primer. Step 3: A poly-A tail was added to the 3′ ends of the first strand cDNA and to any remaining RT primer. Step 4: A tagging primer was used to synthesize the second-strand cDNA that produced double-stranded DNA product with complementary sequences at both ends. Step 5: The byproducts from the remaining RT primers were eliminated through the suppression PCR. Suppression PCR utilizes template DNA that had complementary sequences at both ends that could bind each other. DNA templates that became self-bound was not amplified by PCR. The PCR primer could also binds one end of the template DNA. One end of the template DNA competed with the binding between the PCR primer and one other end of the same DNA template. It was more likely that a short DNA template would bind to itself because of the close proximity of the complementary sequences at the ends of the template. Longer DNA template tend to bind to the PCR primer more readily than binding to itself. The remaining RT primer DNA templates were short and would be not be amplified while the longer cDNA were enriched. Step 6: The amplified cDNA product was purified using a PCR purification column. Figure copied from Sasagawa et al [85]

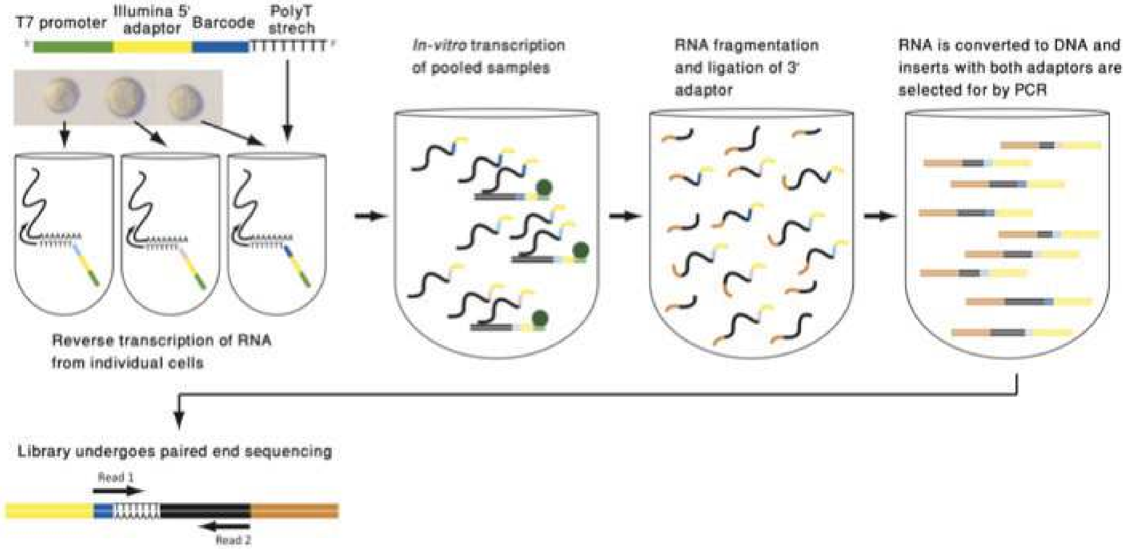
T7 promoter
Illumina 5' adaptor
Barcode
PolyT strech
TTTTTTTT
In-vitro transcription of pooled samples
RNA fragmentation and ligation of 3' adaptor
RNA is converted to DNA and inserts with both adaptors are selected for by PCR
Reverse transcription of RNA from individual cells
Library undergoes paired end sequencing
Read 1
Read 2

Figure 2.3: The CEL-Seq DNA library preparation method with in-vitro transcription. First-strand cDNA synthesis was performed using a primer containing a poly-T sequence, a unique barcode, the 5′ Illumina seqeuncing adaptor, and a T7 promoter. Then, the second-strand synthesis was performed. The double-stranded cDNA samples were then pooled for the in-vitro transcription (IVT) reaction. Next, the amplified RNA was subjected to fragmentation to a size distribution suitable for sequencing. Then, the Illumina 3′ adaptor was ligated to the fragmented RNA. The RNA was then reverse transcribed to DNA. Subsequently, PCR was employed to select for the DNA with both the 5′- and 3′ Illumina adaptors. Then, the DNA library was subjected to paired-end sequencing. Figure copied from Hashimshony *et al*. [33]

a typical reaction tube. The reduction in reaction volume greatly improves the mRNA capture efficiency from 5%-10% to 48%.

2.2 Commercially Available Single-cell RNA Amplification Methods

There are various types of RNA-Seq library construction kits available commercially, depending on the input amounts and the quality of the RNA, and the repertoire of RNAs that one would like to enrich for in the sequencing library (Table 2.1). For this study, I will give an overview of the RNA-Seq library construction kits that are designed to amplify picogram amounts of total RNA, including NuGEN Ovation RNA-Seq v2, Clontech SMARTer Ultra Low Input RNA Kit, Sigma Transplex WTA2-SEQ Kit, and μMACS SuperAmp$^{\text{TM}}$ Kit by Miltenyi Biotec.

2.2.1 NuGEN Ovation RNA-Seq System

The NuGEN Ovation RNA-Seq system is an isothermal linear nucleic acid amplification system for whole-transcriptome sequencing with input total RNA as little as 50 pg [104]. First, total RNA is subjected to the first strand cDNA synthesis through the reverse transcription reaction with a combination of random hexamers and a poly-T DNA/RNA chimeric primer. The resulting cDNA/mRNA heteroduplex contains a unique sequence at the $5'$ end. Then, a heating step is used to degrade the original RNA template. The second strand cDNA is synthesized with the first-strand cDNA

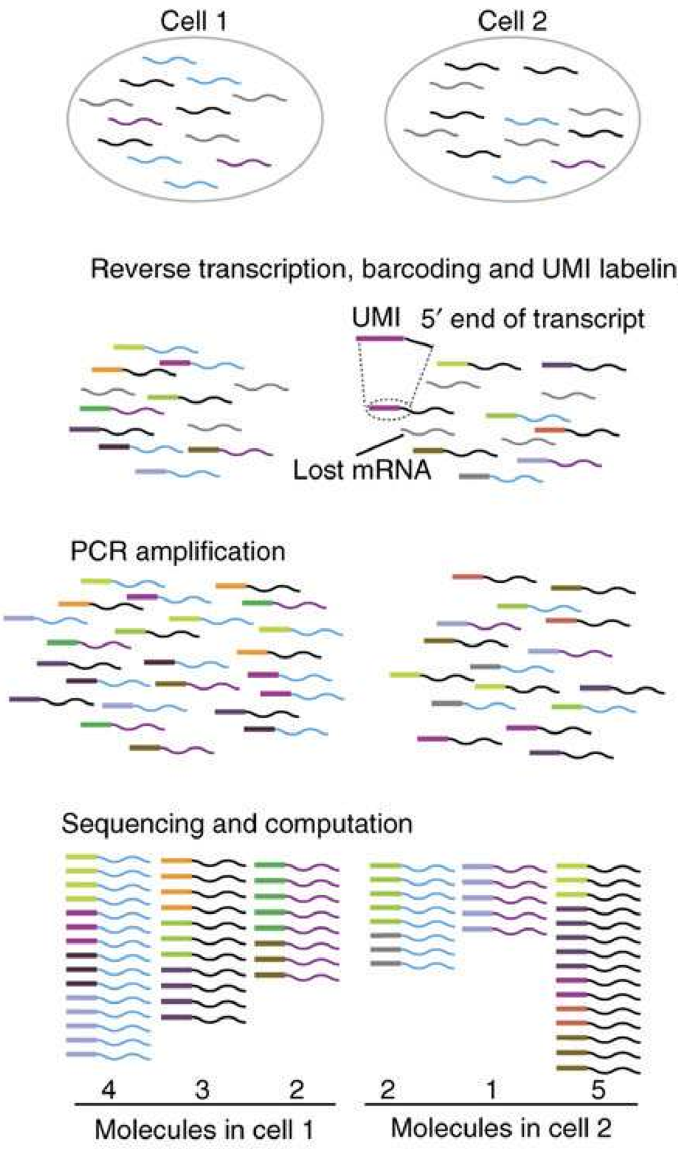

Figure 2.4: Overview of molecular tagging using unique molecular identifiers (UMIs). Two cells containing mRNA molecules (wiggly lines) from different genes represented by distinct colors (top panel). The barcodes and UMIs (the color rectangles attached to the wiggly lines) are attached to the mRNA molecules during reverse transcription. The transcripts that are not tagged with the UMIs (grey wiggly lines) are not reverse-transcribed (middle panel). UMIs make each molecule in a population unique, which allows one to measure the absolute number of mRNA molecule in a single-cell prior to the amplification step. By counting the number of UMIs, one can correct for PCR-induced artifacts and amplification bias that are present in the sequencing data (bottom panel). Figure copied from Islam et al [36]. Reprinted by permission from Macmillan Publishers Ltd: Nature Methods 11:163-166, ©(2014). License number: 3373530538085.

Commerical RNA-Seq library preparation kit	**Total RNA input**	**RNA Quality**	**Enrichment**
Clontech SMARTer Ultra Low Input RNA Kit	10 ng (0.01 ng)*	Single cells, from a few to 1,000 intact cells, or very low amounts of total RNA	poly-A containing mRNA
Sigma Transplex WTA2-SEQ Kit	1-50 ng (0.01 ng)*	High Quality, degraded or FFPE,	mRNA and non-polyadenylated transcripts
μMACS SuperAmp$^{\text{TM}}$Kit by Miltenyi Biotec	100ng (0.01 ng)*	Single cell, from 1 cell up to 10,000 cells	mRNA and non-polyadenylated transcripts
Epicentre ScriptSeq v2 RNA-Seq Library Preparation Kit	25 ng (0.05 ng)*	rRNA-deleted or poly-A selected RNA	mRNA and ncRNA
NuGEN Ovation RNA-Seq v2	10 ng (0.05 ng)*	High quality, degraded or FFPE	mRNA and non-polyadenylated transcripts
Illumina TruSeq Total RNA Sample Preparation Kit	500 ng (100 ng)*	High Quality, degraded or formalin-fixed, paraffin-embedded (FFPE)	mRNA and non-coding RNA (ncRNA), long intergenic noncoding RNA (lincRNA), small nuclear RNA (snRNA), and small nucleolar RNA (snoRNA)
Illumina TruSeq RNA Sample Preparation Kit v2	1000-2000 ng (100 ng)*	High Quality	poly-A containing mRNA
Epicentre RNA Sequencing Ribo-Zero Magnetic Kit	(1000 ng)*	High Quality, degraded or FFPE	mRNA and non-coding RNA, along with other long intergenic noncoding RNA (lincRNA), small nuclear RNA (snRNA), and small nucleolar RNA (snoRNA)

*Minimum Assay Requirements

Table 2.1: A comparison of commercially available RNA-Seq library construction kits. The metrics being compared are input RNA quantity and quality, and the repertoire of RNAs enriched.

as template, using DNA polymerase. The double-stranded cDNA is then purified and amplified using a single-primer, isothermal, linear amplification (SPIA) process. SPIA uses RNase H enzyme to degrade the RNA sequence that is complement to the unique sequence at the 5′ end of the DNA/RNA heteroduplex double-stranded cDNA. This results in the exposure of a DNA sequence for the SPIA DNA/RNA chimeric primer to hybridize to. Subsequently, DNA polymerase initiates replication at the 3′ end of the primer by displacement of the existing forward strand. Once again, RNase H enzyme degrades the RNA portion at the 5′ end of the newly synthesized ds-cDNA, and the hybridization of the SPIA chimeric to the exposed DNA, DNA polymerization, and strand displacement repeats. The SPIA product is then subjected to a sequencing library preparation process (Fig. 2.5).

2.2.2 2.2.2 Clontech SMARTer Ultra Low RNA Kit

The cDNA library amplification process of the Clontech SMARTer Ultra Low RNA Kit is based on the Smart-Seq method developed by Ramskld et al [79], and which is described in Section 2.1.1.

2.2.3 Sigma Transplex WTA2-SEQ Kit

The Sigma Transplex WTA2-SEQ requires a two-step whole transcriptome amplification process [113]. First, total RNA is reverse transcribed with the proprietary library synthesis primer. The 3′ end of this primer consist of a quasi-random, non-self-complementary sequence while the 5′ end is a non-self-complementary, con-

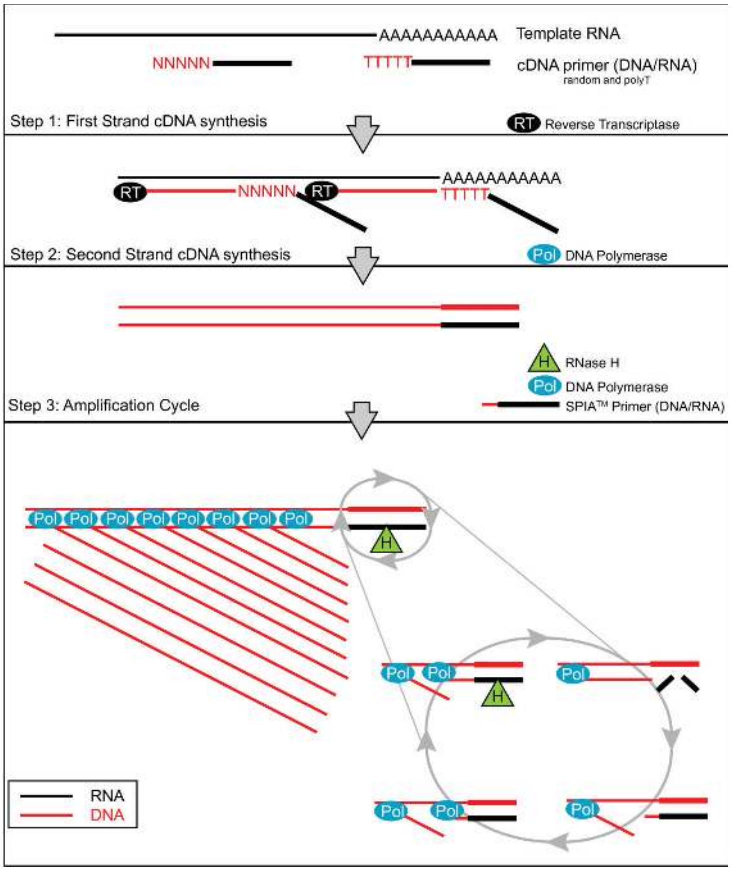

Figure 2.5: NuGEN Ovation RNA-Seq system for cDNA library preparation. In step 1, first strand cDNA is synthesized from total RNA through reverse transcription reaction with a combination of random hexamers and poly-T DNA/RNA chimeric primer. The resulting cDNA/mRNA heteroduplex contains a unique RNA sequence at the 5′ end. In step 2, the original RNA template (black line) is degraded by heat. Then, the second strand cDNA is synthesized with the first-strand cDNA as template using DNA polymerase. The double-stranded cDNA is then purified and amplified. In step 3, linear amplification is performed using a single-primer, isothermal, linear amplification (SPIA) process. The SPIA process first uses the RNase H enzyme to degrade the unique RNA sequence at the 5′ end of the DNA/RNA heteroduplex double-stranded cDNA. Then the SPIA DNA/RNA chimeric primerc can hybridize to the exposure of a DNA sequence. DNA polymerase initiates replication at the 3′ end of the primer by displacement of the existing forward strand. Step 3 is repeated for 2 hours. Figure copied from Watson *et al*. (2008) [115]

stant sequence that serves as the annealing site for the universal amplification primer (Fig. 2.6). Then, the RNA template is degraded using RNase H enzyme. Next, the second cDNA strand is synthesized by strand-displacement polymerization with the library synthesis. The double-strand cDNA library is flanked by a universal end sequence, and is amplified by PCR using a single universal primer with WTA2 polymerase. A restriction enzyme (not specified in the manufacturers specification) is used to remove the universal amplification primer sequence, which contains a type II restriction site, from the cDNA library prior to the downstream library preparation for deep sequencing.

2.2.4 Magnetic μMACS SuperAmp™ Kit by Miltenyi Biotec

Magnetic μMACS SuperAmp™ Kit is a cDNA library preparation kit designed to work directly with cells. After cells are lysed, mRNA is hybridized to the magnetically labeled μMACS Oligo(dT) MicroBeads which contains a complementary tag (Fig. 2.7). The mRNA hybridized to the oligo(dT) beads are placed in the μ-Column. The μ-Column is then place inside the thermoMACS Separator where a magnetic force is applied to immobilized the magnetically labeled mRNA while all other cell components are being washed away from the mRNA. The first-strand cDNA is then synthesized by reverse transcription with random primers. A proprietary Tailing Mix is then added to attach a nucleic-acid tag to the $3'$ end of the first-strand cDNA. By removing the column from the thermoMACS Separator, the cDNA is eluted. After elution, a single primer is annealed to the nucleic-acid tag and used for PCR amplifi-

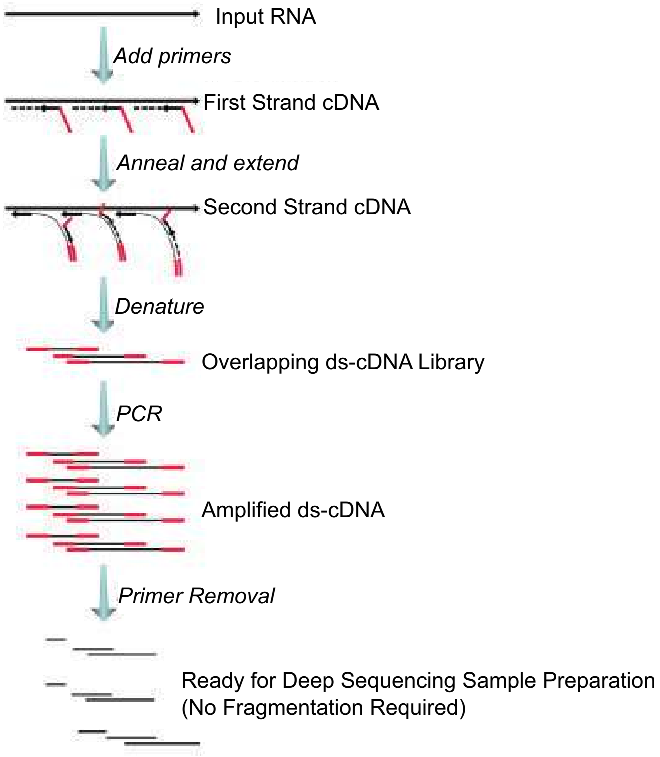

Figure 2.6: Sigma Transplex™ WTA2 Amplification. Total RNA ranging from 20pg to 1ng is used as input material for whole transcriptome amplification. In the first step, library synthesis primer contains a quasi-random 3′ non-self-complementary sequence that facilitates priming throughout the entire RNA template in the first and second strand cDNA synthesis. The 5′ end contains a constant universal, non-self-complementary sequence. RNase H enzyme degrades the RNA template after first strand cDNA synthesis. Then, strand-displacement polymerization generates the second cDNA strand. The double stranded cDNA (ds-cDNA) is flanked by the universal sequence that is subsequently amplified by PCR using a single universal primer. Prior to the downstream sequencing library construction step, a restriction enzyme is used to remove the universal primer sequence from the ds-cDNA. Figure copied from Ward and Heuermann (2010) [113].

cation of the cDNA.

2.3 Evaluation of cDNA Library Preparation Techniques

Exponential-amplification-based methods for cDNA library construction include single-cell tagged reverse transcription (STRT) [35], Smart-Seq [79], and commercially available kits including Sigma Transplex™ WTA2 [113] and Clontech SMARTer Ultra Low RNA Kit [79]. CEL-Seq [33], NuGEN Ovation RNA-Seq system [104], and Magnetic μMACS SuperAmp™ are linear-amplification-based methods for mRNA amplification. When amplifying ultra-low amounts of mRNA, methods such as Smart-Seq can generate a higher transcriptome coverage compared to linear-amplification methods such as CEL-Seq. But the exponential amplification process is more likely to produce spurious PCR products and primer-dimers, and distort the initial transcript abundance levels due to sequence-, length-, and abundance-dependent biases [8, 91]. With about 30 million mapped mRNA-Sequencing reads per single-cell, the Clontech SMARTer Ultra Low RNA Kit and Sigma Transplex™ WTA2 can detect about 20% and 40% more genes, respectively, than that of the NuGEN Ovation RNA-Seq system [118]. A recent study has shown that the NuGEN Ovation RNA-Seq system has successfully amplified femtograms to attograms of viral RNA for sequencing on the Illumina HiSeq and MiSeq sequencing platforms [60]. The *de novo* assembly of viral reads generated consensus sequence for the complete, or nearly complete, coding sequences (CDS) of several viral genomes [60]. One of the advantages of the linear cDNA amplification

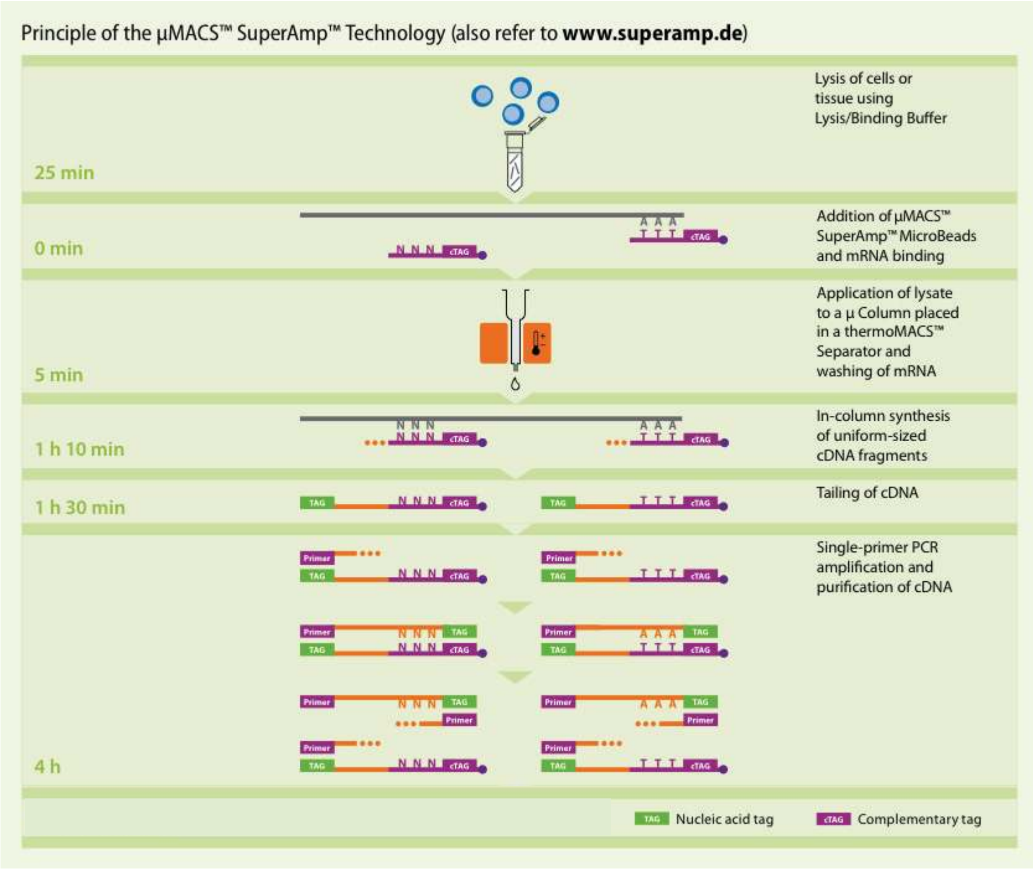
Principle of the µMACS™ SuperAmp™ Technology (also refer to **www.superamp.de**)
25 min
Lysis of cells or tissue using Lysis/Binding Buffer
0 min
A A A
N N N
cTAG
Addition of µMACS™ SuperAmp™ MicroBeads and mRNA binding
5 min
Application of lysate to a µ Column placed in a thermoMACS™ Separator and washing of mRNA
1 h 10 min
In-column synthesis of uniform-sized cDNA fragments
1 h 30 min
TAG
T T T
Tailing of cDNA
Primer
Single-primer PCR amplification and purification of cDNA
4 h
TAG Nucleic acid tag
cTAG Complementary tag

Figure 2.7: Magnetic μMACS SuperAmp$^{\text{TM}}$ Technology. First, the mRNA is enriched by directly adding a dT-oligo tethered to superparamagnetic MACS MicroBeads to the cell lysate. Then, the magnetically labeled mRNA is added to the μ-Column that is placed in the magnetic field of a thermoMACS Separator. Other cell components are washed away while the magnetically labeled mRNA is immobilized by the strong magnetic field. The cDNA synthesis and cDNA purification steps are performed in the same column to avoid loss of material. The proprietary MicroBead mixture is added to the mRNA to generate first-strand cDNA fragments of uniform size. Subsequently, cDNA is amplified by PCR with a single primer. Figure copied from Miltenyi Biotec website, `https://www.miltenyibiotec.com/~/media/Images/Products/Import/0002400/IM0002465.ashx`

system in the NuGEN Ovation RNA-Seq system is the ability to minimize the chance of amplifying nucleotide incorporation errors in cDNA sequences introduced by DNA polymerase during the early cycles of amplification. Only the second-strand cDNA fragments are used in the amplification process, and none of the amplicons will be re-amplified. Therefore, any nucleotide mis-incorporated during the early cycles of the amplification process will not be re-amplified in the pool of cDNA.

2.4 Paclitaxel Resistance in Breast Cancer

Paclitaxel is one of the most commonly used chemotherapy drugs for treating breast cancer, however, resistance of Paclitaxel has previously been observed in human cancer cell line of breast origin [4]. Paclitaxel is a cytotoxic agent, originally derived from the bark of the Pacific yew tree, *Taxus bravifoliaa* [1]. The substance arrests cells at G2/M phase by interacting with the β-tubulin to promote the stabilization of the microtubules, and prevents normal spindle assembly and cell division [23]. Despite the benefits offered by Paclitaxel for overall and disease-free survival in early-stage and metastatic breast cancer patients, the disease often recurs in a drug resistant manner [23, 100].

A number of Paclitaxel-resistance mechanisms involving the regulation of cell cycle and apoptosis have recently been identified. Previous work has shown the involvement of genes *CDK1*, *CDK2* [68], and the Hippo pathway component *TAZ* and its downstream transcriptional targets *Cyr61* and *CTGF* [46] in Paclitaxel resistance. These genes encode for proteins which regulate cell cycle and apoptosis [34, 55], respectively. In addition, estrogen receptor (ER) is found to play a role in Paclitaxel sensitivity in breast cancer cells. ER-positive cell lines were found to be resistant to Paclitaxel associated with *Bcl-2* expression mediated by ER [100]. Although ER-negative cell lines appeared to be more sensitive to Paclitaxel than ER-positive cells, ER-negative cells were able to slip out of Paclitaxel-induced mitotic arrest mediated by the Bcl-xL/Bak interaction. Downregulation of Bak was reported to suppress Paclitaxel-induced apoptosis in MDA-MB-231 cells, an ER-negative metastatic breast cancer cell line [126]. The proteins encoded by *Bcl-2*, *Bcl-xL*, and *Bak* belong to the BCL2 protein family, in which there are about 20 known members with either pro-apoptotic or anti-apoptotic function [87]. A number of proteins in the BCL2 protein family that are key players in the mitochondrial intrinsic apoptotic pathway have been linked to Paclitaxel resistance [23, 45, 114]. Aberrant expression or mutation in these genes could enable cells to escape the damage induced by Paclitaxel, which induces prolonged mitotic arrest and ultimately activates the mitochondrial intrinsic apoptotic pathway [24].

Chapter 3

Single Nucleotide Variants at the Single-Cell Level

High-throughput sequencing allows one to study the genetic changes across the entire genome or transcriptome. But there is a limit of detection with this technology where signals from rare single nucleotide variants (SNVs) in a cell population are often drowned out by signals from the major alleles [79]. Thus far, all the previously published single-cell RNA-Seq studies focused on single-cell gene expression. However, Ramsköld *et al*. suggests that it is feasible to detect SNVs using the single-cell RNA-Seq technique [79]. RNA-Seq not only can detect mutations propagated from the DNA templates to the RNA transcripts, but can also detect all other expressed variants that could be a result of RNA editing. Although ultra-deep sequencing of the whole genome with bulk cells can potentially improve the chance of identifying rare variants, the cost of performing ultra-deep sequencing is very high. On average, one sequencing run for the whole genome of human using the Illumina HiSeq 2000 with a read length at 100 bp can generate roughly 30x depth of coverage, and each run cost about $22,000 [15, 96]. In order to obtain a depth of coverage of 500x of whole genome sequencing, it would cost more than $360,000. I hypothesize that rare variants not detected through bulk-cells sequencing can be identified by sequencing at the single-cell level when performing ultra-deep sequencing is not feasible. Here I leveraged the power of single-cell RNA sequencing technology to identify SNVs in a drug-tolerance experimental paradigm with Paclitaxel and the metastatic breast cancer cells MDA-MB-231. A linear RNA amplification system, the NuGEN® RNA-Seq system, was employed in this study to preserve the transcript stoichiometry, as well as to minimize the number of single-nucleotide mutations introduced during the cDNA amplification step. In this chapter, I discuss the detection and comparison of SNVs within single-cells and populations of cells. First, I validated of a set of SNVs using pyrosequencing. To compare the single-cell variant frequencies in this study with those in normal human cells and other cancer cells, I analyzed two single-cell RNA-Seq datasets from two previously published papers using the same methods that I employed for this single-cell study. I also identified variants that were likely to be responsible for Paclitaxel resistance in the MDA-MB-231 cell line.

3.1 Methods and Materials

3.1.1 Cell culture, drug treatments and the Paclitaxel paradigm

MDA-231 cells were obtained from the Princeton Physical Sciences Oncology Center tissue biorepository and routinely cultured in DMEM supplemented with 10% fetal bovine serum. Taxol (Paclitaxel, Sigma, St. Louis, MO) was prepared as a 5 mM stock solution in ethanol and serial dilutions were prepared for toxicity assays.

The Paclitaxel treatment paradigm was established as indicated in the diagram of Fig. 3.1A. Briefly, 1×10^6 cells were plated in 100 mm culture dishes for 24 hours, and then treated with 100 nM Paclitaxel. After 3 days, fresh 100 nM Paclitaxel-containing media was added for another 2 days, totaling 5 days of Paclitaxel treatment. Cells were then rinsed with PBS and maintained in drug-free culture with media replacement every 48 hours and clones of drug-tolerant cells were expanded by the ring cloning technique. Cells still alive 1 day after Paclitaxel removal were considered residual cells undergoing a stress response, most of which died within the next 2-4 weeks. The clones of cells that resumed proliferation are considered recurrent drug-tolerant cells. The frequencies of stressed and drug-tolerant cells is calculated by dividing the number of the counted stressed or drug-tolerant cells by the total number of cells submitted to drug treatment.

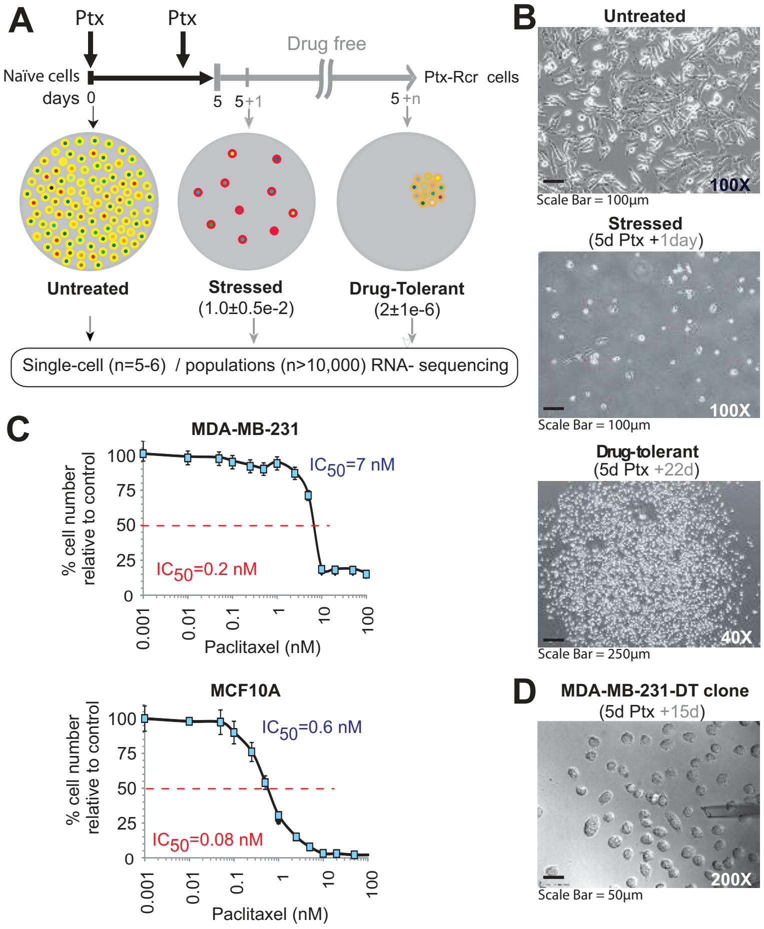

Figure 3.1: The response to Paclitaxel in cancer cells. (A) Regimen for expansion of Paclitaxel (Ptx) stress-tolerant cells. Highly metastatic MDA-MB-231 naïve (yellow) cells were treated with Ptx (100nM) on Day 1 and Day 3. After 5 days, Ptx was removed and cells were left in a drug free culture. Most stressed cells arrested (red) and ultimately died, while rare drug-tolerant cells (orange) resumed proliferation after 10-15 days and clones were expanded. Five single-cells per group were analyzed including before treatment, 1 day after Ptx removal, and from recently established (n<64) or long-term expanded, drug-tolerant clones. Populations were analyzed from long-term expanded clones. Frequencies of surviving stressed and drug-tolerant cells observed are indicated between parentheses. Cell-to-cell heterogenous RNA content is indicated with varying colors. (B) Bright field images of untreated, stressed, and drug-tolerant cells at the indicated times after drug removal. Total magnification is indicated. (C) Paclitaxel toxicity assays on naïve MDA-MB-231 cells (top) and MCF10A cells (bottom). Growth Inhibitory Concentrations 50% (IC_{50}) are indicated. Data shown are the mean ± SEM from a quadruplicated representative experiment. (D) Bright field image of an MDA-MB-231-Ptx-tolerant clone (n<64) during single-cell collection by micromanipulation. The opening of the micropipette of roughly 20 microns is shown.

3.1.2 Paclitaxel toxicity assays

Cell growth of naïve or expanded recurrent drug-tolerant cells was determined as follows. Briefly, 25,000 cells were plated in each well of 12-well plates and after 24 hour were treated with vehicle-ethanol or up to 100 nM Paclitaxel containing media. After 4 days, cells were fixed with 10% formaldehyde and the IC_{50} (concentration for 50% growth inhibition) was established by Giemsa staining. Cell number was plotted as a percent of cells relative to vehicle control with standard error from 4 replicated wells used in a representative experiment.

3.1.3 Cell analysis experimental design

For the single-cells, RNA sequencing was performed for 5 naïve (untreated) cells, 5 stressed (day 5+1 day drug free) cells, and 5 drug-tolerant cells from one clone at early growth (5 days Ptx + 15 days drug free). Thus, the RNA-Sequencing for the 5 drug tolerant cells was from a unique clone. The drug-tolerant cells shown in the bottom panel of Fig. 3.1B was a clone expanded from an individual cell to over 8 million cells (>23 population cell-doublings). The population cells that were used in RNA sequencing include 10,000 naïve MDA-MB-231 cells, 10,000 stressed cells (day 5+1 drug free, non-clonal) and 3 independent drug-tolerant clones, each with 10,000 drug-tolerant cells. Pyrosequencing was performed for additional single-cells from different drug-tolerant clones as well as from additional, untreated single-cells obtained as described above.

3.1.4 Isolation of single-cells and cell populations, and cDNA synthesis

Five single-cells from populations of untreated, stressed, or proliferating drug-tolerant cells obtained from single clones as indicated in Fig. 3.1A were collected as follows. Media was removed and replaced by PBS at room temperature. Single cells were picked within the next 10 minutes with <20 μm-diameter glass needles using Narshige MO-188 and MN-188 hydraulic micromanipulators over an inverted microscope, washed and immediately lysed in Prelude™ Direct Lysis Module (NuGEN Technologies, Inc., San Carlos, CA) on glass-mounted microdroplets. For population analyses, $>$10,000 cells from untreated, stressed, or drug-tolerant cells were lysed. Snap frozen lysates were stored at -80°C. cDNA was generated for each single-cell lysate using the Ovation® RNA-Seq system (NuGEN Technologies, Inc., San Carlos, CA) per manufacturer's recommended protocols and as described previously in Tariq *et al.* [104]. For the single-cell cDNA synthesis and library preparation methods, please refer to Appendix B.1 and Appendix B.2.

3.1.5 Quality control and mapping of the sequencing reads

The sequencing reads were subjected to a three-step quality control process. First, the quality of the sequencing reads was evaluated with FastQC (`http://www.bioinformatics.babraham.ac.uk/projects/fastqc/`). Then, sequencing adapter sequences were removed from the reads using SeqPrep (`https://github.com/jstjohn/SeqPrep`). In the single-cell RNA-Seq reads, the first six bases from the 5′ appeared to have biased nucleotide usage due to the usage of random hexamers in the first-strand cDNA synthesis. Therefore, the six bases from the 5′ end of the sequencing reads were trimmed. No additional end-trimmings were done on sequencing reads for the population RNA-Seq and the DNA sequencing of the MDA-MB-231 cell line.

There were three types of samples for whole transcriptome analyses – single-cells, 5-cell pooled samples, and population. The 5-cell pooled samples were generated by concatenating all the fastq files from five single-cells into one pooled sample. The preprocessed sequencing reads were aligned against the UCSC hg19 human reference genome as paired-end reads using Tophat (version 1.3.2) [108] with default settings. Uniquely mapped reads were used for differential gene expression analyses and SNV calling. These reads were tagged with "NH:i:1" (NH stands for the number of reported alignments that contains the query in the current record) and were extracted from the bam files generated by Tophat using the GNU fgrep package (`http://www.gnu.org/s/grep`). PCR duplicates were removed using the rmdup function in samtools [53]. To facilitate the identification of DNA-RNA variants, DNA sequencing reads were mapped to the UCSC hg19 human reference genome as paired-end reads using Bowtie2 (version 2.0.0-beta6) [47]. Read-mapping quality analysis for 5′- and 3′ read biases was performed using RSeQC (version 2.3.1) [112].

3.1.6 SNV identification

The SNVs in single-cell RNA were called using BamBam [84] with sequencing read alignment data in each BAM file format as input. Each variant was assigned a confidence score according to the genotype accuracy likelihood. Variants with supporting reads only in the first or last third of a read's data were removed. Variants with a genotype accuracy likelihood score lower than 30 were discarded, and the rest of the variants were used in the downstream analyses only if they had passed two additonal filters: the strand bias filter and the read alignment quality filter. A recent study had shown that variant allele reads that were present exclusively on one strand are often associates with false positive variant calls [50]. Therefore, I applied the strand-bias filter to variants that had at least four supporting reads, and remove those that had more than 90% of the supporting reads on either only the forward strand or the reverse strand. The read alignment quality removed variants that did not have at least one supporting read with a base alignment quality (BAQ) score of 15. SNVs were written in VCF (Variant Call Format) file format. The SNVs were divided into two groups: known SNVs (those catalogued in the single nucleotide polymorphism database, dbSNP, Build ID: 137), and novel SNVs (those not present in the dbSNP). Although the quality of data cataloged in the dbSNP has been questioned [67] where half of the SNPs are still candidate SNPs and have not yet been validated in a population, both novel SNVs and dbSNP variants were analyzed in this study. Some true novel SNVs might not be accounted for if they were mistakenly annotated as SNPs in the dbSNP.

The SNVs were filtered to find those within the exons of UCSC's known gene canonical transcripts, where the exon's average mapped read coverage was greater than 50. Each single-cell variant rate was calculated by summing the total number of variants that pass this filter, and dividing by the total number of bases in exons with average coverage greater than 50.

3.1.7 Identification of common and unique SNVs amongst single-cells and populations of cells

To compare the SNVs between a single-cell and its corresponding population, I first identified the comparable genomic regions where both the single-cell and the populations of the same group have at least 10× RNA-Seq read coverage. I used the depth function in samtools [53] to measure the read depth, extracted all the genomic locations where the read depth is at least 10, and output the results in BED file format. I then identified the common and different SNVs between the single-cell and the population that are within the comparable genomic regions using the --intersect and --difference operators in BEDOPS (version 1.2.3) [69], respectively. For identifying common and unique SNVs between any two single-cells, I performed all pair-wise comparisons of single-cells in the same manner I did for comparing single-cell to population SNVs. I first identified comparable genomic regions where both single cells have at least 10× RNA-Seq read coverage. Then, I identified common and different SNVs between the two single cells that are within the comparable genomic regions.

3.1.8 Detection of DNA-RNA variants and candidate RNA variants

I used RADIA [77] to identify DNA-RNA variants and RNA-variants. DNA-RNA variants are the SNVs that are only present in the RNA but not in the DNA. By comparing the genomic DNA of MDA-MB-231 cell line sequencing data with RNA-Seq data from single-cells, I identified the DNA-RNA variants. DNA-RNA variants were detected for each of the three groups of single cells (untreated, stressed, and drug-tolerant). I first identified the DNA variants that were specific to the cell line by comparing the cell line DNA to the human reference genome (UCSC hg19). The MDA-MB-231 DNA data were from two sources: one from our whole genome DNA sequencing (20×), and the other from ultra-deep exome sequencing (200×) (GEO accession number: GSE48215 [17]). Next, I identified additional DNA-RNA variants by compared untreated RNA to human reference genome (UCSC hg19) and all the cell-line specific variants were excluded. A subset of DNA-RNA variants were then classified as RNA variants if there was enough read coverage in the RNA to support the variant and enough coverage in the DNA to determine that the variant seen in the RNA was not a DNA variant. Specifically, RNA variants must be covered by at least 10 reads, and at least four of the reads need to support the variant. In addition, at least 10% of the RNA reads must support the variant. I also require 10 or more reads in the cell line DNA, and none of the reads can support the RNA variant. I identified the high-confidence RNA variants by requiring at least 100 reads in the cell line DNA at those loci and none of the reads can support the RNA variant. All the aforementioned parameters were carefully selected and tested using validated DNA and RNA sequencing dataset from tumor and matched-normal samples [77]. I continued to determine candidate RNA variants that were newly emerged in the stressed single-cells by comparing them to the cell line DNA, human reference, and the untreated RNA. Last, I identified RNA variants that had only occurred in the drug-tolerant cells by comparing them to the cell line DNA, human reference, untreated RNA, and stressed single-cells. I performed additional filtering steps for all the RNA variants and removed all the RNA variants that overlapped with SNP sites in dbSNP. I only retained RNA variants that were within the accessible genome defined by the 1000 Genome Project Consortium [26]. To eliminate false positive RNA variants, I used BLAT (BLAST-like alignment tool) [39] to ensure unique mapping of reads that support any RNA variant.

3.1.9 PCR amplification for targeted SNV pyrosequencing

To validate the fidelity of sequencing platform, the Illumina HiSeq 2000, and the mutation calling accuracy of BamBam, ten SNVs were selected for validation with pyrosequencing using cDNA from nine different single-cells: 2 untreated cells, 2 stressed cells, and 5 drug-tolerant cells. PCR primers and internal sequencing primers were designed using Pyrosequencing™ Assay Design Software (Biotage, Uppsala, Sweden) and were synthesized by IDT (Coralville, IA). Amplicons were designed to be 100-200 bp long. Amplicons used in pyrosequencing were amplified from cDNA that was used to generate the HiSeq libraries. Each PCR reaction in a 50 μL volume contained the following: 5 ng cDNA, 0.1μM of each forward and reverse primer, 2.0 mM $MgCl_2$, 200 μM dNTPs, 75 mM Tris-HCl (pH 8.0), and 1.5 U of Titanium® Taq polymerase (Clontech Laboratories, Inc., Mountain View, CA). The amplification was performed in a Gene Amp PCR System 9700 Thermal Cycler (Applied Biosystems, Foster City, CA) under the following conditions: 95°C for 5 min, followed by 25 cycles of denaturing at 95°C for 30 seconds and annealing at the primer specific annealing temperature for 30 seconds, and a final extension at 72°C for 4 min.

3.1.10 Validating SNVs with pyrosequencing

Biotinylated PCR amplicons (50 μL) were immobilized onto streptavidin-coated paramagnetic beads (Dynabeads M-280-streptavidin; Dynal AS, Oslo, Norway) in 2× binding wash buffer (10mM Tris-HCl pH 7.5, 1mM EDTA, 2M NaCl) and incubated at room temperature for 15 min. The immobilized PCR product was treated with 100 μL of 20 mM NaOH for 5 min to denature into single-stranded DNA. Single-stranded DNA attached to the beads was washed twice with 1× annealing buffer (200 mM magnesium acetate, 0.1 M Tris-acetate, pH 7.75). Immobilized single-stranded DNA was resuspended in 20 μL of 1x annealing buffer and 5 μL of sequencing primer at 10 μM. The sequencing primer was annealed to single-stranded template at 95°C for 2 min and then 50°C for 8 min. Primed single-stranded template was sequenced using the PyroMark Q24 system (Qiagen, Hilden, Germany). SNV quantification was performed using the PyroMark Q24 1.010 software (Qiagen, Hilden, Germany).

3.1.11 Private RNA variant frequencies and SNV per mapped reads in normal human single-cells and cancer cells

To compare our RNA-Seq variant calls and variant calls using other single-cell RNA-Seq dataset that used normal human cells and other cancer cells, I performed SNV analysis with two other published single-cell RNA-Seq datasets, including single-cells collected from human early embryos, human embryonic stem cells (hESCs), and human melanoma cells. The raw sequencing read data from Ramsköld *et al*,. 2012 [79] and Yan *et al*. 2013 [121] were downloaded from the Gene Expression Omnibus repository, with GEO accession ids GSE38495 and GSE36552, respectively. The number of SNV per mapped reads were calculated by dividing the number of SNVs that passed all the filters mentioned in the Methods Section 3.1.6 by the total number of mapped reads. Private RNA variant frequencies were calculated by dividing the number of novel variants (variants not present in dbSNP) that are unique to one cell but not in any other single-cell of the same type in the comparable regions (where both single-cell and the rest of the cells have at least 10× read coverage) by the number of transcriptomic bases where all single-cells of the same type have at least 10× coverage.

3.1.12 Data simulation experiment for determining if RNA variants found in three out of five drug-tolerant cells occurred by chance

In order to determine the probability that a RNA variant found in three out of five drug-tolerant cells occurred by chance, I wrote a python script that was designed to create a data set which consists of key and value pair corresponding to the genomic locus and the allele. The data set consists of a dictionary of 3000 randomly generated unique keys for the loci where random mutations were found in the human genome, with the assumption that mutation rate is 10^{-6} and the human genome has 3 billion bp. The script creates five of these dictionary data sets, and then it merges these data sets into one larger dictionary. The idea behind this is to create a new dictionary of overlapped keys. The overlapping keys represent common mutation loci found more than one cell. When an overlap happens during the merging of the five data sets, all values that match that key will be appended, as a list of values associated with the same key position. The length of the list indicates how many single-cells have mutation at a particular locus. The generation of five dictionary data sets was repeated 100 times to determine the probability that a RNA variant occurs in the same locus in three of five single-cell.

3.2 Results

3.2.1 Generation of a Paclitaxel tolerance paradigm in metastatic human cancer cells and isolation of single-cells

To investigate the molecular events associated with cancer cells response to drug-treatment followed by drug withdrawal potentially associated with drug tolerance, cells from the Paclitaxel-sensitive ($IC_{50} < 10$nM) metastatic human breast cancer cell line MDA-MB-231 [7] were exposed to Paclitaxel (100 nM) according to the regimen diagrammed in Fig. 3.1A. After 5 days of drug exposure, most cells had died. Residual cells alive 1 day after Paclitaxel removal were considered to be a “stressed” cell population, and the majority of these cells underwent apoptosis within 2-4 weeks. A small number of residual stressed cells resumed proliferation and established clones, and such cells were considered to be “drug-tolerant” cells (Fig. 3.1B). A drug-toxicity curve was also constructed using a range of Paclitaxel concentrations (Fig. 3.1C). The IC50 was $\sim$7 nM with $\sim$20% of viable cells.

3.2.2 Early drug tolerance dynamics analysis at the single-cell Level

To better understand the early events occurring soon after the onset of proliferation of the rare drug-tolerant cells, I conducted whole transcriptome sequencing analyses at the single cell level for untreated, stressed and drug-tolerant (collected from a proliferating clone at less than six cell divisions) populations. Five single cells were isolated from each treatment group by picking single cells with glass needles using micromanipulators over an inverted microscope and immediately placing each cell in lysis buffer (Fig. 3.1D). For whole population analyses, >10,000 pooled cells were collected from each group. We used a linear RNA amplification system for the whole transcriptome sequencing [44]. The use of such a system prevents reproduction of an error introduced in earlier amplification cycles, a concern in exponential amplification systems.

I generated similar average numbers of sequencing reads for individual single cells and each cell population, 77 million reads and 100 million reads, respectively (Appendix, Table A.1). With a somewhat similar number of sequencing reads, RNA-Seq from single cells generated a much greater sequencing depth than it did for cell populations. On average, there were 117 times coverage for single cells and 23 times depth of coverage for cell populations. By contrast, RNA sequencing reads of the cell populations covered 5.4 times more genomic regions compared with that of a single cell (Appendix, Table A.2)). This result indicates that with a comparable number of reads generated, the single-cell RNA sequencing generates less coverage than the cell population RNA sequencing, with the consideration that each individual cell may be expressing only a fraction of the genes that are expressed in the bulk population. Indeed, the fraction of genes expressed above 1 RPKM (or 1 adj-RPKM; Methods Section) in single cells compared with their bulk populations is only 20%, whereas pooling and mapping the reads from each cell within the same group resulted in a much greater approximation of the number of genes expressed above the same threshold (Appendix, Table A.3).

3.2.3 The novel RNA variants in single-cells are not the major alleles found in population

One of the main goals of performing single-cell sequencing is to exam the genetic heterogeneity within a cell population. I suspect that each single-cell carry some private variants that are not present in most cells in a population. The single-cell private SNVs may consist of somatic mutations propagated from DNA or RNA variants that are introduced by processes such as RNA editing or errors in transcription. RNA variants in this study are supported by sufficient evidence that they are only present in the RNA sequencing reads and not in any of the DNA sequencing reads. Novel SNVs are variants that are not present in dbSNP (The Single Nucleotide Polymorphism Database) [92]. Variants in dbSNP are common SNPs that are found in at least 1% of the human population; therefore, they are not rare variants. Most of the novel SNVs identified in single cells were not the major alleles at the cell population level, despite the fact that there were 2-10 times more total SNVs found in cell populations than in single cells (Appendix, Table A.4) and that SNVs detected in the cell populations cover more genomic regions than those from single cells. Within comparable genomic regions where there was at least 10× depth of coverage, there were about 6 times fewer SNVs detected at the population level than in single cells. In most cases, the novel variants in single cells were not the major variants in the cell populations whereas most dbSNP variants were shared between single cells and population cells (Fig. 3.2). Since the number of RNA variants called could be directly related to the depth of sequencing, therefore, I also compared the amount of SNVs detected in both single cells and cell populations at various depth of read coverage thresholds (Fig. 3.3)). The number of SNVs was normalized by the number of genomic bases with the corresponding depth of read coverage to ensure that the difference in the number of SNVs was not due to differences in genome coverage breadth. Strikingly, many SNVs were found at genomic regions with less than 60x read coverage, while the genomic regions with deeper read coverage do not present more SNVs. Moreover, more novel (non-dbSNP) variants were detected from single cells than from populations regardless of the depth of coverage. In contrast, more dbSNP variants were detected at the population-cell level compared to the single-cell level at all depths of coverage. Additionally, I observed that with a similar number of uniquely mapped reads for single-cells vs. populations, the latter have only slightly more transcriptomic bases with reads at lower depth of coverage but this difference is minimal or even reverts in regions with higher depth of coverage (Fig. 3.4). Thus with a similar amount of resources and effort RNA sequencing from single cells has increased sensitivity to detect novel SNVs which are not apparent from RNA-Seq from populations.

3.2.4 RNA variation is similar in drug tolerant cells and other cancer cells

Cells from cancer cell-line typically contain more SNVs compared to normal cells. Here, I compared the RNA variant frequencies in single-cells in this study with those found in single-cells with normal human single-cells and human cancer cell-line single-cells from two recently published dataset. I also examined the amount of RNA variants that are shared between any two single-cells of the same type to show the degree of heterogeneity in single-cells.

To compare our RNA-Seq variant calls and variant calls using other single-cell RNA-Seq datasets that used normal human cells and other cancer cells, I performed SNV analysis with two other published single cell RNA-Seq datasets using the SNV analysis method described in the Methods Section, including single cells collected from human early embryos [121], human embryonic stem cells (hESCs) [121, 79], and human melanoma cells [79]. To ensure that these datasets are comparable, I first examined the number of SNV per mapped read in each sample in each dataset. The number of SNV per mapped reads were comparable between single-cells from this study and those from human early embryos, hESCs, and human melanoma cells (Table 3.4).

With the single-cell in this study, I measured the number of novel variants shared between any two cells in the genomic regions where each single cell has at least 10x read coverage. Prior to Paclitaxel treatment, untreated single cells shared about 30% of novel variants (not present in the DNA) with any other untreated cell.

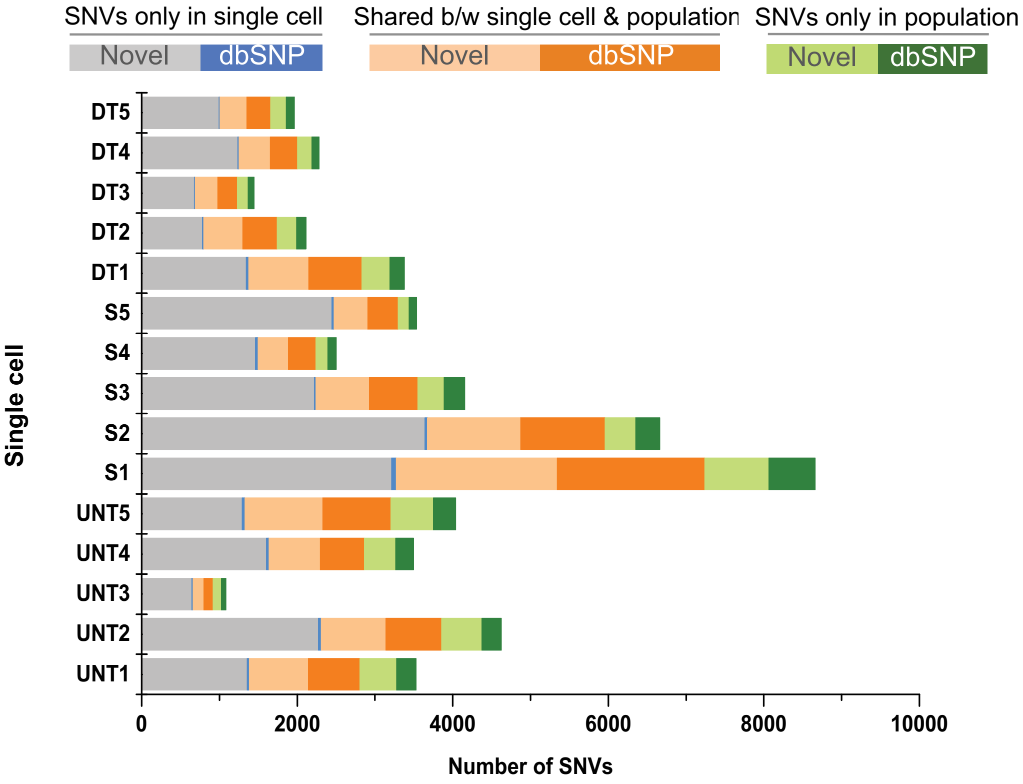

Figure 3.2: The majority of novel variants in single-cells was unique to the single-cells (gray bars), and these single-cell novel variants were not the majority alleles at the population level. Most of the common variants that were present in a single-cell and its corresponding population were known variants catalogued in dbSNP (orange bars). A relatively small number of variants SNVs that were unique in the population that were not the alleles found in the single-cells (green bars). An insignificantly small number of dbSNP variants that were unique to single-cell, which could be due to the differences between cell-line DNA and the normal human DNA.

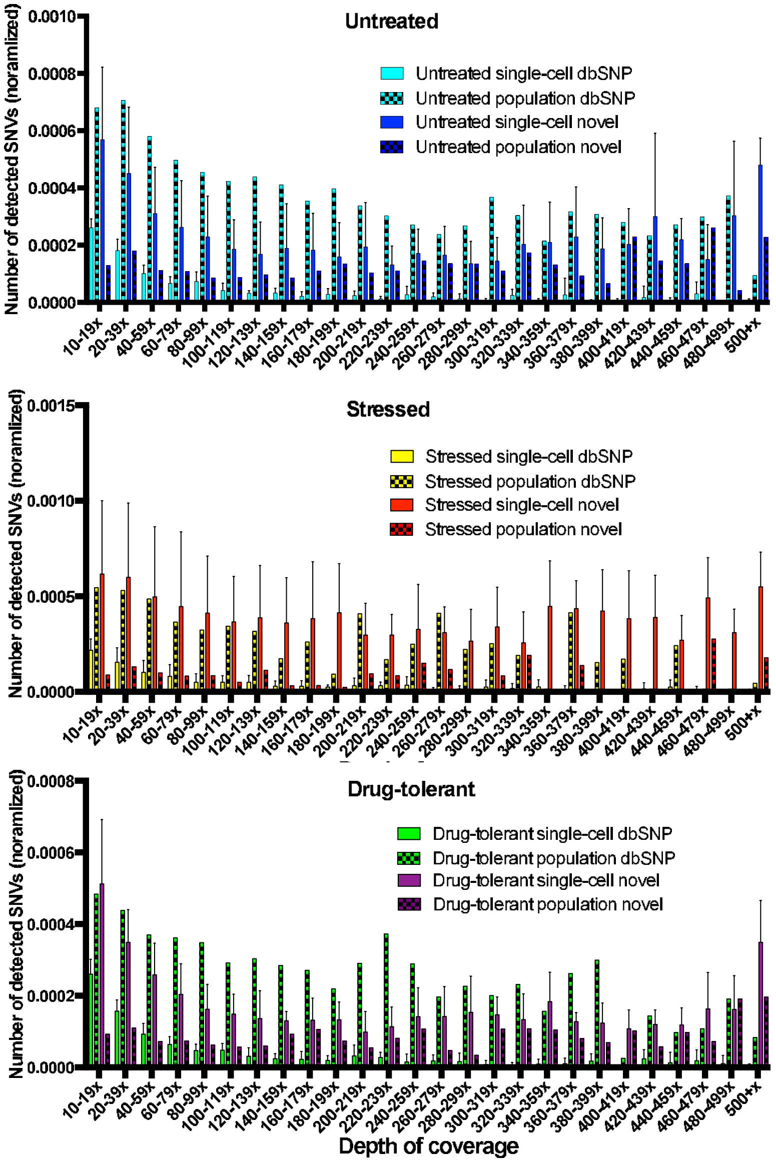

Figure 3.3: The number of SNVs detected in single cells and population regions cells at various depth of read coverage. The number of SNVs was normalized by the number of genomic bases with the corresponding depth of read coverage to ensure that the difference in the number of SNVs was not due to the difference in the breadth of genome coverage. Many SNVs were found at genomic regions with less than 60x read coverage, while the genomic regions with deeper read coverage do not present more SNVs.

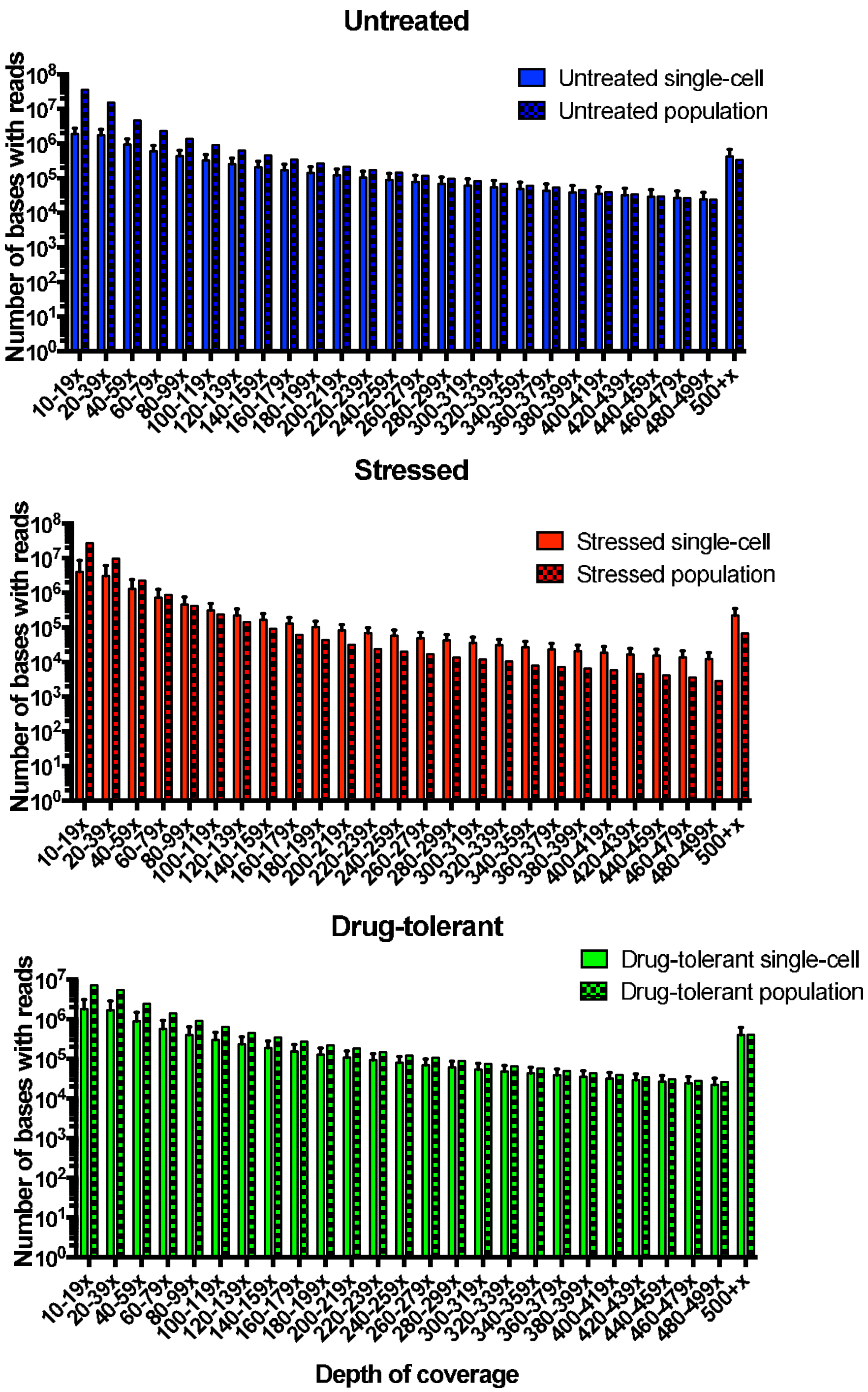

Figure 3.4: Number of bases with reads at various depth of coverage. The number of bases with reads in different genomic regions presenting low to high depth of sequencing was plotted to detect biases in coverage/depth of sequencing between single cells vs. cell population RNA-Seq data.

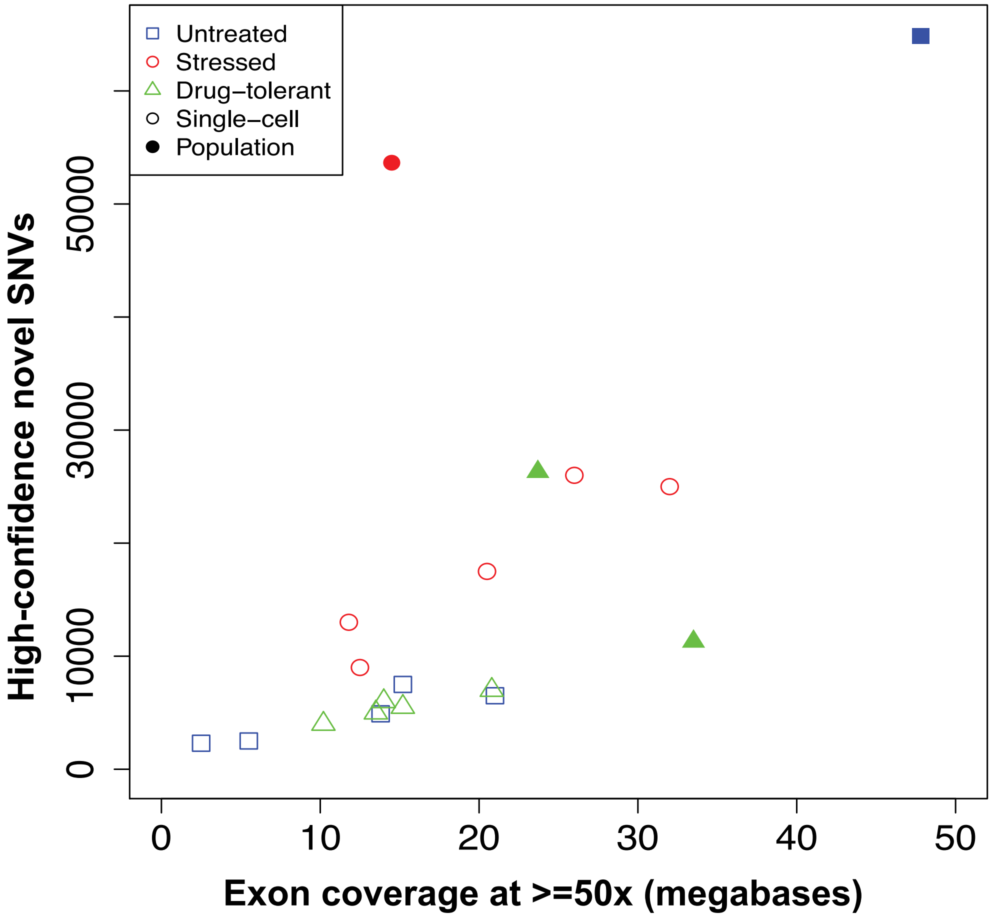

Figure 3.5: Novel SNV rates of single-cells and population cells from different treatment conditions. There were highly disparate variant rates within the different treatment conditions. Single cells from the stressed cell group (red circle) contained about 2x more novel SNVs than did single untreated cells or single drug-tolerant cells. Drug-tolerant cells had a variant rate similar to that of untreated cells. Untreated: blue square, Stressed: red circle, Drug-tolerant: green triangle, Single-cell: Unfilled shapes, Population: Filled shapes.

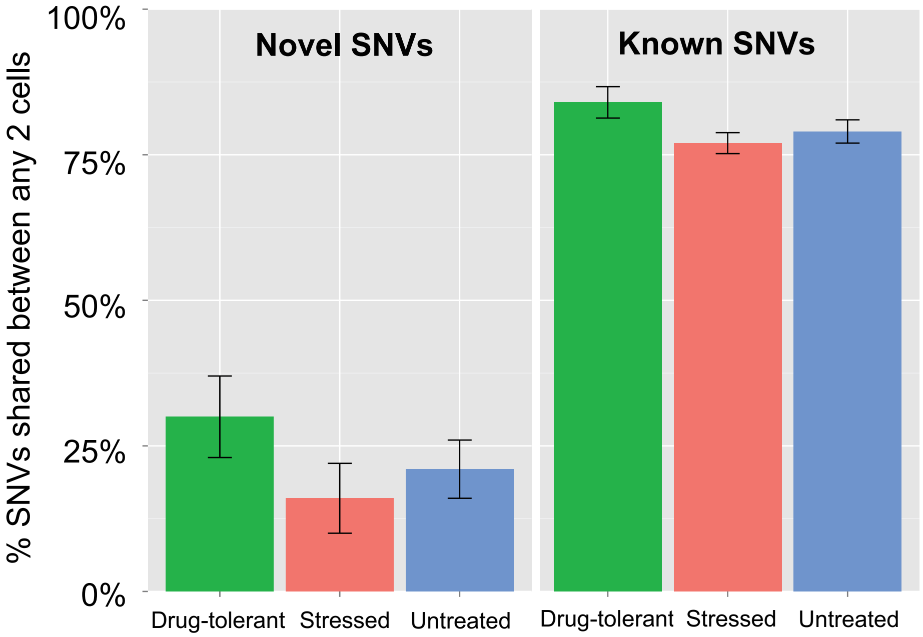

Figure 3.6: The amount of novel SNVs and known SNPs shared between single-cells of the same treatment group. Novel variants are the ones that are not present in the dbSNP database. The bar plot shows the average percent of novel shared variants between any two single-cells for each group. Most known variants present in one cell were present in another cell of any different group. The bar plot shows the average percent of known (dbSNP) shared variants between any two single-cells for each group.

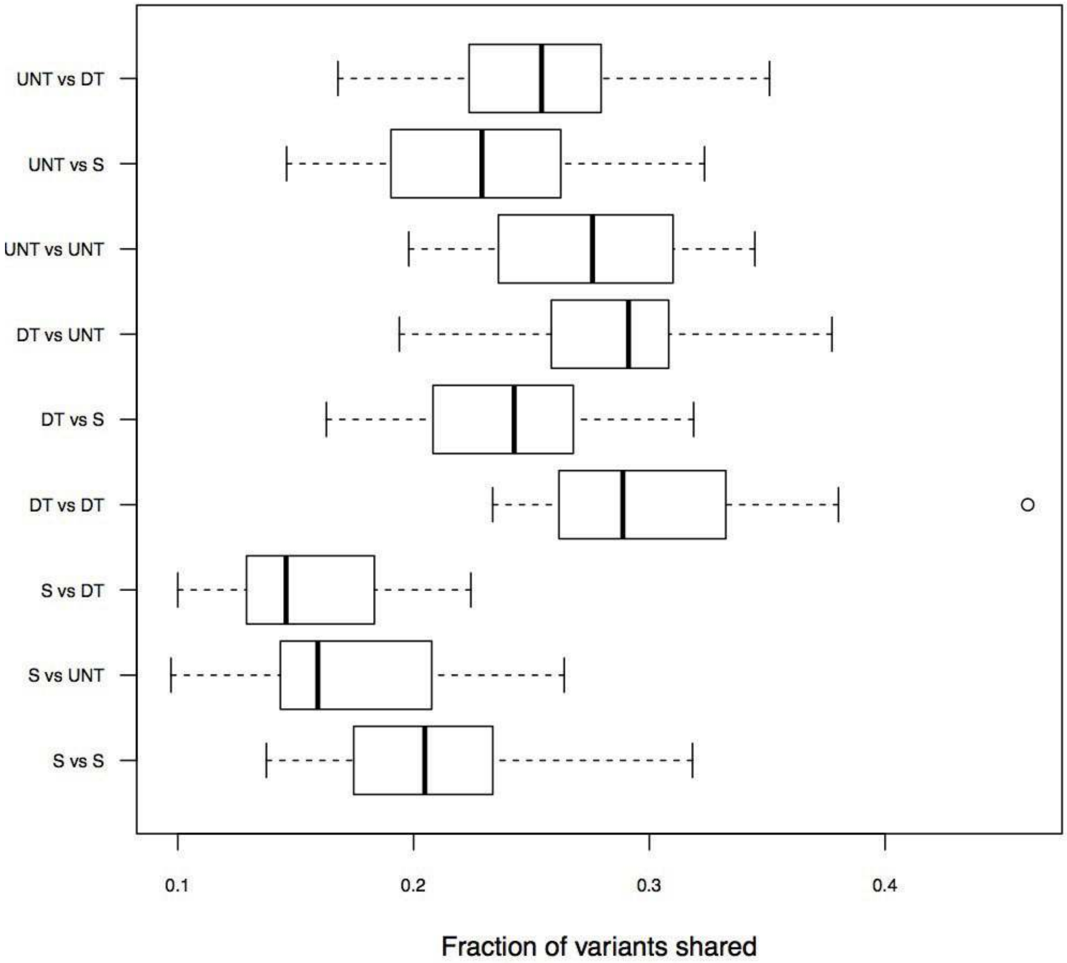

Figure 3.7: The fraction of novel variants shared between any two single-cells. A high heterogeneity is observed between single-cells within and between groups. UNT: untreated cells, S: stressed cells, DT: drug-tolerant cells.

Upon exposing the cells to 5 days of Paclitaxel treatment, the stressed cells appeared to have accumulated additional novel variants that were not previously present in the untreated cells (Fig. 3.5). On average, stressed cells shared 24% of novel variants with each other, but fewer than 20% novel variants in stressed cells were found in any single cell in either the untreated- or drug-tolerant group (Fig. 3.6 and Fig. 3.7). Although drug-tolerant cells were clonal, they shared similar percentages of novel SNVs among themselves compared to untreated single cells, about 25-45%. Drug-tolerant cells and untreated cells shared about 30% of novel variants. Overall, most novel variants in one cell were unique (Fig. 3.6 and Fig. 3.7), and these novel variants could arise from DNA-RNA transcription error or RNA editing. Furthermore, all single cells shared more than 75% of the known dbSNP variants with any other cell of any of the three groups (Fig. 3.6). This shows that those variants catalogued in the dbSNP are already present in the DNA.

Single-cell RNA-Seq from human early embryos including oocytes, 2-cell embryos, and 4-cell embyros shows that as cells go through each cell division, the number of novel variants progressively increases (Table 3.3). The polymorphism frequencies from the other two datasets were 3.3e-4/bp for hES cells, 7.0e-4/bp for the cancer cells [79]; 1.4e-4/bp for 2-cell stage human embryos and 4.7e-4/bp for 4-cell stage human embryos [121] (Fig. 3.9). Importantly, the frequency of cell-specific SNVs in this study is about 4.7e-4/bp, which is higher than the polymorphism frequencies of normal human cells but comparable to that found in cancer cells from Ramsköld *et al* [79] (Table 3.4). Moreover, although neither untreated cells nor long-term stressed cells are monoclonal, the frequency of cell-specific SNVs in the latter is greater, suggesting either that cellular stress may increase errors in transcription such as when RNA polymerase inserts the wrong base into the transcript or RNA editing events.

To identify the RNA-editing events, one needs to compare DNA and RNA from the same cell. However, it is not yet possible to sequence whole genome DNA and whole transcriptome RNA simultaneously from a single cell. To gain insight into whether the single-cell RNA variants in this study result from RNA editing, I compared the base substitution patterns between our single-cell RNA variants and other previously published RNA editing events. A-to-G substitution is typically the most frequently occurring RNA variants detected in other RNA editing studies [6, 41, 73, 75]. Curiously, I found that after T-to-C, A-to-G substitutions were the more frequent substitutions identified in our study (Fig. 3.8A). In addition, most of the A-to-G RNA variants observed in the single cells occurred in the intronic and untranslated regions (UTRs) (Fig. 3.8C), in agreement with previous A-to-G RNA editing studies [30, 70, 73]. One way to confirm that these A-to-G variants are indeed resulting from RNA editing events is to conduct ADAR (adenosine deaminase acting on RNA) knockdown experiment. ADAR is an enzyme that is known to mediate adenosine to inosine (A-to-I) editing, where inosine is interpreted as guanosine (G) during translation [6].

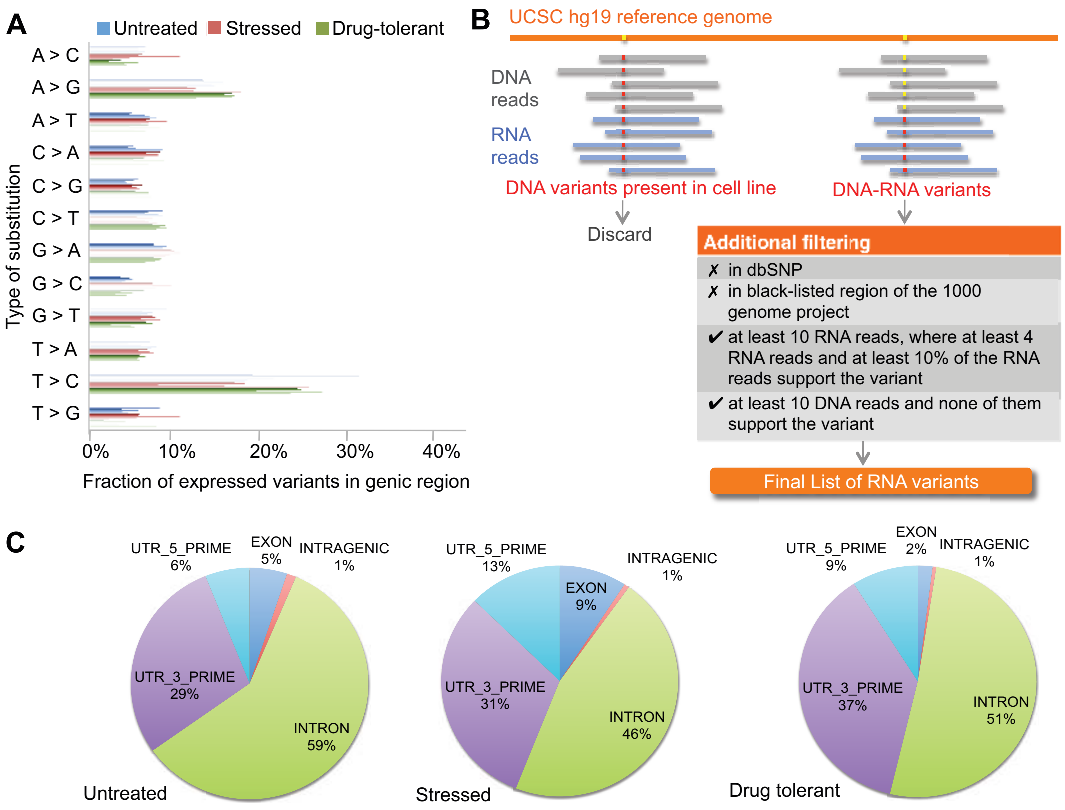

Figure 3.8: RNA variants identified at the single-cell level. (A) The distribution of the 12 RNA variants at the single-cell level showed that the most abundant types of RNA variants were A-to-G and T-to-C. (B) Multiple filters were applied to identify candidate RNA variants. Any SNV in the DNA of the cell line that did not match the human genome reference was considered to be a DNA variant specific to the MDA-MB-231 cell line. DNA-RNA variants were those in which the base call in the single-cell RNA reads differed from that in the cell line DNA reads, and the base call in the reference genome agreed with that in the cell line DNA. The DNA-RNA variants were first subjected to two filters that removed all known variants and variants that were not within the accessible genome defined by the 1000 Genome Project Consortium. Two filters were applied to the rest of the DNA-RNA variants to ensure that the RNA variants have enough sequencing reads to support an RNA variant call. (C) The distribution of A-to-G RNA variants relative to gene boundaries. The majority of the A-to-G RNA variants were clustered in non-coding regions including introns and 5′ and 3′ untranslated regions (UTRs).

3.2.5 RNA variants found only in drug-tolerant cells are involved in microtubule stabilization and organization

One of the goals of this study is to identify RNA variants that reside in genes associated with Paclitaxel resistance. Although it is challenging to elucidate the precise role of these alterations in Paclitaxel resistance, the identification of these RNA variants at the single-cell level provides new opportunities for understanding tumor heterogeneity and treatment of cancer.

The DNA-RNA variants and RNA variants in this study were identified using a somatic mutation caller, RADIA [77]. In any single-cell, there were approximately 5,000 cell-line specific SNVs that were different from the human reference genome (hg19), and about 63,000 cell-line specific SNVs were found in the population cells of all three groups. After removing all cell line-specific variants, the remaining DNA-RNA variants that passed all additional filters were considered to be RNA variants (Fig. 3.8B). One of the filters was for removing RNA variants that overlap with dbSNP. To accurately identify RNA variants, the most ideal way is to sequence both the transcriptome and the genome with great depth from the same sample and compare the sequence differences between the ”matched” RNA and DNA. Since it is not yet possible to sequence both the genome and transcriptome from a single cell, therefore, I followed a commonly used method by other studies that used only RNA-Seq to identify RNA variants – mapping the RNA-Seq reads to a (nonmatched) genomic reference sequence, and remove the known SNPs to eliminate potential germline variants [78, 75]. An additional filter was applied to remove all the RNA variants that reside in reads that were mapped to inaccessible sites in the genome defined by the 1000 Genomes Project [26]. The inaccessible sites mainly consist of segmental sequence duplications and high-copy repeats. Sequencing reads are often incorrectly aligned to the inaccessible sites, and leading to false positive variant calls [26]. The parameters being used in selecting the RNA variants from the DNA-RNA variants (Fig. 3.8B) come from multiple parameter optimization experiments to achieve a maximum specificity while maintaining an acceptable balance between specificity and sensitivity. These parameters allowed RADIA to achieve a 98% specificity/84% sensitivity and a 99% specificity/85% sensitivity balance in two independent TCGA validation experiments on data collected from over 500 patients [77].

The accuracy of the RNA variant calls was further validated through pyrosequencing of 10 randomly selected SNVs (Table 3.1). I validated these SNVs using a new set of single-cells from independent groups of the untreated MDA-MB-231 cell line and different drug tolerant clones. All the SNVs identified by pyrosequencing agreed with the ones detected using Illumina HiSeq 2000.

Each untreated cell had an average of 526±92 RNA variants, and about 84±9 of them were high-confidence rare RNA variants where there were at least 100 DNA reads and none of them support the RNA variants. After exposing the cells to Paclitaxel treatment for five days, there were 110±92 new RNA variants that were found in stressed cells; 31±15 are high-confidence rare RNA variants, and none were detected in any of the untreated cells. Drug-tolerant cells contained about 94±52 new RNA variants that were not previously detected in untreated and stressed cells, and 29±15 were high-confidence rare RNA variants.

As described in Section 2.4, Paclitaxel blocks the G2/M phase in cells by stabilizing the microtubules such that the cell cannot form the normal mitotic apparatus for cell division. Therefore, any mutation found in genes that encode for proteins associated with microtubule functions and cell-cycle regulation is relevant and important for understanding how it can potentially lead to Paclitaxel-resistance. There were 38 RNA variants in at least three out of five drug-tolerant cells that were not present in any untreated or stressed cells and were not detected in the population sequencing (Table 3.2). I did a data simulation experiment and concluded that these 38 RNA variants did not simply occur in three of the five cells by chance (see the Methods section *** put ref). Interestingly, four of the 38 RNA variants resided in genes that encode for proteins involved in microtubule stabilization and organization (*PCM1*, *NUDCD3*, *RAPGEF4*, and *KIAA1671*) and two of them were located in genes that were implicated in Paclitaxel resistance (*RAPGEF4* and *AMOTL1*) (Table 3.5). One of the variants present in all five drug-tolerant single-cells, was located on chromosome 8 (chr8:17885150) and represented a missense mutation in the *PCM1* gene (pericentriolar material 1). PCM1 encodes a protein essential for anchoring microtubules to the centrosome [25, 19]. PCM1 is involved in microtubule stabilization and assembly of centrosomal proteins [19]. Centrosome function is essential for completion of interphase and mitosis [109] and aberrant centrosomal activity has been implicated in tumor progression [56, 13]. The two other missense mutation were found in genes that were involved in microtubule organization and stabilization during mitosis: *RAPGEF4* and *NUDCD3*. *RAPGEF4*, Rap guanine nucleotide exchange factor 4, was previously shown to interact with protein complexes that were involved in microtubule polymerization and organization [59, 88]. RAPGEF4 protein is also known as Exchange Protein Directly Activated by cAMP 2 (EPAC2) and is one of the binding partners of MAP1A (microtubule-associated protein 1A) [59]. MAP1A is known to promote elongation and nucleation of tubulin [74]. The gene *NUDCD3* encodes the NudCL (nuclear distribution gene C-like) protein. NudCL has been shown to interact with the dynein complex, a minus-end-directed microtubule motor [128], and is required for mitosis and cytokinesis [127]. Depletion of NudCL causes loss of dynein function, which leads to insufficient recruitment of γ-tubulin to spindle poles and mislocalization of the dynein complex during mitosis [128]. The last mutation listed in Table3.5 resides in the gene *KIAA1671* that encodes a protein involved in mitosis and chromosome segregation [71, 20]. Antibodies against this protein were found in sera of breast cancer patients that had developed auto-antibodies [22].

The aforemented gene *RAPGEF4* was also implicated in Paclitaxel resistance. Depletion of RAPGEF4 showed a significant increase in Paclitaxel-induced microtubule stabilization in Paclitaxel-resistant A549-T12 lung carcinoma cells and partially restored Paclitaxel sensitivity in a previous study [3]. Another mutation was found in the $3'$-UTR of *AMOTL1*. AMOTL1 protein was known to interact with the Hippo pathway component TAZ, which was implicated in Paclitaxel resistance in breast cancer cells [46, 16].

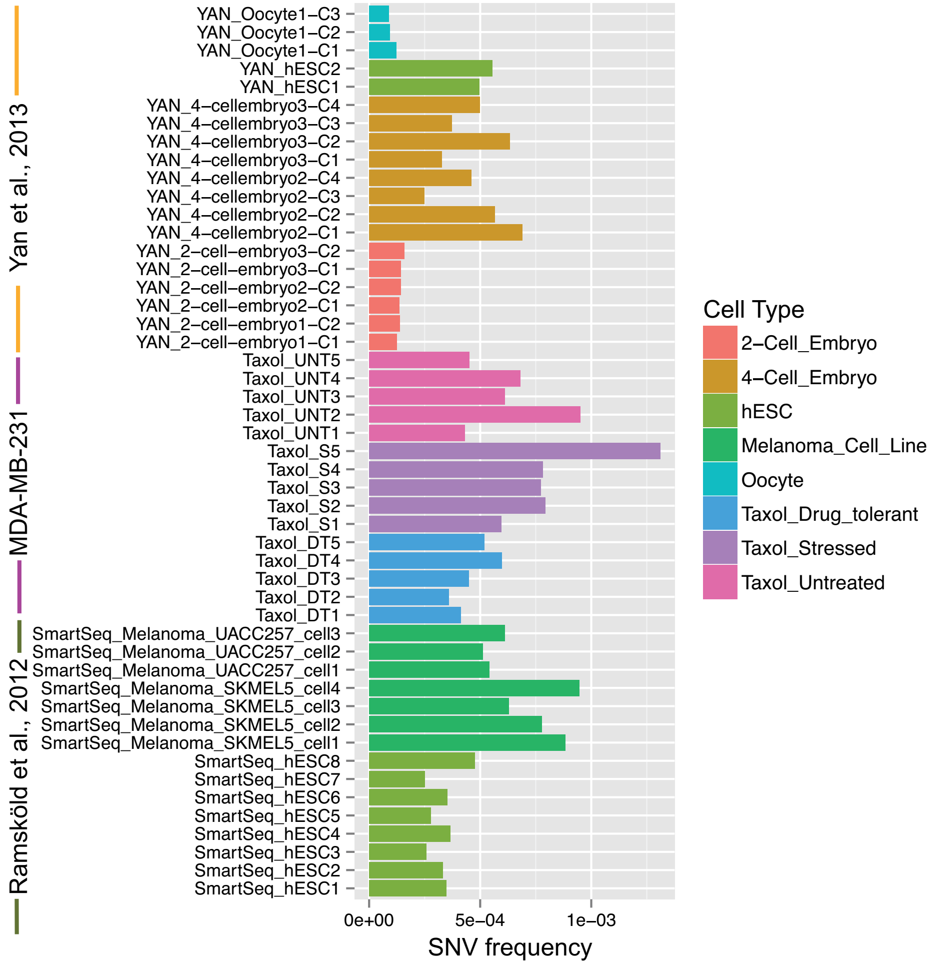

Figure 3.9: Comparing single-cell SNV frequencies between cells from normal human cells and cancer cell line cells. The Illumina sequencing platform is quite low (<0.4% [76]), therefore, I expect a very small number of SNVs that are due to sequencing error. However, it is the important to determine if the amount of SNVs found in the single-cells in this study are comparable to that found in other single-cell RNA-Seq studies that used the same sequencing platform. Here, I compared single-cell SNV frequencies between cells from normal human cells and cancer cell line cells. The single-cell SNV frequencies are calculated by dividing the number of private novel SNVs in a single-cell by the total number of novel SNVs in that cell. Private novel SNVs are unique SNVs only present in the single-cell and not in any other single-cell of the same type type. I utilized the single-cell RNA-Seq data from Yan *et al*. 2013 [121] including three oocytes, one pair of 2-cell embryo cells, and two sets of four single-cells from a 4-cell embryo. From Ramsköld *et al*. 2012 [79] single-cell RNA-Seq dataset, I analyzed two sets of single-cells from two different melanoma cancer cell lines (UACC257 and SKMEL5), and eight human embryonic stem cells.

Locus	**Cell IDs**	**HiSeq variant calls**	**Pyrosequencing results**
chr17:33478229	DT-cell #4 DT-cell #9B.1 DT-cell #9B.2	A-to-T	A-to-T
chr3:170078232	DT-cell #1 DT-cell #2 DT-cell #3 DT-cell #9B.2	G-to-A	G-to-A
chr17:6917703	DT-cell #1 DT-cell #2 DT-cell #9B.2	G-to-A	G-to-A
chr10:27459670	DT-cell #1 DT-cell #9B.1	C-to-T	C-to-T
chr13:76378459	S-cell #1 S-cell #2 DT-cell #3.1	T-to-C	T-to-C
chr16:2815237	DT-cell #2 DT-cell #4 DT-cell #9B.2	T-to-G	T-to-G
chr3:196612295	DT-cell #1 DT-cell #9B.1	G-to-T	G-to-T
chr3:196769982	S-cell #1 S-cell #2 S-cell #3 DT-cell #3.1	G-to-C	G-to-C
chr16:33963248	UNT-cell #4 UNT-cell #5 UNT-cell #6	T-to-C	T-to-C
chr9:33625096	UNT-cell #3 UNT-cell #6	T-to-C	T-to-C

Table 3.1: SNV validation using pyrosequencing. Ten randomly selected SNV calls were tested in single-cells from all three groups (untreated, stressed, and drug-tolerant), and all were confirmed by pyrosequencing. The variant calls are made by using the Allele Quantification (AQ) Pyrosequencing Assay in the PyroMark Q24 1.010 software. Cells with ID number greater than 5 are from repeated drug-treatment experiments. DT: Drug-tolerant, S: Stressed, UNT: Untreated.

Locus	**Gene affected**	**Mutation type**	**Gene Ontology**
chr1:54232975	*TMEM48*	3′-UTR	RNA localization and protein transport
chr1:54269670	*TMEM48*	Missense	RNA localization and protein transport
chr2:128744486	*SAP130*	Missense	Chromatin organization and regulation of transcription
chr2:141816502	*LRP1B*	Missense	Receptor-mediated endocytosis
chr2:166626700	*GALNT3*	Missense	Glycoprotein biosynthetic process
chr2:173916571	*RAPGEF4*	Missense	Ras-like GTPases
chr2:55201845	*RTN4*	Missense	Negative regulation of anti-apoptosis
chr2:55200973	*RTN4*	Missense	Negative regulation of anti-apoptosis
chr2:55200710	*RTN4*	Missense	Negative regulation of anti-apoptosis
chr3:45007193	*ZDHHC3*	Intron	Transition metal ion binding
chr3:63601583	*SYNPR*	3′-UTR	cytoplasmic membrane-bounded vesicle
chr3:185211018	*ZDHHC3*	Missense	transition metal ion binding
chr4:27010057	*STIM2*	Misense	Ion transport
chr5:139908435	*ANKHD1*	Missense	Negative regulation of translation
chr6:7882933	*MUTED/TXNDC5*	Missense/Silent	Protein-disulfide isomerase
chr6:8015778	*MUTED/TXNDC5*	Missense/Silent	Protein-disulfide isomerase
chr6:76412735	*SENP6*	Missense	Protein catabolic process
chr6:122734789	*HSF2*	Missense	Regulation of transcription
chr7:44425714	*NUDCD3*	Missense	Protein binding and maintain the stability of dynein intermediate chain
chr7:93592725	*BET1*	3′-UTR	Vesicle-mediated transport
chr7:115894125	*TES*	Intron	Focal adhesion
chr7:138822678	*TTC26*	Missense	Cilium assembly
chr8:17885150	*PCM1*	Missense	Microtubule cytoskeleton organization
chr9:95068105	*NOL8*	Missense	Positive regulation of cell growth
chr9:95072953	*NOL8*	Misense	Positive regulation of cell growth
chr9:123555243	*FBXW2*	Missense	Protein catabolic process
chr10:12199974	*SEC61A2*	Missense	Intracellular protein transport
chr10:71977528	*PPA1*	Intron	Phosphorus metabolic process
chr11:83182669	*DLG2*	Missense	Cytoskeleton
chr11:94607183	*AMOTL1*	3′-UTR	Cell-cell junction
chr12:27542113	*ARNTL2*	Missense	Regulation of transcription
chr12:42792740	*PPHLN1*	Stop Lost	Epithelial cell differentiation
chr12:69743928	*LYZ*	Silent	Lysozyme activity
chr13:21044267	*CRYL1*	Intron	Fatty acid metabolic process
chr15:89021827	*MRPS11*	3′-UTR	DNA damage response
chr17:64208161	*APOH*	3′-UTR	Negative regulation of endothelial cell proliferation
chr:19:46253959	*AC074212.3*	Silent	Uncharacterized protein
chr22:25592835	*KIAA1671*	3′-UTR	Uncharacterized protein

Table 3.2: This table shows the 38 novel RNA variants that are unique to the drug-tolerant single-cells, and they are found in at least three of out of the five drug-tolerant cells. These variants reside in genes with a wide variety of molecular functions, including DNA binding, catalytic activity, enzymatic regulator activity, transcription factor activity, receptor activity, structural molecule activity, and transporter activity.

Cell1 and cell2 comparison	**Shared novel variants**	**Novel variants only in cell1**	**Novel variants only in cell2**	**% Novel shared in cell1**	**% Novel shared in cell2**	**% Private variants in cell1**	**% Private variants in cell2**
Oocyte1-C1 & Oocyte1-C2	2441	721	565	77.20%	81.20%	22.80%	18.80%
Oocyte1-C1 & Oocyte1-C3	2277	672	472	77.21%	82.83%	22.79%	17.17%
Oocyte1-C2 & Oocyte1-C3	2289	566	493	80.18%	82.28%	19.82%	17.72%
2-Cell-Emb1-C1 & Emb2-C1	2455	732	827	77.03%	74.80%	22.97%	25.20%
2-Cell-Emb1-C1 & Emb2-C2	2580	740	953	77.71%	73.03%	22.29%	26.97%
2-Cell-Emb1-C1 & Emb3-C1	2290	813	1006	73.80%	69.48%	26.20%	30.52%
2-Cell-Emb2-C1 & Emb2-C2	2546	821	934	75.62%	73.16%	24.38%	26.84%
2-Cell-Emb2-C1 & Emb3-C1	2242	888	1000	71.63%	69.15%	28.37%	30.85%
2-Cell-Emb2-C2 & Emb3-C1	2323	1012	997	69.66%	69.97%	30.34%	30.03%
4-Cell-Emb1-C1 & Emb1-C2	2747	3548	3833	43.64%	41.75%	56.36%	58.25%
4-Cell-Emb1-C1 & Emb1-C4	2406	3088	3274	43.79%	42.36%	56.21%	57.64%
4-Cell-Emb1-C2 & Emb1-C4	2304	3287	3075	41.21%	42.83%	58.79%	57.17%
4-Cell-Emb2-C1 & Emb2-C1	2396	2759	2472	46.48%	49.22%	53.52%	50.78%
4-Cell-Emb2-C1 & Emb2-C3	2395	2862	1524	45.56%	61.11%	54.44%	38.89%
4-Cell-Emb2-C1 & Emb2-C4	2439	2906	2552	45.63%	48.87%	54.37%	51.13%
4-Cell-Emb2-C2 & Emb2-C3	2317	2634	1627	46.80%	58.75%	53.20%	41.25%
4-Cell-Emb2-C2 & Emb2-C4	2446	2791	2812	46.71%	46.52%	53.29%	53.48%
4-Cell-Emb2-C3 & Emb2-C4	2373	1708	2792	58.15%	45.94%	41.85%	54.06%
4-Cell-Emb3-C1 & Emb3-C2	2555	1713	2895	59.86%	46.88%	40.14%	53.12%
4-Cell-Emb3-C1 & Emb3-C3	2370	1572	1514	60.12%	61.02%	39.88%	38.98%
4-Cell-Emb3-C1 & Emb3-C4	2663	1872	2489	58.72%	51.69%	41.28%	48.31%
4-Cell-Emb3-C2 & Emb3-C3	2333	2623	1445	47.07%	61.75%	52.93%	38.25%
4-Cell-Emb3-C2 & Emb3-C4	2598	2961	2390	46.74%	52.09%	53.26%	47.91%
4-Cell-Emb3-C3 & Emb3-C4	2433	1499	2160	61.88%	52.97%	38.12%	47.03%

Table 3.3: The number of private novel RNA variants increases with the number of cell division. This table shows the novel RNA variants found in single-cells of early human embryos from Zang *et al.* 2013 dataset. The number of private RNA variants found in single-cell increases with the number of cell-division, from oocyt (1-cell stage), 2-cell stage, and 4-cell stage. Here, oocytes from the same individual are compared and the number of private RNA variants in a single-cell is around 600. After one round of cell division, the number of private RNA variants in a single-cell increased by 54% to about 900. After two rounds of cell division, the number of private RNA variants increased to about 2,500 (a 328% increase from the one-cell stage). Emb: Embryo.

	Single cell	Single-cell Private RNA variant frequency	Private RNA variant frequency ratio (cell-line vs human oocytes)	Avg. Number of SNV per mapped read
MDA-MB-231 cells Paclitaxel-paradigm	UNT1	4.30E-04	6.1	1.06E-04
	UNT2	9.51E-04	13.6	
	UNT3	6.12E-04	8.7	
	UNT4	6.80E-04	9.8	
	UNT5	4.52E-04	6.5	
	S1	5.96E-04	8.5	1.33E-04
	S2	7.94E-04	11.3	
	S3	7.74E-04	11.1	
	S4	7.82E-04	11.2	
	S5	1.31E-03	18.8	
	DT1	4.14E-04	5.9	8.94E-05
	DT2	3.58E-04	5.1	
	DT3	4.50E-04	6.4	
	DT4	5.97E-04	8.5	
	DT5	5.19E-04	7.4	
Early human embryos (Ref: Yan *et al.* 2013 [121])	Oocyte1-C1	1.23E-04	1.8	6.94E-04
	Oocyte1-C2	9.37E-05	1.3	
	Oocyte1-C3	8.95E-05	1.3	
	2-cell-embryo1-C1	1.24E-04	1.8	6.13E-04
	2-cell-embryo1-C2	1.39E-04	2.0	
	2-cell-embryo2-C1	1.36E-04	1.9	
	2-cell-embryo2-C2	1.42E-04	2.0	
	2-cell-embryo3-C1	1.42E-04	2.0	
	2-cell-embryo3-C2	1.58E-04	2.3	
	4-cell-embryo2-C1	6.91E-04	9.9	8.53E-04
	4-cell-embryo2-C2	5.66E-04	8.1	
	4-cell-embryo2-C3	2.48E-04	3.5	
	4-cell-embryo2-C4	4.60E-04	6.6	
	4-cell-embryo3-C1	3.28E-04	4.7	
	4-cell-embryo3-C2	6.34E-04	9.1	
	4-cell-embryo3-C3	3.72E-04	5.3	
	4-cell-embryo3-C4	4.98E-04	7.1	
	ESCp0-1-C1	4.96E-04	7.1	7.70E-04
	ESCp0-1-C2	5.54E-04	7.9	
Human ES cells and cancer cells (Ref: Ramsköld *et. al.*, 2012 [79])	ESC1	3.47E-04	5.0	5.96E-04
	ESC2	3.33E-04	4.8	
	ESC3	2.58E-04	3.7	
	ESC4	3.66E-04	5.2	
	ESC5	2.79E-04	4.0	
	ESC6	3.52E-04	5.0	
	ESC7	2.50E-04	3.6	
	ESC8	4.77E-04	6.8	
	SKMEL5 cell1	8.84E-04	12.6	5.09E-04
	SKMEL5 cell2	7.77E-04	11.1	
	SKMEL5 cell3	6.30E-04	9.0	
	SKMEL5 cell4	9.47E-04	13.5	
	UACC257 cell1	5.42E-04	7.7	
	UACC257 cell2	5.11E-04	7.3	
	UACC257 cell3	6.10E-04	8.7	

Table 3.4: This table shows the SNV frequencies of single-cells in this study and single-cells from two other published datasets with normal human cells and human cancer cells. The single-cell SNV frequencies found in this study are slightly higher than those found in normal human cells from Yan *et al*. and human embryonic stem cells (ESC) from Ramsköld *et al*. [79].

Function	Gene		Mutation	Locus	∆aa*	Ref.
Paclitaxel resistance	*RAPGEF4*	Rap guanine nucleotide exchange factor (GEF) 4	Missense	chr2:173916571	L1785M	[3]
	AMOTL1	Angiomotin like 1	3′-UTR	chr11:94607183	--	[16, 46]
Microtubule organization and stabilization	*PCM1*	Pericentriolar material 1	Missense	chr8:17885150	G227R	[19, 25]
	NUDCD3	NudC domain containing 3	Missense	chr7:44425714	H131D	[127]
	RAPGEF4	Rap guanine nucleotide exchange factor (GEF) 4	Missense	chr2:173916571	L1785M	[3]
	KIAA1671	Uncharacterized protein	3′-UTR	chr22:25592835	--	[20, 71]

*Amino acid change

Table 3.5: This is a subset of the RNA variants listed in Table 3.2 that reside in genes implicated in microtubule stabilization/organization and Paclitaxel resistance. These mutations are useful for followup functional studies to determine if or how they are indeed associated with Paclitaxel resistance.

3.3 Summary

In this chapter, I have demonstrated that single-cell RNA-Seq can identify many private SNVs that are not detectable in bulk cells. I have also shown that the single-cell RNA-Seq technique in this study has produced similar base call fidelity compared to published datasets from previous single-cell RNA-Seq studies. Between single-cells, the majority of the share SNVs are catalogued in the dbSNP database and are not rare variants. Only a quarter of the novel SNVs are shared between single-cells. A number of SNVs only present in the drug-tolerant single-cells reside in genes that are involved in Paclitaxel resistance and microtubules organization and stabilization, and they are interesting targets for future studies for their role in Paclitaxel resistance.

Chapter 4

Whole-transcriptome Gene Expression Analyses at the Single-cell Level

RNA-Seq technology not only has improved our understanding of the transcriptomic landscape of humans and many other organisms, it has also provided a higher dynamic range in the detection and quantification of gene transcripts compared to microarray technology. Thus far, most RNA-Seq experiments were performed with bulk cells and the gene expression levels detected were merely an average of many cells. Aberrant gene expression that drives disease progression is often found in a rare subpopulation of cells or even a single-cell. Therefore, there is a pressing need to study gene expression at the single-cell level.

The aim of this chapter is to highlight the single-cell heterogeneity at the gene expression level, and to demonstrate that the gene expression profile of a cell population is not representative of that in a single cell. Here, I discuss the methods I used in determining the overall gene expression profile and the differentially expressed genes among single-cells and bulk-cells from three conditions in the Paclitaxel-tolerant experimental scheme: untreated, stressed, and drug-tolerant. I also identified the differentially expressed genes that are likely to be responsible for the drug-tolerant mechanism.

4.1 Methods and Materials

4.1.1 Whole transcriptome gene expression analysis

Gene expression variability between samples can occur at many levels, biological and technical. Due to the minute amount of starting RNA material from a single-cell, it was not possible to generate technical replicates from a single-cell and that is one of the limitations of this study. Single cells in the same condition were analyzed as biological replicates. One way to normalize the direct read counts is to normalize the counts with respect to the library sizes and with respect to the length of the transcripts, such as RPKM (Reads per kilobase per million) [66].

$$\text{RPKM} = \frac{\text{RPK}}{\text{million mapped reads}} \tag{4.1}$$

$$\text{RPK} = \frac{\text{number of mapped reads}}{\text{length of transcript in kilobase}} \tag{4.2}$$

However, normalizing the reads by the length of the transcript is based on the assumption that longer transcripts give more read counts, but this is not entirely valid in regards to the single-cell RNA-Seq data from this study where some parts of the transcript have highly uneven read coverage (Fig. 4.1). This phenomenon could be partly due to the technical limitations in evenly amplifying a minute amount of input genetic materials from a single cell, and it could also be due to sequence biases in the cDNA synthesis step using random hexamers. Using the typical RNA-Seq gene expression quantification such as RPKM or FPKM with single-cell RNA-Seq data, one could underestimate the expression level if the read coverage is highly uneven (Fig. 4.2). Therefore, the read counts for single-cells were normalized with respect to the library sizes and with respect to the number of bases in the transcript that has at least 10 uniquely mapped reads. It is referred to as the adjusted-RPKM.

$$\text{Adjusted-RPKM} = \frac{\text{Adjusted-RPK}}{\text{million mapped reads}} \tag{4.3}$$

$$\text{Adjusted-RPK} = \frac{\text{No. of mapped reads in regions with at least 10x coverage}}{\text{positions in transcript in kilobase with at least 10x coverage}} \tag{4.4}$$

The total number of mapped reads for each transcript were obtained using the RNA-Seq quality control package, RSeQC (version 2.3) [112], with the RPKM_count.py script using the following parameter settings: --strand=none, --skip-multi-hits, and using the reference gene model in bed format. The reference gene model was downloaded from the Table Browser in the UCSC Genome Browser with the following query (genome: Human, assembly: Feb. 2009 GRCh37/hg19, track: UCSC Genes, table: knownGene, region: genome) and the output format was set to BED (browser extensible data).

4.1.2 Characterizing single-cells and bulk-cells using gene expression data

The gene expression levels of 15 single-cells (5 cells from each condition), 5-cell pooled samples, and bulk-cells from the three groups were characterized using principal component analysis (PCA) and hierarchical clustering with 1,000 bootstrapping replications. A matrix was generated with adjusted-RPKM for each gene in each single-cell sample. Only genes with adjusted-RPKM > 0 in at least one sample were retained for further analyses. The principal component analysis was performed using FactoMineR [52]. PCA is more suitable in this analysis compared to factor analysis since the main goal here is to reduce a large number of observed variables to a smaller set of important independent composite variables without any prior assumptions or variables model. I used the Pvclust package (version 1.2-2) in R [98] to perform the hierarchical clustering analysis on log2 transformed adjusted-RPKM using the Ward's method with distance measured in Euclidean distance. Psuedo count of 1 was added to all counts prior to log2 transform of adjusted-RPKM.

4.1.3 Differential gene expression and functional classification analyses

Differential expression analysis was performed using adjusted-RPMK for single-cells and population cells using DEGSeq (version 1.10.0) [111]. DEGSeq uses a non-parametric approach with re-sampling to account for the different sequencing depths. Nonparametric methods are more robust in selecting significant features than parametric method when the read counts do not follow any known distribution. Based on the statistical methods defined by Tusher *et al*. (2001) [110], DEGSeq assigns a score to

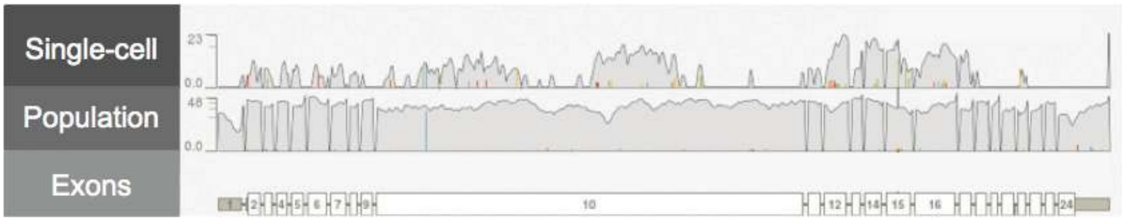

Figure 4.1: An example of uneven read coverage of single-cell RNA-Seq. The top track contains the RNA-Seq read coverage of a single-cell that spans the 5′-UTR, 23 exons, and the 3′-UTR. The middle track contains the RNA-Seq read coverage of population cells that spans the same genomic regions as the single-cell read coverage track. The y-axis on the top and middle tracks shows the number of reads. The bottom track shows the 5′-UTR, 23 exons, and the 3′-UTR that the reads are aligned to. The thin colored vertical lines along the top two tracks indicate where SNVs are detected.

each gene based on the change in gene expression relative to the standard deviation of repeated measurements, and it uses uses permutations of repeated measurements from a shuffled data set to determine the percentage of differentially expressed genes identified by chance, the False Discovery Rate (FDR). Functional classification of the differential expressed genes was performed using the PANTHER Classification System, version 8 [106] (`http://www.pantherdb.org/`). Hierarchical clustering of differentially expressed genes was performed using the heatmap function in R (version 2.15.1) [105].

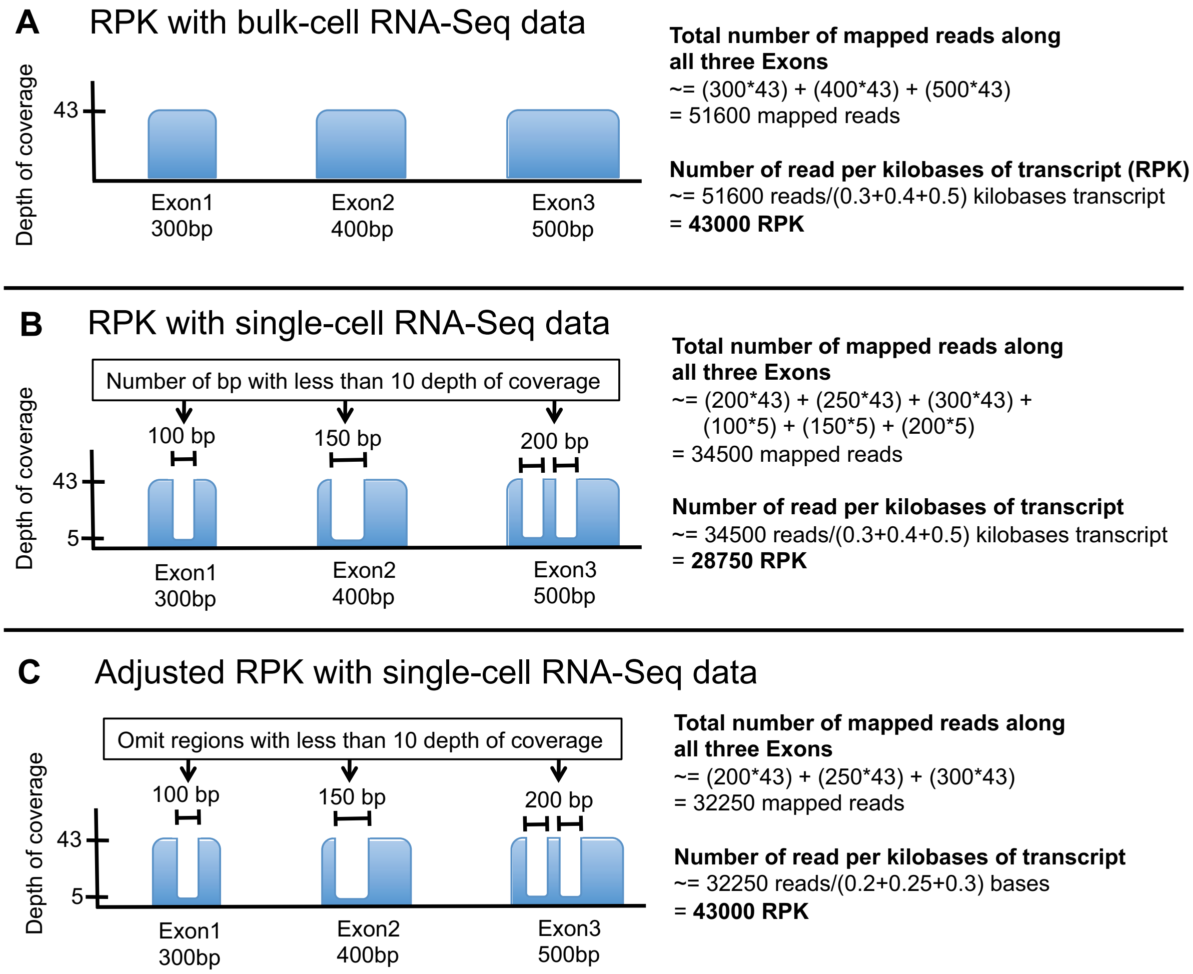
A
RPK with bulk-cell RNA-Seq data
Depth of coverage
43
Exon1
300bp
Exon2
400bp
Exon3
500bp
B
RPK with single-cell RNA-Seq data
Number of bp with less than 10 depth of coverage
100 bp
150 bp
200 bp
Depth of coverage
43
5
Exon1
300bp
Exon2
400bp
Exon3
500bp
C
Adjusted RPK with single-cell RNA-Seq data
Omit regions with less than 10 depth of coverage
100 bp
150 bp
200 bp
Depth of coverage
43
5
Exon1
300bp
Exon2
400bp
Exon3
500bp

Total number of mapped reads along all three Exons
~= (300*43) + (400*43) + (500*43)
= 51600 mapped reads

Number of read per kilobases of transcript (RPK)
~= 51600 reads/(0.3+0.4+0.5) kilobases transcript
= **43000 RPK**

Total number of mapped reads along all three Exons
~= (200*43) + (250*43) + (300*43) +
(100*5) + (150*5) + (200*5)
= 34500 mapped reads

Number of read per kilobases of transcript
~= 34500 reads/(0.3+0.4+0.5) kilobases transcript
= **28750 RPK**

Total number of mapped reads along all three Exons
~= (200*43) + (250*43) + (300*43)
= 32250 mapped reads

Number of read per kilobases of transcript
~= 32250 reads/(0.2+0.25+0.3) bases
= **43000 RPK**

Figure 4.2: A new method for normalizing the number of reads aligned to transcript for single-cell RNA-Seq data. A) RNA-Seq with bulk-cells usually generates a fairly even depth-of-coverage over transcriptomic regions. In order to compare gene expression levels between samples, it is common to normalize the number of mapped reads by the transcript length, RPK (read per kilobase of transcript). B) Single-cell RNA-Seq often results with uneven depth-of-coverage along the transcriptomic regions. If the number of mapped reads along a transcript is simply normalized by the length of the transcript, one could potentially underestimate the actual gene expression level. C) This is a new method for normalizing the number of reads aligned to transcript for single-cell RNA-Seq data. To correct for the underestimation of gene expression level due to highly uneven depth of coverage, the kilobase of transcript length and the number of reads aligned to the transcriptomic regions with less than 10× depth of coverage are excluded from the RPK calculation.

4.2 Results

4.2.1 Stressed cells undergo a Paclitaxel-induced transcription response that is not apparent in drug-tolerant cells

Although acute changes in gene expression (4-24 hours) have been extensively analyzed for a number of stressors including chemotherapeutic compounds, the gene expression profiles in long-term stressed cells are largely unknown. Single cells from our long-term stressed cell group exhibited distinct gene expression patterns. I first characterized the cell type using the adjusted reads per kilobase per million (RPKM) for 15 single-cells using principal component analysis (PCA). The first and second PCA components explained 25% of the variation in all the single-cells, and they separated the stressed single-cells from the untreated and drug-tolerant cells (Fig. 4.3A). And the hierarchical clustering analysis also showed similar clustering pattern (Fig. 4.4A).

To further examine the molecular functions of the differentially expressed genes that separate the stressed cells from the unstressed cells (untreated/drug-tolerant), I performed hierarchical clustering and functional classification of the 50 most significantly differentially expressed genes between the stressed- and unstressed cells. The differentially expressed genes showed a long-term stress-induced response and the effects of Paclitaxel on microtubules and mitosis in stressed cells including down-regulation of genes involved in maintenance of chromatin architecture, microtubule motor activity, mitosis, DNA repair, mRNA splicing, mRNA polyadenylation, and chromatin binding. In addition, gene expression was up-regulated in the following functional areas: cell-cell adhesion and signaling, stress-induced response, apoptosis, glycolysis, amino acid biosynthesis, translation, protein folding, and protein modification (Fig. 4.5). The differential gene expression analysis between stressed and drug-tolerant cells showed a reversed trend in up- and down-regulation compared with that observed between untreated and stressed cells (Fig. 4.6).

Although the untreated and drug-tolerant cells appeared to exhibit similar gene expression patterns, genes that were differentially expressed between these two group could potentially explain the drug-resistance capability of the drug-tolerant cells. Differential gene expression analysis between untreated and drug-tolerant cells showed that microtubule motor activity, microtubule binding, and protein kinase activity were up-regulated in drug-tolerant cells. Furthermore, genes involved in mRNA splicing, mRNA transcription factor activity, translation, and cell adhesion were down-regulated in drug-tolerant cells. Interestingly, I found that expression of ITGA6 (integrin alpha 6), histone demethylase KDM5A, and IGF1R (IGF1 receptor) were each up-regulated in drug-tolerant cells but not in untreated or stressed cells (Fig. 4.6 and Fig. 4.7). Expression of these genes was observed in the majority of single cells as well as the population. Importantly, our data are consistent with studies by Sharma *et al.* that implicated IGF1R signaling and an altered chromatin state conferred, in part, by KDM5A as being required to maintain a dynamic Palitaxel-tolerant phenotype [90]. Overexperssion of *ITGA6* has a synergistic effect on the suppression of Paclitaxel-mediated cell death via the PI3K/AKT pathway mediated by a survival gene, *Evi1* [57, 120]. In this single-cell study, *Evi1* expression level was 2-fold higher in the drug-tolerant cells compared to untreated cells.

4.2.2 Gene expression profile of single-cells is distinct from that of the population

As one cell expand into a clonal population, it is unclear if the gene expression profile of the population is representative of that in a single-cell from that population. I speculate that RNA-Seq for bulk-cells can provide an average gene expression profile of all the cells in the population. To answer this question, I performed PCA and hierarchical clustering with the gene expression data from single cells, pooled single-cells (combing all paired-end reads of five single-cells and treated them as one sample for read mapping and gene expression analysis), and bulk-cells. The hierarchical clustering and PCA showed that pooled cells clustered closer to the population cells in the untreated and drug-tolerant groups (Fig. 4.3B and Fig. 4.4B). The single cells did not cluster with their corresponding population, except for the stressed cells. However, each stressed cell appeared to have distinct gene expression patterns; therefore, they did not cluster together as tightly as untreated and drug-tolerant single cells (Fig. 4.3B and Fig. 4.4B). I also examined the expression level of the genes extracted from the first PCA component which separated the single-cells from the bulk-cells (pooled-cells and population). It appeared that the gene expression level of those genes fluctuates more in single-cells (with some single-cells having zero gene expression while other single-cells having high gene expression) compared to bulk-cells. When I examined

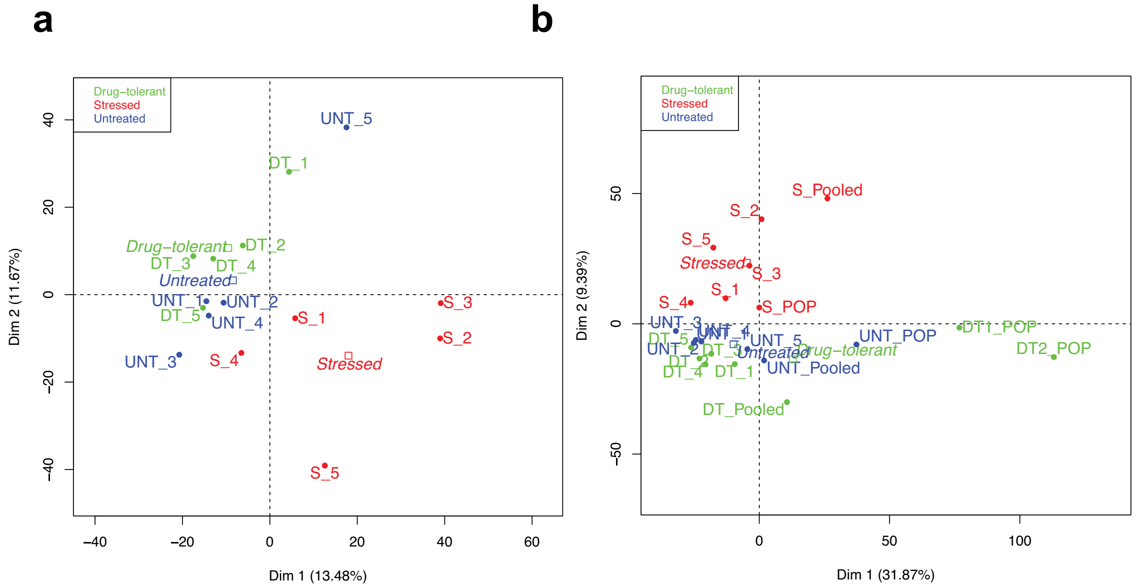

Figure 4.3: Single-cell and population cells were classified using Principal Component Analyses. (A) Principal components analysis plot of adjusted-RPKM for 15 single-cell samples from the untreated, stressed, and drug-tolerant group showed that gene expression profiles of stressed cells (red) were much different from those of untreated (blue) and drug-tolerant cells (green). (B) Clustering gene expression data in adjusted-RPKM from single cells, pooled cells and population cells using PCA showed that single-cells clustered closer to their corresponding pooled-cells than the population sample. The round dots represent each sample (single-cell, pooled-cell or population). The unfilled squares depict the barycenter of each cluster categorized by the cell type (untreated, stressed, or drug-tolerant). Dim: Principal component dimension. POP: population cells, Pooled: 5-cell-pooled sample.

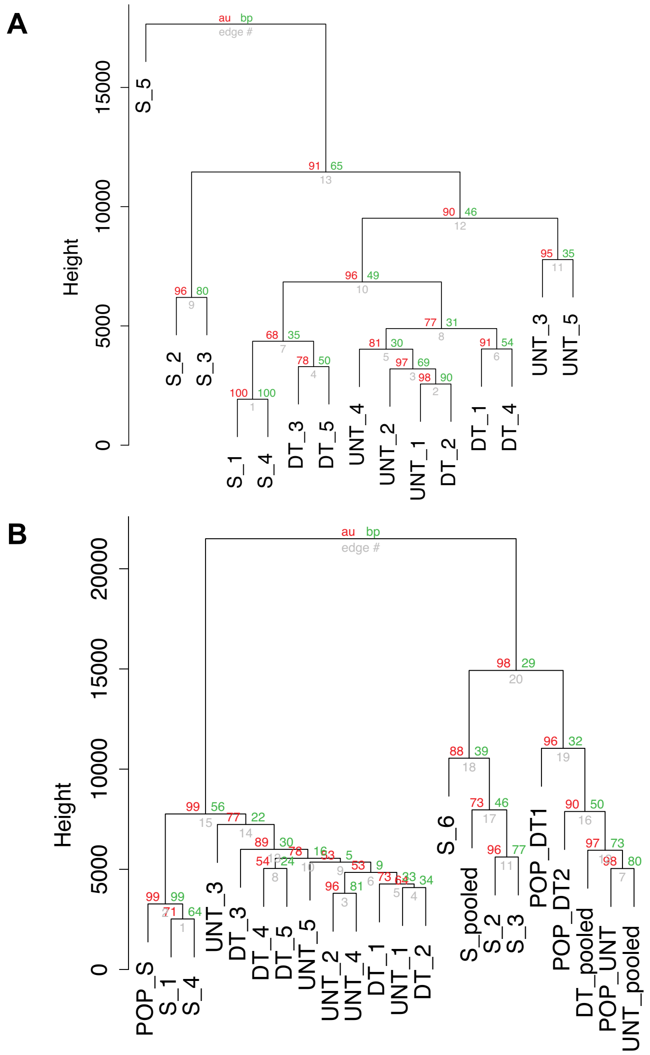

Figure 4.4: The gene expression profile of stressed single-cells is different than that of untreated and drug-tolerant cells. A) Hierarchical clustering of log2-transformed of adjusted RPKM for single-cells for all genes in Euclidean distance with 1,000 bootstrap replications. B) Hierarchical clustering of log2-transformed of adjusted RPKM for single cells, pooled cells, and population cells in Euclidean distance with 1,000 bootstrap replications. Values at branches are approximately unbiased (au) *p*-values (left, red), bootstrap probability (bp) values (right, green), and sample labels (bottom). The edge number is in gray at each branch.

the drug-tolerant single-cells, which were collected from a single clonal population, a divergence of gene expression was found between any drug-tolerant single cell and the averaged expression of the five-cell group. These results indicated that gene expression in a single cell is not reflected by the average expression found in the five-cell group or in a large population of cells (Fig. 4.3B and Fig. 4.4B). These results underscore the value of single-cell RNA-Seq to enhance the resolution of gene expression analysis otherwise masked by averaged values of gene expression in a bulk population.

The higher variability of single-cell gene expression compared with bulk measurements makes it more difficult to find clear patterns of differential gene expression in single cells, particularly for those that are highly variable, as has been recently described when performing RNA-Seq from normal single nuclei from human neurons [82]. Moreover, a much larger sample size would empower a better examination for those transcripts that are consistently highly variable.

4.3 Summary

In this chapter, I have shown that single-cell gene expression profiles are different than those of bulk cells. The 50 most significant differentially expressed genes between untreated cells and stressed cells were those involved in the stress response. Genes that are up-regulated in stressed cells are involved in apoptosis, glycolysis, protein synthesis, cell-to-cell adhesion and signaling. Genes required for chromatin architecture, DNA repair, DNA replication, mRNA splicing, mRNA polyadenylation, microtubule motor activity, and mitosis are down-regulated in stressed cells, and their expression levels are similar between untreated and drug-tolerant cells. The differential gene expression analysis between untreated and drug-tolerant cells suggested multiple drug-tolerant mechanisms including altering the chromatin state, switching Integrin signals, and shifting the balance of pro- and anti-apoptotic signals in the intrinsic apoptotic pathway. Thus, a single molecular mechanism for drug tolerance might not be needed since the diversity will ensure at any time that a given cancer cell containing the right gene expression will be able to overcome massive stress.

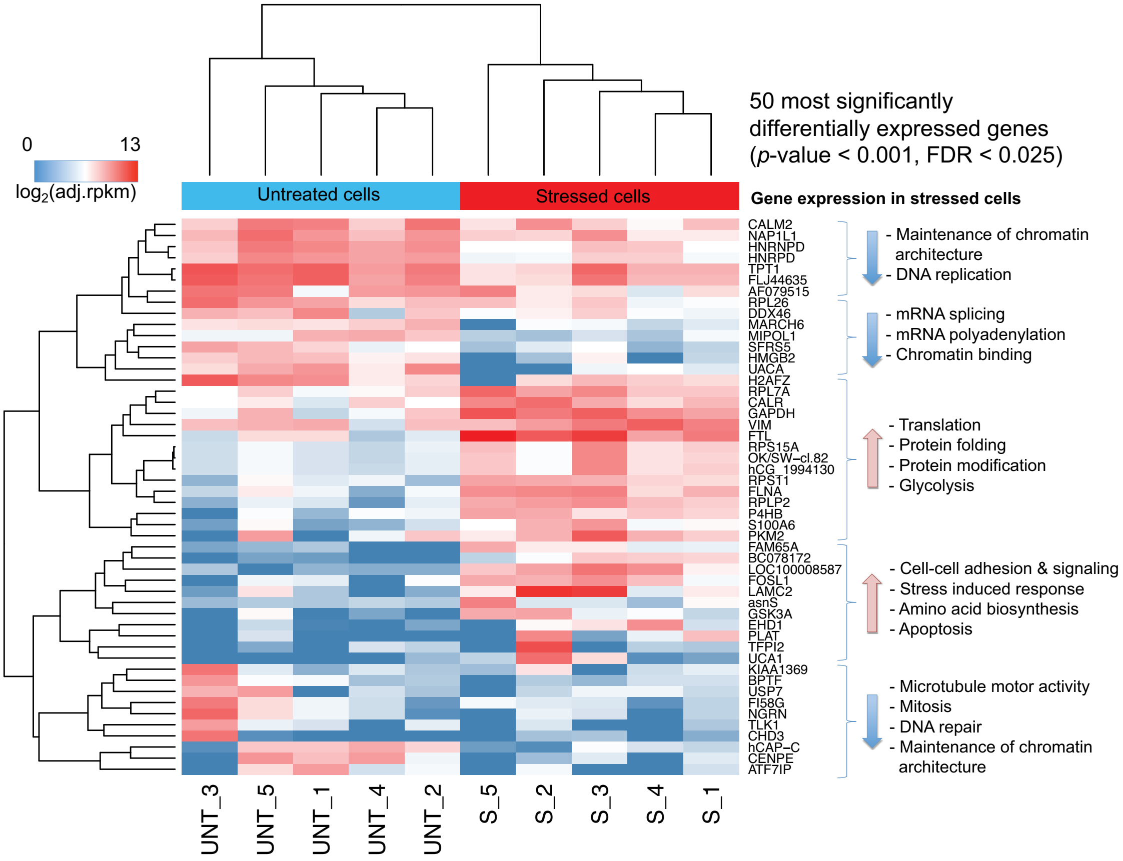

Figure 4.5: Paclitaxel-induced stress response at the single-cell level. Hierarchical clustering of gene expression data for the 50 most significantly differentially expressed genes between untreated and stressed single cells. These differentially expressed genes showed the Paclitaxel-induced effects of Paclitaxel on microtubules and mitosis in stressed cells including down-regulation of genes involved in maintenance of chromatin architecture, microtubule motor activity, mitosis, DNA repair, mRNA splicing, mRNA polyadenylation, and chromatin binding. In addition, gene expression was upregulated in stressed cells in the following functional areas: cell-cell adhesion and signaling, stress-induced response, apoptosis, glycolysis, amino acid biosynthesis, translation, protein folding, and protein modification.

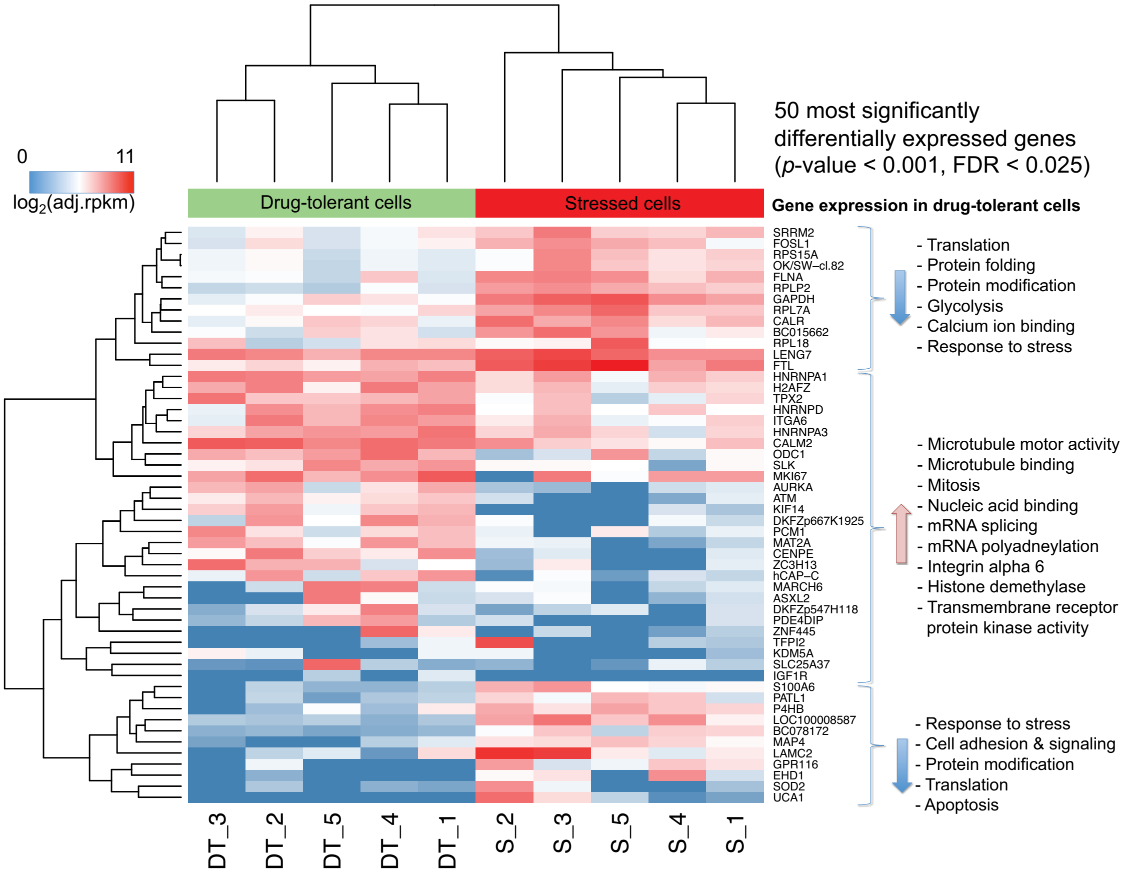

Figure 4.6: The stress response observed in stressed cells subsided in drug-tolerant cells. Hierarchical clustering of gene expression data of the 50 most significantly differentially expressed genes between stressed and drug-tolerant cells showed that the Paclitaxel-induced effect observed in stressed cells did not linger in the drug-tolerant surviving cells after the drug was removed.

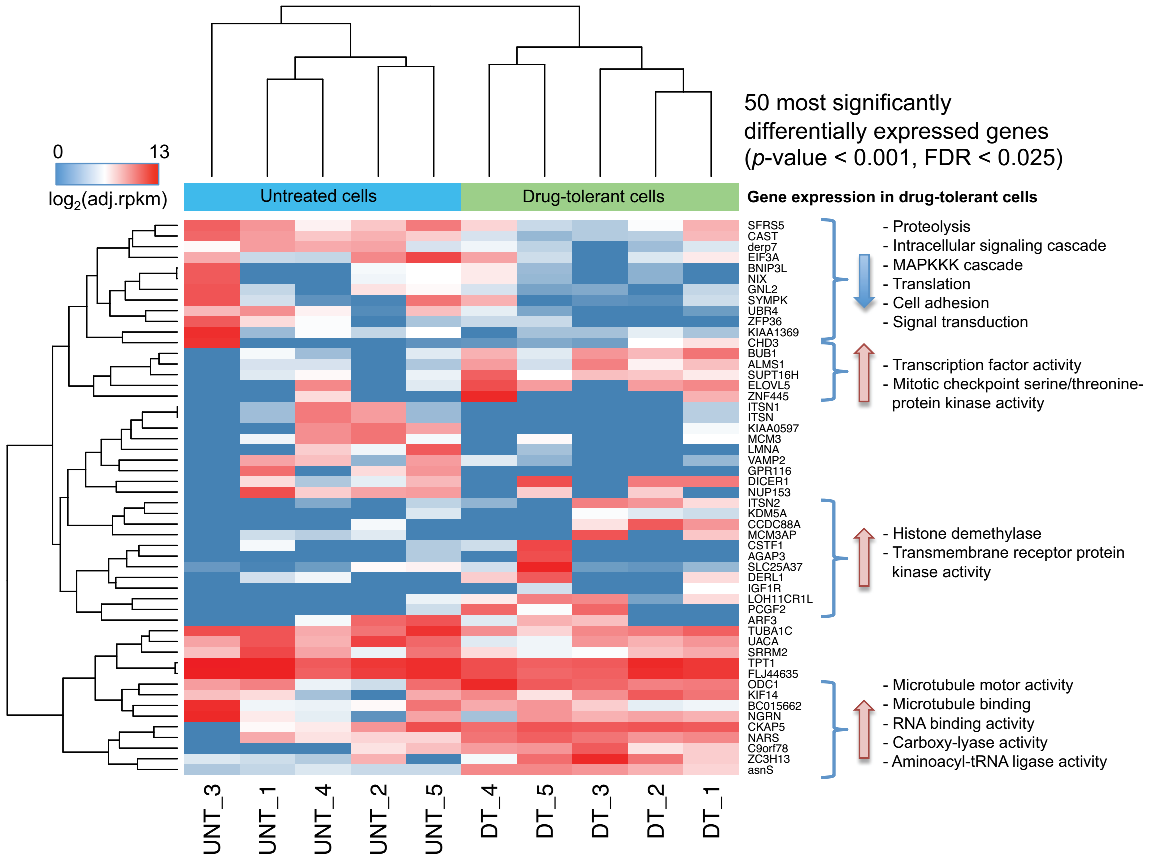

Figure 4.7: Differential gene expression between untreated and drug-tolerant cells. Hierarchical clustering of the 50 most significant differential expressed genes between untreated and drug-tolerant cells (p-value $<$ 0.001, FDR $<$ 0.025).

Chapter 5

Mitochondria Specific SNV and Gene Expression Analyses

Altered mitochondrial metabolism can stimulate cancer cell proliferation. Mitochondria also play a critical role in regulating apoptosis and necrotic cell death. Tian and colleagues [107] had previously shown that tubulin and mitochondrial proteins were the major cellular components exhibiting changes associated with Paclitaxel treatment, and suggested that mitochondria may play a role in Paclitaxel resistance. Although the regulation, transcription, and posttranscriptional processing of the human mitochondrial genome had been extensively studied, very little is known about the extent and distribution of sequence variation in the mitochrondrial transcriptome at the single cell level. In this chapter, I discuss the single-cell transcriptomic mutations and gene expression analyses of mitochondrial genes and nuclear genes that encode proteins involved in mitochondrial functions that could be implicated in Paclitaxel resistance.

5.1 Methods

5.1.1 Mapping single-cell RNA-Seq reads to the mitochondrial reference genome

For mitochondria-specific analyses, I first custom-built a Bowtie index using the bowtie-build function in Bowtie (version 0.12.8) [48] with the UCSC hg19 human reference genome where the DNA sequence for chromosome M was replaced by the Revised Cambridge Reference Sequence (rCRS) of the human mitochondrial DNA (NCBI reference sequence: NC_012920.1). Then, the pre-processed paired-end single-cell and population RNA-Seq reads were mapped against this custom-built Bowtie index with Tophat (version 1.3.2) with default settings [108]. Aligning the reads to the rCRS reference allows for easy comparison with MITOMAP gene annotation [80]. Uniquely mapped reads were used for differential gene expression analyses and SNV calling. These reads were tagged with "NH:i:1" (NH stands for the number of reported alignments that contain the query in the current record) and were extracted from the bam files generated by Tophat using GNU fgrep package (`http://www.gnu.org/s/grep`). PCR duplicates were removed using the rmdup function in samtools [53].

5.1.2 Detecting homoplasmic and heteroplasmic variants in mitochondrial RNA

Uniquely mapped reads against the rCRS human mitochondrial reference in BAM file format were used for the identification of mitochondria homoplasmic (mtDNA sites that only carry one allele for all mitochondrial genomes in an individual) and heteroplasmic (sites that carry more than one allele in an individual) variants using loFreq (version 0.6.0) with default settings [117]. SNVs that are supported by reads with extreme strand bias, especially for novel non-synonymous variants, are more likely to be due to false positive variant calls [31]. Therefore, I used the lofreq_filter.py program to remove variants with significant strand bias (Holm-Bonferroni-corrected p-value$<$0.05). To identify heteroplasmic variants with high confidence, at least 100× read coverage is needed [123], therefore, I removed variants that were not supported by at least 100× depth of coverage prior to subsequent analyses.

5.1.3 Identify SNVs in nuclear-encoded genes involved in mitochondrial functions

A list of 933 nuclear-encoded mitochondrial genes was compiled by querying two databases, the Human Mitochondrial Protein Database (HMPDb, `http://bioinfo.nist.gov`) and the MitoCarta database [72]. SNVs found in these genes were extracted from the filtered VCF files generated by the BamBam as described in the SNVs Identification section in the previous chapter.

5.1.4 Differential expression of genes that encode for proteins involved in mitochondrial functions

The differential gene expression analyses for mitochondria-encoded genes and nuclear-encoded genes were performed independently since these two groups of genes are mapped to two different genomes, rCRS human mitochondrial reference genome and the UCSC hg19 human reference genome, respectively. The gene expression level is measured in adjusted-RPKM and is calculated by first getting the read counts per transcript using the RPKM_count.py script in the RNA-Seq quality control package, RSeQC (version 2.3) [112], using the following parameter settings: --strand=none, --skip-multi-hits, and using the reference gene model in bed format. The read counts for single-cells were normalized with respect to the library sizes and with respect to the number of positions in the transcript that has at least 10 uniquely mapped reads. This is referred to as the adjusted-RPKM (Equation 4.3 in section 4.1.1). The UCSC hg19 human reference gene model was downloaded from the Table Browser [38] in the UCSC Genome Browser [40] with the following query (genome: Human, assembly: Feb. 2009 GRCh37/hg19, track: UCSC Genes, table: knownGene, region: genome) and the output format was set to BED (browser extensible data). The rCRS human mitochondrial gene model was downloaded from the MITOMAP (`http://www.mitomap.org/bin/view.pl/MITOMAP/GenomeLoci`) [80]. Differential expression analysis was performed using adjusted-RPMK for single-cells and population cells using DEGSeq (version 1.10.0) [111]. Based on the statistical methods defined by Tusher *et* *al*. (2001) [110], DEGSeq assigns a score to each gene based on the change in gene expression relative to the standard deviation of repeated measurements from a shuffled data set, and it uses uses permutations of repeated measurements to determine the percentage of differentially expressed genes identified by chance, the False Discovery Rate (FDR). Hierarchical clustering of differentially expressed genes was performed using the heatmap function in R (version 2.15.1) [105].

5.1.5 Knockdown experiment of BNIP3L

RNAi of BNIP3L for the knock-down experiment was expressed from bacteria that carry the plasmid with the RNAi sequence and ampicillin resistance genes, Bnip3L RNAi pSuper (Addgene, Cambridge, MA). The plasmid carrying bacteria were streaked onto LB-ampicillin-agar plates, from which individual colonies were inoculated into 5 mL LB broth cultures and grown overnight at 37°C shaking. Overnight cultures were pelleted and resuspended in 250μL resuspension buffer with RNase A. The plasmid DNA was then extracted and purified using the Invitrogen Mini kit (Life technologies, Foster City, CA) and the QIAGEN Plasmid Midi kit (QIAGEN, Venlo, Limburg), respectively. The purified Bnip3L RNAi plasmids was then transfected into the untreated MDA-MB-231 cells that were cultured to >90% confluency.

5.1.6 Cell viability assay

Cells were seeded in six well plates to 90% confluency and transfected using either the Bnip3L RNAi plasmids with Lipofectamine 2000®(Life technologies, Foster City, CA) or using only Lipofectamine without expression vector (negative control) for 72 hours. Paclitaxel (100 nM, the same concentration that was used throughout this study) was subsequently administered and cells were grown for 48-72 hours. The viability of each well was measured by combining the suspended media with the corresponding trypsinized adherent cells per individual well and the percentage of live cells was counted using Bio-Rad TC-10 Automated Cell Counter (Bio-Rad, Hercules, CA). The viable-cell-count between Paclitaxel-treated and untreated cells was compared to determine if BNIP3L knockdown could increase survival rate of Palitaxel-treated.

5.2 Results

5.2.1 Mitochondria-encoded gene expression profile is unique when cells are under stress

The mitochondrial genome contains 37 genes which encode for 2 ribosomal RNAs (rRNAs), 22 transfer RNAs (tRNAs), and 13 subunits of the respiratory chain [21]. Single-cell and population RNA-Seq data in this study show that the majority of the sequencing reads that did not mapped to the nuclear transcriptome aligned to rRNA and mRNA in the mitochondrial transcriptome (Fig. 5.1). The small mitochondrial genome produced a very high depth of read coverage. The average read coverage of the mitochondria genome is about 3650× per single cell, and is about 7270× per cell population. A number of mitochondria-encoded genes were up-regulated in the stressed single-cells, including cytochrome c oxidase, and 12S and 16S ribosomal RNAs.

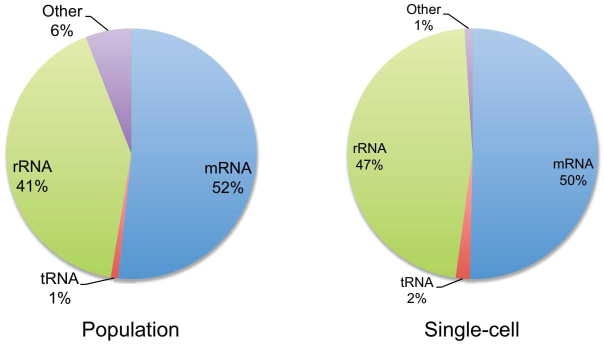

Figure 5.1: Proportion of RNA-Seq reads (that did not map to the nuclear genome) aligning to rRNA, tRNA, mRNA, and other regions (including integenic and antisense regions) of the mitochondrial genome. The majority of the RNA-Seq reads aligned to the rRNA and mRNA regions of the mitochondrial genome. The pie chart on the left shows the proportion of RNA-Seq reads from population cells aligning to the mitochondrial genome. The pie chart on the right shows the fraction of RNA-Seq reads from single-cells to the mitochondrial transcriptome.

Mitochondrial genes encoding NADH dehydrogenase and ATPase are downregulated in stressed cells (Fig. 5.2), compared to untreated cells and drug-tolerant cells, which share similar gene expression profiles. Paclitaxel did not have a significant effect on tRNA production.

5.2.2 Nuclear-encoded mitochondrial genes

Since the majority of the mitochondrial proteins (more than 99%) are synthesized in the cytosol of the cell and are imported into the mitochondria [11], it is important to study the expression level of the nuclear-encoded mitochondrial genes to get a complete picture of the overall mitochondrial gene expression profile in the Paclitaxel-resistance experimental scheme. A number of nuclear-encoded mitochondrial genes were significantly differentially expressed in drug-tolerant cells compared to untreated cells and were implicated in the cell death mechanisms (Table 5.1). Two genes involved in the intrinsic apoptotic pathway were down-regulated in the drug-tolerant cells, *BNIP3L* and *BCL2L1*. The intrinsic apoptotic pathway is regulated by the mitochondria. BNIP3L, also known as NIX, is a pro-apoptotic protein that has been shown to interact with adenovirus E1B19kD protein and the anti-apoptotic protein BCL2 [63]. BNIP3L protein was found to be down-regulated in lung cancer and erythroleukemia cells[2, 97]. *BCL2L1* has two known splice variants, *BCL-*x_L and *BCL-*x_S [95]. *BCL-*x_L is the longer isoform that encodes for an anti-apoptotic protein, 233 amino acids in length. BCL-x_S is 63 amino acids shorter than BCL-x_L and is has pro-apoptotic effects. Chemotherapeutic drugs are found to induce apoptosis by shifting the splicing of *BCL2L1* pre-mRNA in favor of pro-apoptotic *Bcl-*x_S [93]. Cytotoxic agents, such as Paclitaxel, can shift the balance of the pro- and anti-apoptotic proteins in favor of pro-apoptotic proteins, which increase the permeability of the mitocondrial membrane, resulting in the release of cytochrome c from the mitochondrion. Cytochrome c, pro-caspase-9, and Apaf-1 form the apoptosome complex that activates pro-caspase-9 by changing its conformation. The activated caspase-9 then triggers the downstream caspase cascade which executes apoptosis [95]. The down-regulation of pro-apoptotic genes could potentially shift the balance of pro- and anti-apoptotic proteins and enhance the anti-apoptotic effects in the cells.

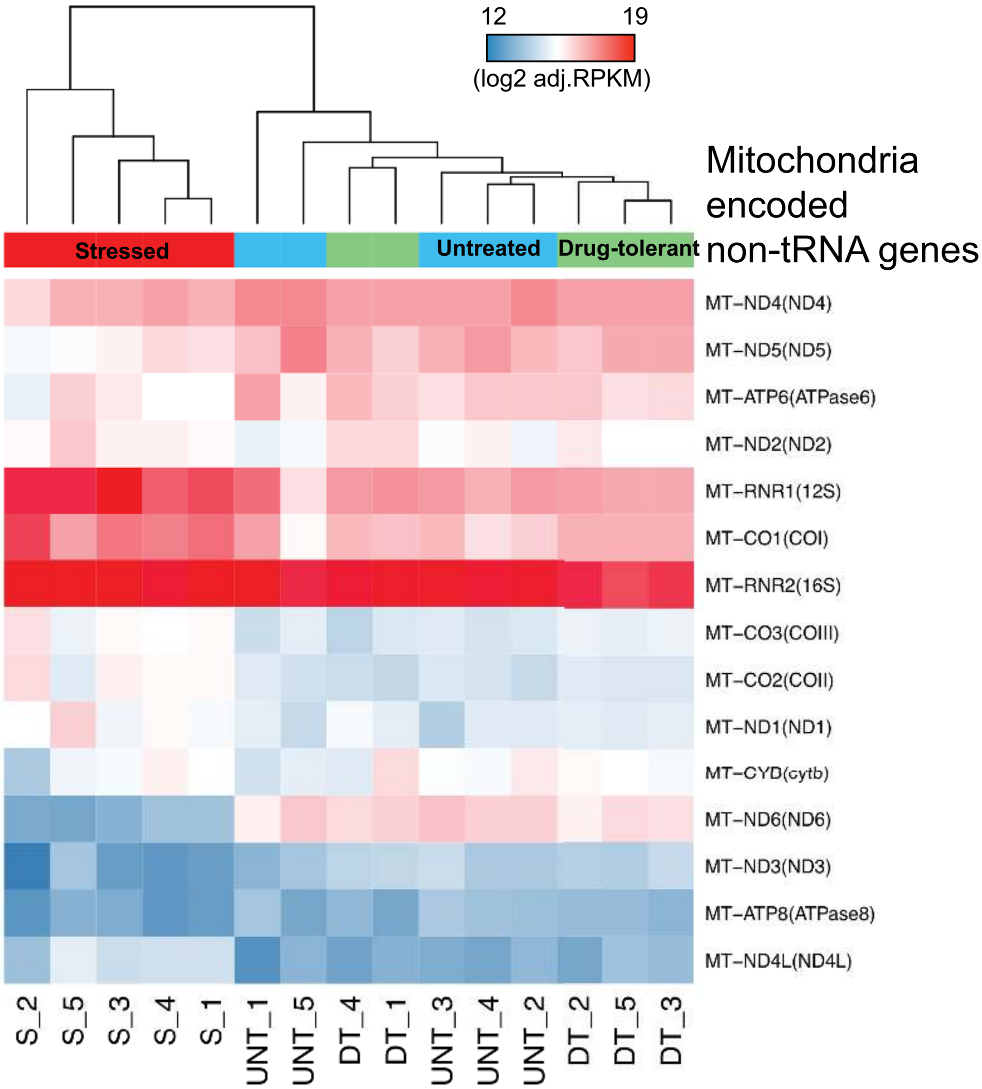

Figure 5.2: Stressed cells exhibit distinct mitochondrial expression pattern in genes encoded for proteins of the mitochondrial respiratory chain complex. Hierarchical clustering of mitochondrial mRNAs and rRNAs expression across 15 single-cells. Genes that encode for rRNAs (RNR1 and RNR2) and cytochrome c oxidase (CO1, CO2, and CO3) were up-regulated whereas ATPase (ATPase6 and ATPase8) and NADH dehydrogenases (ND3, ND4, ND5, and ND6) were down-regulated in the stressed cells compared to untreated and drug-tolerant cells.

5.2.3 SNVs in mitochondrial genes

Mutations present in genes encoding for mitochondrial proteins can potentially affect mitochondrial functions, including energy production through cellular respiration, maintenance of the proper cellular calcium ions concentration, and regulation of intrinsic apoptosis. Three different missense mutations were detected in the *RTN4* gene in three different drug-tolerant cells. RTN4 protein was previously shown to sequester the anti-apoptotic proteins BCL2 and BCL-x_L in the endoplasmic reticulum and prevent them from entering mitochondria [101]. The missense mutations in RTN can potentially alter its binding affinity for BCL2 and BCL-xL, and increase the concentration of the anti-apoptotic proteins in the mitochondria. With the down-regulation of pro-apoptotic genes, it is possible that the shift in balance of pro-apoptotic proteins and anti-apoptotic proteins is the cellular mechanism for drug-tolerance (Fig. 5.4).

5.2.4 Recapitulate the drug-tolerant phenotype by manipulating the expression level of BNIP3L

The genes that encode for the pro-apoptotic proteins BNIP3L was found down-regulated significantly in the drug-tolerant single cells compared to untreated and stressed cells, which were discussed in Section 5.2.2. To further understand the role of BNIP3L protein in the drug-tolerant experimental scheme, I designed and performed a knockdown experiment of this pro-apoptotic gene. I speculated that if *BNIP3L* was not expressed, then the pro-apoptotic effect in the cell would decrease and fewer Paclitaxel-

Gene	Up-regulated	Down-regulated	$\log_2$FoldΔ	Function	Ref.
BNIP3L	Untreated	Drug-tolerant	3.3	A pro-apoptotic protein	[63]
BCL2L1	Untreated	Drug-tolerant	3.8	It has both pro-survival, Bcl-X_L, and pro-apoptotic, Bcl-X_S, gene products through alternative splicing	[116]
C1QBP	Drug-tolerant	Untreated	1.5	Promotes cell proliferation, migration and resistance to cell death	[64]
TMABADH (ALDH9A1)	Drug-tolerant	Untreated	2.3	Aldehyde dehydrogenase family of proteins. ALDH-positive breast cancer cells are resistant to Paclitaxel	[54]
MRPS27	Drug-tolerant	Untreated	4.7	It encodes a 28S subunit protein that may be a functional partner of the death associated protein 3 (DAP3 - a positive mediator of cell death)	[103]

Table 5.1: Nuclear-encoded mitochondrial genes involved in cell death and were significantly differentially expressed when compared between untreated and drug-tolerant single-cells.

treated cells would undergo Paclitaxel-induced apoptosis. Knockdown of Bnip3L gene appeared to enhance the cell survival against Paclitaxel killing from three independent knockdown experiments (Fig. 5.3).

5.2.5 Heteroplasmic mitochondrial variants

Heteroplasmic mitochondrial mutations (present in only a fraction of the mitochondrial DNA) are often disease related and have been associated with tumor activity and cancer progression [12, 42]. I examined the extent of heteroplasmic variants present at the single-cell level (Fig5.5). There were heteroplasmic sites along the mitochondrial genome, but no unique heteroplamsic variant arise from Paclitaxel-induced stress.

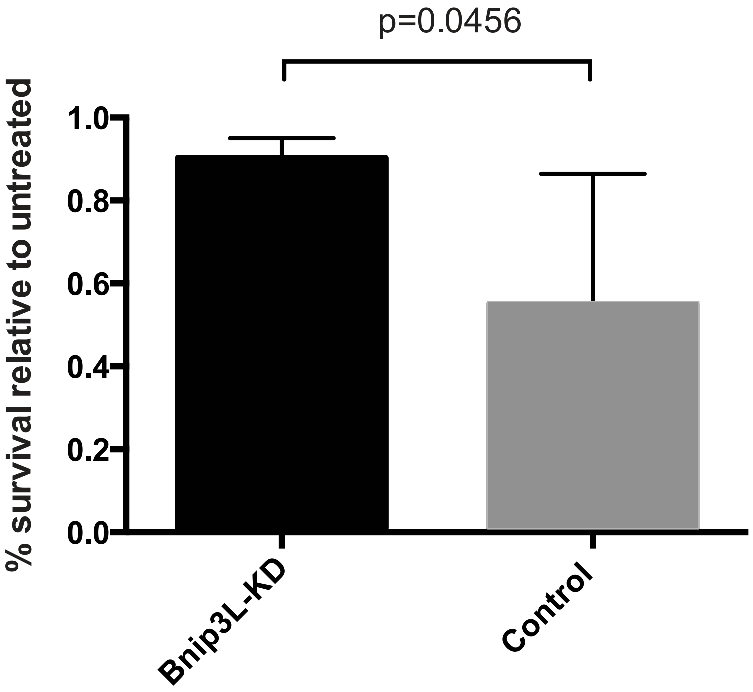

Figure 5.3: Knockdown of Bnip3L gene appeared to enhance the cell survival against Paclitaxel killing. The percent survival relative to untreated was calculated by dividing the number of viable cells of the Paclitaxel-treated samples by that of the untreated samples. Bnip3L-KD samples were cells that had been transfected with the Bnip3L RNAi plasmids using Lipofectamine. The Control samples were the negative control that had undergone the mock transfection using Lipofectamine alone, without the Bnip3L RNAi plasmids. This result was obtained from three independent knockdown experiments.

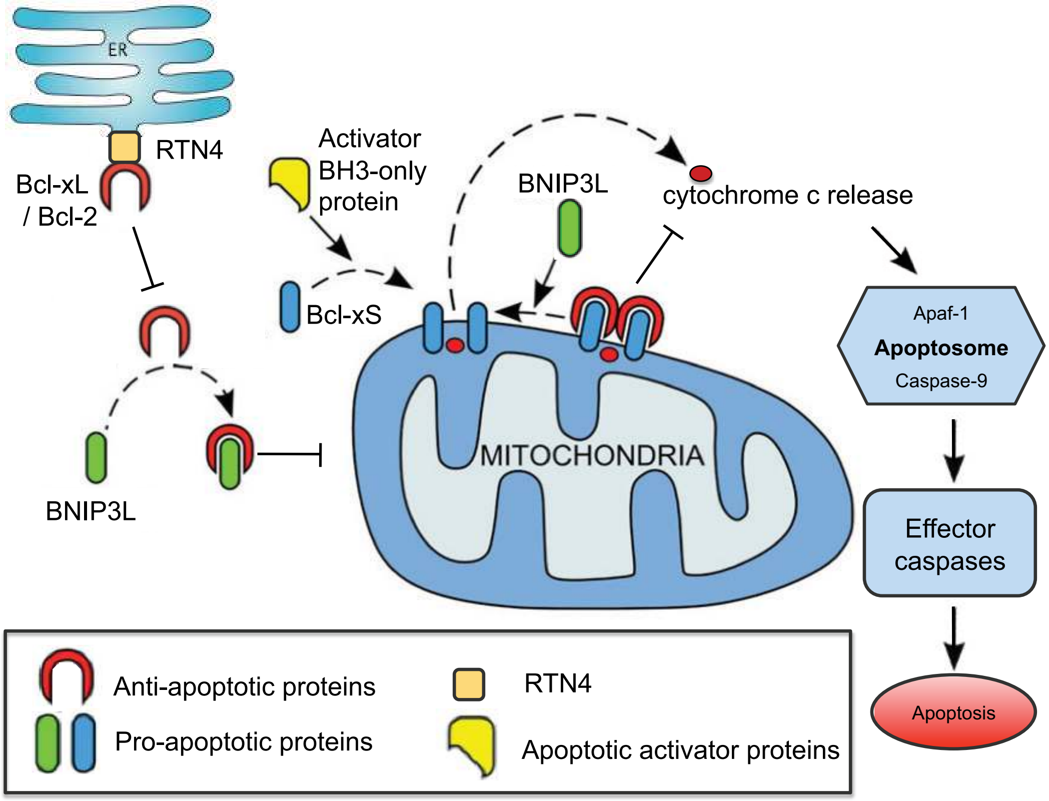

Figure 5.4: Proposed drug-tolerance mechanism. The missense mutations found in *RTN4* gene can potentially reduce the ability of RTN4 to keep the anti-apoptotic proteins, BCL-2 and BCL-x_L, in the endoplasmic reticulum (ER), and allow more anti-apoptotic proteins to localize in the mitochondria. If the pro-apoptotic protein (BNIP3L) and the apoptotic activtor (BCL-x_S) are both down-regulated in drug-tolerant cells, then it is possible that the anti-apoptotic signal will become stronger than the apoptotic signal in the mitochondria, preventing the cell from entering apoptosis.

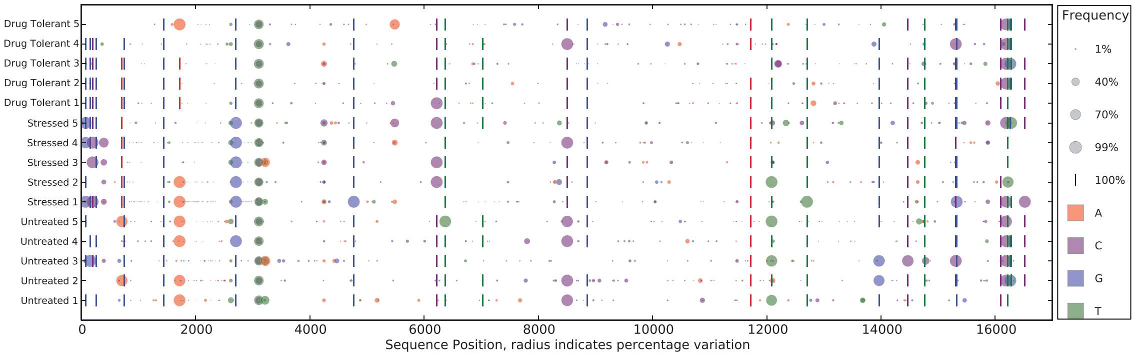

Figure 5.5: Heteroplasmic and homoplasmic variants across the mitochondrial genome at the single-cell level. The variants in each single-cell are plotted along the mitochondria genome (along the x-axis) as a circle (a heteroplasmic variant, where the bigger the circle, the higher the frequency of that variant at the locus) or a vertical line (homoplasmic variant). The color of the circle/vertical line represents the alternative base compared to the reference.

5.3 Summary

Mitochondria are not only the powerhouses of cells, they also determine if cells should live or die through the instrinsic apoptotic pathway. Paclitaxel inhibits the microtubules in achieving the metaphase spindle configuration, and ultimately, activates the intrinsic apoptotic signal by prolonging the activation of mitotic checkpoint. From the single-cell RNA-Seq data in this study, I observed that stressed cells had elevated gene expression for 12S and 16S ribosomal RNAs and cytochrome c oxidase while NADH dehydrogenase and ATPase were down-regulated compared to untreated and drug-tolerant cells. Paclitaxel-induced stress did not appear to alter the level of tRNA transcript production and the frequency of heteroplasmy. I have discovered three different nonsense mutations in the gene encoding the RTN4 protein in three different drug-tolerant cells that are not present in untreated or stressed cells.

RTN4 is known to sequester anti-apoptotic proteins, BCL2 and BCL-x$_L$, in the endoplasmic reticulum, hence, reduces the anti-apoptotic components in the mitochondria. Mutations in RTN4 could affect the binding affinity between RTN4 and anti-apoptotic proteins, BCL2 and BCL-x$_L$. In addition, two genes involved in the intrinsic apoptotic pathways were down-regulated in the drug-tolerant cells compared to the untreated cells: *BNIP3L* and *BCL2L1*. Aberrant and down-regulation of the pro-apoptotic genes can affect the balance of the pro- and anti-apoptotic proteins and allow cells to escape from apoptosis.

Chapter 6

Discussion

It has become technically and economically feasible to sequence RNA from single-cells, which enables highly sensitive detection of rare single-nucleotide variants (SNVs). Such technologies will be critical for examining individual cells from tissue biopsies of heterogenous cell populations. Although not all rare variants are relevant to personalized cancer treatment, some have the potential to drive drug resistance or serve as biomarkers of therapeutic success. Thus, the ability to detect rare SNVs and specific gene expression profiles distinguishing drug-terminally-arrested versus drug-tolerant single-cells at the very early onset of recurrence offers extremely valuable information as this may potentially provide diagnostic/prognostic value to assess success or failure of cancer chemotherapies shortly after administration, and guide the selection of appropriate treatments that will ultimately increase therapeutic efficacy.

Here, by using a single-cell RNA sequencing approach, I interrogated both the single-nucleotide variants and the expression levels present at very early onset of the evolution of a monoclonal population of drug-tolerant cells. I demonstrated that the majority of novel RNA variants in a single-cell were unique to that cell. Most of the RNA variants shared among single cells or between cell populations were SNPs catalogued in the dbSNP database. There were more SNVs detected in stressed cells than in untreated and drug-tolerant cells. This could be the result of Paclitaxel-associated down regulation of DNA repair that was detected in the differential gene expression analysis. I identified drug-tolerant-specific RNA variants residing in genes that were involved in Paclitaxel resistance and microtubule stabilization and organization.

Although it would be more rigorous to measure SNV frequency at the DNA level, my data provides an indirect approximate estimation of the maximum effective SNV rate of cancer cells from individual cells at the RNA level. Furthermore, the cell-specific SNV frequencies I found in the previously published single-cell RNA-Seq datasets by Ramsköld *et al.* [79] and Yan *et al.* [121] were very similar to ours and among themselves, regardless whether the cells were normal or cancerous, and despite the different protocols used in each study. This suggests that our single-cell RNA-Sequencing appears to show equivalent base call fidelity to those previously published.

Classifying cells using gene expression data could be valuable in predicting the clinical significance of residual cancer cells after chemotherapy. In this study, I was able to apply Principal Component Analysis (PCA) and hierarchical clustering analysis to the gene expression data to differentiate the distinct gene expression profiles of stressed cells from that of untreated and drug-tolerant cells. Drug-tolerant cells presented gene expression profiles more similar to untreated cells than to long-term stressed cells. These drug-tolerant cells could be either cells that became stressed and then resolved the stress, or cells that had been in a pre-existing condition and were never engaged in a stress response. Some SNVs in the drug-tolerant cells reside in genes related to tubulin metabolism, showing a cellular memory of the damage previously encountered. This would suggest that these cells have been stressed, but obviously they enacted a rare program that ensured survival. Drug-tolerant cells might originate from stressed cells. I identified SNVs in different subset of drug-tolerant cells that reside in genes associated to a wide variety of molecular functions, including DNA binding, enzymatic regulator activity, transcription factor activity, receptor activity, structural molecule activity, transporter activity, intrinsic apoptosis, microtubule stability and organization, and regulation of cell growth 3.2. I speculate that a single molecular mechanism for drug tolerance might not be needed since the diversity will ensure at any time that a given cancer cell containing the right gene expression and/or RNA variant will be able to evade killing by cytotoxic agents.

Paclitaxel acts on cells by stabilizing the microtubules that leads to a mitotic arrest in the late G2/M-phase of the cell cycle. Prolonged mitotic arrest will trigger the activation of intrinsic apoptosis, which is regulated by the mitochondria. Interestingly, I identified differentially expressed genes involved in the intrinsic apoptotic pathway between untreated and drug-tolerant cells. Two of these genes, *BNIP3L* and BCL2L1, encode for pro-apoptotic proteins that have not been previously implicated in Paclitaxel resistance in cells under normal physiological oxygenation condition. The gene knockdown experiment in this study showed that the downregulation of *BNIP3L* appeared to enhance the survival rate of the Paclitaxel-treated cells.

RTN4 is another protein that controls the concentration and the balance of pro- and anti-apoptotic proteins in the mitochondria, which is known to interact with the pro-apoptotic proteins BCL-2 and BCL-x$_L$ in the endoplasmic reticulum, preventing them from entering the mitochondria to enhance cell survival. Interestingly, three different missense mutations were found in the gene *RTN4* in three different drug-tolerant single-cells but not in any untreated or stressed cell. These missense mutations can potentially affect the binding affinity between RTN4 and BCL-2 and/or BCL-x$_L$ and promote anti-apoptotic responses in the cell. Further studies will be needed to confirm the localization of BCL-2 and BCL-x$_L$ in cells with these mutations in *RTN4*.

Drug-resistance can be a result of aberrant gene expression or genetic mutations, but the phosphorylation states of proteins also play an important role in regulating the intrinsic apoptosis. One of the major pro-apoptotic proteins in the intrinsic apoptotic pathway is the Bcl-2-associated death promoter (BAD), which inactivates anti-apoptotic proteins BCL-2 and BCL-x$_L$ when it is in its dephosphorylated form [125]. In this study, the Insulin-like growth factor receptor (IGF1R) is upregulated in the drug-tolerant cells. IGF1R can activate phosphatidylinositol 3-kinase (PI3K) signaling cascade, and ultimately, inactivates BAD by phosphorylating it [32]. The inactivation of BAD will lead to the activation of anti-apoptotic proteins BCL-2 and BCL-x$_L$, which can promote cell survival. In another study, Sharma *et al.* found that activation IGF1R signaling, together with the histone demethylase KDM5A activity, can alter the chromatin state in a subpopulation of cells, and provides those cells with a reversible Paclitaxel resistance capability [90].

In sum, drug-tolerant mechanisms can arise from genetic, transcriptomic, and epigenetic alterations. Figure 6.1 provides a summary of the genes I have identified, from the single-cell RNA-Seq data in this study, that are involved in various drug-tolerance mechanisms. I believe that many of the drug-tolerant mechanisms can also be identified using population RNA-Seq data (but I cannot be sure since I did not have biological replicates for most of the population RNA-Seq data due to the experimental resource constraints). But what makes single-cell RNA-Seq unique and worthwhile, is that it allows us to detect cell-to-cell transcript heterogeneity at the single-nucleotide level, and it can also identify gene expression heterogeneity among single cells.

Analyzing cell populations only generates an averaged gene expression level in all cells. Interestingly, Marinov and colleagues have recently reported the stochastic gene expression heterogeneity found between single cells. They were able to reconstitute the averaged gene expression given by an entire population of cells by pooling the single-cell RNA sequencing results from 30 to 100 single cells [62]. In this study, the 5-cell-pooled samples did cluster closer to their corresponding populations compared to single-cells. The data in this study suggest that pooling five cells from the same biological conditions is not sufficient to accurately reconstitute the averaged expression of the populations.

Here I demonstrated that single-cell gene expression profiles differ from profiles of their corresponding populations in significant and illuminating ways. Single-cell RNA-Seq allows one to study gene expression and single-nucleotide variants at a higher resolution which can help identify genes that are not yet implicated in cancer, cancer treatment, or other disease states.

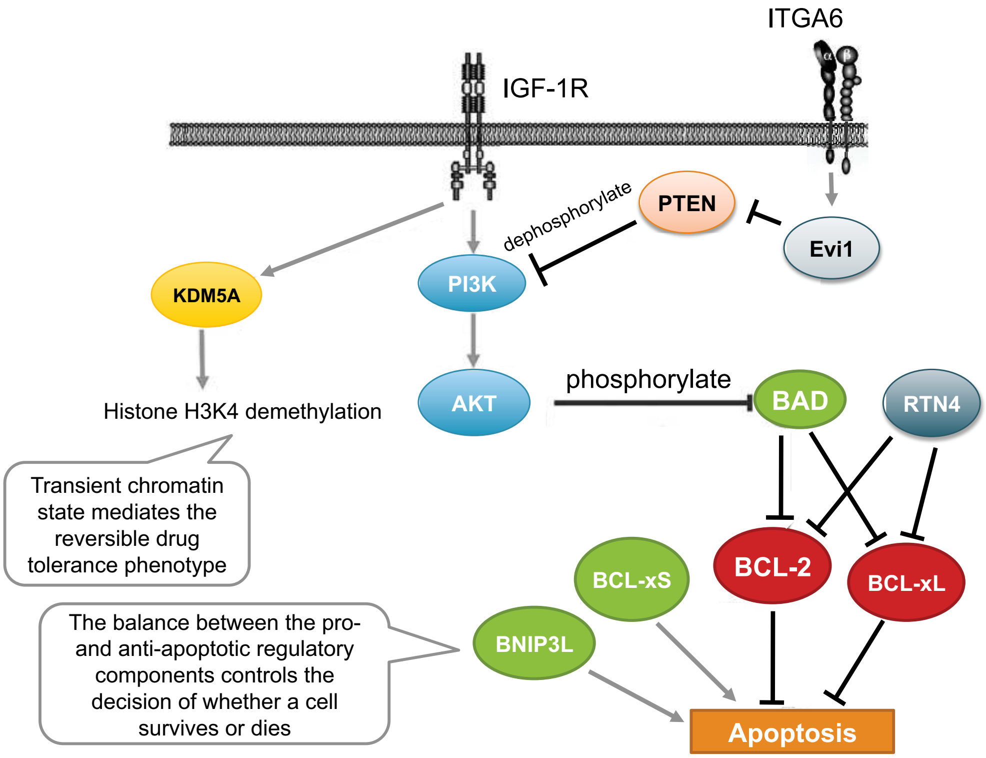
ITGA6
IGF-1R
PTEN
dephosphorylate
Evi1
KDM5A
PI3K
AKT
phosphorylate
BAD
RTN4
Histone H3K4 demethylation
Transient chromatin state mediates the reversible drug tolerance phenotype
BCL-xS
BCL-2
BCL-xL
BNIP3L
The balance between the pro- and anti-apoptotic regulatory components controls the decision of whether a cell survives or dies
Apoptosis

Figure 6.1: Multiple drug-tolerance mechanisms regulated by the genes that were identified in this study. IGF-1R was found to be up-regulated the drug-tolerant cells. Upon activation of IGF-1R, it phosphorylates and activates phosphoinositol-3-kinase (PI3K). Phosphorylated PI3K, in turn, phosphorylates and activates protein kinase B, also known as AKT. The activated AKT can then phosphorylate and inhibit pro-apoptotic protein BAD from binding to anti-apoptotic proteins BCL-2 and BCL-x$_L$. BAD inhibits the anti-apoptotic proteins only when it is in its non-phosphorylated form. RTN4, also known as Reticulon 4, has been shown to interact with BCL-2 and BCL-x$_L$ and reduces their anti-apoptotic activities by keeping them in the endoplasmic reticulum. Pro-apoptotic genes, BNIP3L and BCL-x$_S$, were both down-regulated in the drug-tolerant cells. IGF1R signaling and the histone demethylase KDM5A activity, together, alter the chromatin state and provide cells with a reversible Paclitaxel resistance capability. Another gene that was found to be up-regulated in the drug-tolerant cells is Integrin alpha-6 (ITGA6). Increased expression of ITGA6, together with a high expression level of Evi1, is known to enhance Paclitaxel resistance. Evi1 activates the PI3K pathway by repressing PTEN expression (PTEN expression was not detected in any single-cell or population in this study). PTEN suppresses PI3K activity by dephosphorylating PIP3, an important signaling component of the PI3K.

Appendix A

RNA-Seq read mapping statistics for single-cells and bulk-cells

Samples	Total number of paired-end reads sequenced	Total number of properly paired mapped-reads without PCR duplicates
UNT_1	72,398,342	42,429,918
UNT_2	97,896,104	69,651,740
UNT_3	32,434,019	25,731,672
UNT_4	86,764,133	62,280,876
UNT_5	55,056,490	22,804,666
UNT_Pop	94,393,218	80,834,490
S_1	93,752,892	89,363,318
S_2	77,374,749	59,347,478
S_3	57,117,251	27,832,072
S_4	76,309,928	56,447,554
S_5	63,019,868	46,954,348
S_Pop	89,785,654	73,548,017
DT_1	94,547,328	47,021,098
DT_2	86,555,396	46,399,478
DT_3	69,507,808	43,944,268
DT_4	86,185,154	66,641,812
DT_5	105,928,132	61,132,450
DT_Pop1	110,801,220	85,512,326
DT_Pop2	106,855,138	70,235,819

Table A.1: Number of sequencing reads and mapping statistics. This table shows the total number of paired-end reads that were sequenced for each single-cell and bulk-cells, as well as the total number of mapped reads that both paired-end reads are properly paired after removing PCR duplicates. We generated similar number of sequencing reads for individual single-cells and each cell population. Pop: population, UNT: untreated, S: stressed, DT: drug-tolerant.

	Samples	**% Genomic coverage**
Single cells	UNT_1	6.5%
	UNT_2	7.1%
	UNT_3	2.3%
	UNT_4	6.5%
	UNT_5	11.0%
	S_1	20.9%
	S_2	14.2%
	S_3	12.1%
	S_4	5.1%
	S_5	5.1%
	DT_1	9.9%
	DT_2	6.1%
	DT_3	3.9%
	DT_4	5.5%
	DT_5	5.8%
Population	UNT_Pop	49.5%
	S_Pop	48.2%
	DT_Pop_1	36.7%
	DT_Pop_2	41.9%

Table A.2: RNA sequencing reads of the population cells cover more genomic region than that of single cells. For each sample, the percent genomic coverage is calculated by dividing the total number of transcriptomic-bases with at least 1x read coverage by the total number of transcriptomic bases.

Samples	**Number of genes with RPKM>1**	**% detected genes compared to population**	**Number of genes with adj-RPKM>1**	**% detected genes compared to population**
UNT_1	2484	20%	2212	17%
UNT_2	2431	19%	2172	17%
UNT_3	1266	10%	959	7%
UNT_4	2288	18%	2040	16%
UNT_5	3635	29%	3070	24%
UNT_Pooled_5cells	8175	65%	10146	79%
UNT_Pop	12541	-	12854	-
S_1	4442	32%	4565	38%
S_2	3992	29%	3835	32%
S_3	3869	28%	3383	28%
S_4	2011	15%	1665	14%
S_5	1909	14%	1644	14%
S_Pooled_5cells	10209	74%	12855	107%
S_Pop	13796	-	12007	-
DT_1	3261	24%	2927	25%
DT_2	2641	20%	2137	18%
DT_3	2091	15%	1564	13%
DT_4	2247	17%	1902	16%
DT_5	2310	17%	1879	16%
DT_Pooled_5cell	8175	60%	9760	82%
DT_Pop_1	12443	-	11981	-
DT_Pop_2	14609	-	11795	-

Table A.3: Number of genes with RPKM>1 and adjRPKM>1 in single cells and population cells. Pop: population, UNT: untreated, S: stressed, DT: drug-tolerant.

Cell Type	All SNVs in population passed all filters	Single-cell ID	All SNVs in single-cell passed all filters	Comparable SNVs in single-cell	Comparable SNVs in population	Novel SNVs only in single-cell	Novel SNVs only in population	Novel SNVs in both single-cell and population	dbSNP variants only in single-cell	dbSNP variants only in population	dbSNP variants in both single-cell and population
Untreated	63578	1	6284	2109	2411	1356	470	760	28	93	663
		2	8382	3097	2809	2270	516	834	36	104	715
		3	2267	784	451	644	107	142	15	17	116
		4	7595	2257	2155	1602	402	658	35	108	566
		5	4000	2292	2919	1292	545	1003	33	144	877
Stressed	35227	1	13756	5278	5439	3211	824	2071	59	309	1897
		2	8886	4832	2967	3641	392	1196	34	127	1086
		3	6152	2902	2000	2217	336	687	23	142	623
		4	4342	1850	1025	1464	152	392	31	58	351
		5	5748	2873	1021	2442	139	435	30	42	390
Drug-tolerant	11857	1	8100	2112	1913	1343	363	773	31	98	683
		2	3684	1280	1248	780	251	503	14	63	442
		3	2688	965	728	677	137	289	11	28	251
		4	6933	1630	977	1233	186	401	18	43	349
		5	4315	1336	955	992	199	348	11	50	305

Table A.4: The number of common and unique SNVs detected in single-cells and population in three different groups. Related to Fig. 3.2. Comparable SNVs are the variants located in genomic regions where there is at least 10× RNA read coverage in both the single-cell and the population. SNVs variants in single-cell and/or in population are parts of the comparable SNVs. SNVs consist of novel and dbSNP variants.

Appendix B

Additional Methods and Materials

B.1 Single-cell cDNA synthesis

Total RNA of cell lysate was reverse-transcribed to first-strand cDNA using a combination of random hexamers and poly-T chimeric primers and then converted to double-stranded (ds) DNA using fragmentation and RNA-dependent DNA polymerase. Finally, the ds cDNA was amplified linearly using a SPIA process and purified by using MyOne$^{\text{TM}}$ carboxilic acid-coated superparamagnetic beads (Invitrogen, Carlsbad, CA). The cDNA was prepared for fifteen individual single-cells for library preparation. The quality and quantity of single-cell cDNA were evaluated using the Agilent Bioanalyzer 2100 DNA High Sensitivity chip (Agilent, Palo Alto).

B.2 RNA-Seq library preparation and sequencing

For paired-end whole transcriptome library preparation, $\sim$0.5-1.0 μg cDNA of each sample was sheared to a size ranging between 200-300 bp using the Covaris-S2 sonicator (Covaris, Woburn, MA) according to the manufacturer's recommended protocols. Fragmented cDNA samples were used for the preparation of RNA-Seq libraries using TruSeq v1 Multiplex Sample Preparation kit (Illumina, San Diego, CA). Briefly, cDNA fragments were end-repaired, dA-tailed and ligated to multiplex adapters according to manufacturer's instructions. After ligation, DNA fragments smaller than 150 bp were removed with AmPure XP beads (Beckman Coulter Genomics, Danvers, MA). The purified adapter ligated products were enriched using polymerase chain reaction (14 cycles). The final amplified libraries were resolved on 2.0% agarose gel and manually size-selected in the range of 350-380 bp. The final RNA-Seq libraries were quantitated using the Agilent bioanalyzer 2100 and pooled together in equal concentration for sequencing. The pooled multiplexed libraries of single-cells were sequenced in four independent sequencing runs, with eight flow cell lanes per run which generated 2×50 bp paired-end reads on HiSeq 2000 (Illumina, Inc; San Diego, CA). On the same sequencing platform, population RNA-Seq was performed in two flow cell lanes in one run, generating 2×100 bp paired-end reads. Due the timing and the cost of sequencing, the sequencing read-length generated for single-cells and population are not the same. However, since both single-cell and population sequencing generated paired-end reads, the read-length difference should have a minimal impact on the read alignment accuracy.

B.3 Whole genome DNA sequencing of naïve MDA-MB-231 cells

For high-throughput sequencing, high-molecular weight genomic DNA (gDNA) was obtained from MDA-MB-231 cells (Princeton PSOC). For the DNA library prep, 1μg of gDNA was first sheared down to 200-300 bp using the Covaris S2 (Woburn, Massachusetts) per manufacture recommendations. A target insert size of 200-250 bp was then size-selected using the automated electrophoretic DNA fractionation system, known as LabChip XT (Caliper Life Sciences, Hopkinton, Massachusetts). Paired-end sequencing libraries were prepared using Illumina's TruSeq DNA Sample Preparation Kit (San Diego, CA). Following DNA library construction, samples were quantified using the Agilent Bioanalyzer per manufacturer's protocol (Santa Clara, CA). DNA libraries were sequenced using the Illumina HiSeq 2000 in two flow cell lanes with sequencing paired-end read lengths of 2×100 bp. Reads were de-multiplexed using CASAVA (version 1.8.2).

Bibliography

[1] J. D. Adams, K. P. Flora, B. R. Goldspiel, J. W. Wilson, S. G. Arbuck, and R. Finley. Taxol: a history of pharmaceutical development and current pharmaceutical concerns. *J Natl Cancer Inst Monogr*, (15):141–7, Jan 1993.

[2] W. Aerbajinai, M. Giattina, Y. T. Lee, M. Raffeld, and J. L. Miller. The proapoptotic factor Nix is coexpressed with Bcl-xL during terminal erythroid differentiation. *Blood*, 102(2):712–7, Mar 2003.

[3] A. A. Ahmed, X. Wang, Z. Lu, J. Goldsmith, X. F. Le, G. Grandjean, G. Bartholomeusz, B. Broo m, and Jr. Bast, R. C. Modulating microtubule stability enhances the cytotoxic response of cancer cells to Paclitaxel. *Cancer Res*, 71(17):5806–17, Sep 2011.

[4] G. M. Ajabnoor, T. Crook, and H. M. Coley. Paclitaxel resistance is associated with switch from apoptotic to autophagic cell death in MCF-7 breast cancer cells. *Cell Death Dis*, 3:e260, Jan 2012.

[5] V. Almendro, A. Marusyk, and K. Polyak. Cellular heterogeneity and molecular evolution in cancer. *Annu Rev Pathol*, 8:277–302, Jan 2013.

[6] J. H. Bahn, J. H. Lee, G. Li, C. Greer, G. Peng, and X. Xiao. Accurate identification of A-to-I RNA editing in human by transcriptome sequencing. *Genome Res*, 22(1):142–50, Jan 2012.

[7] J. A. Bauer, F. Ye, C. B. Marshall, B. D. Lehmann, C. S. Pendleton, Y. Shyr, and J. A. Arteaga, C. L. a nd Pietenpol. RNA interference (RNAi) screening approach identifies agents that enhance paclitaxel activity in breast cancer cells. *Breast Cancer Res*, 12(3):R41, Jun 2010.

[8] V. Bhargava, S. R. Head, P. Ordoukhanian, M. Mercola, and S. Subramaniam. Technical variations in low-input RNA-seq methodologies. *Sci Rep*, 4:3678, Jan 2014.

[9] J. F. Bishop, J. Dewar, G. C. Toner, J. Smith, M. H. Tattersall, I. N. Olver, S. Ackland, I. Kennedy, D. Goldstein, H. Gurney, E. Walpole, J. Levi, J. Stephenson, and

R. Canetta. Initial paclitaxel improves outcome compared with CMFP combination chemotherapy as front-line therapy in untreated metastatic breast cancer. *J Clin Oncol*, 17(8):2355–64, Aug 1999.

[10] C. Bock and T. Lengauer. Managing drug resistance in cancer: lessons from hiv therapy. *Nat Rev Cancer*, 12(7):494–501, Jun 2012.

[11] Boengler, K. and Heusch, G. and Schulz, R. Nuclear-encoded mitochondrial proteins and their role in cardioprotection. *Biochim Biophys Acta*, 1813(7):1286–94, Jul 2011.

[12] M. Brandon, P. Baldi, and D. C. Wallace. Mitochondrial mutations in cancer. *Oncogene*, 25(34):4647–62, Aug 2006.

[13] B. R. Brinkley and T. M. Goepfert. Supernumerary centrosomes and cancer: Boveri's hypothesis resurrected. *Cell Motil Cytoskeleton*, 41(4):281–8, Dec 1998.

[14] G. M. Cann, Z. G. Gulzar, S. Cooper, R. Li, S. Luo, M. Tat, S. Stuart, G. Schroth, S. Sr inivas, M. Ronaghi, J. D. Brooks, and A. H. Talasaz. mRNA-Seq of single prostate cancer circulating tumor cells reveals recapitulation of gene expression and pathways foun d in prostate cancer. *PLoS One*, 7(11):e49144, Nov 2012.

[15] J. G. Caporaso, C. L. Lauber, W. A. Walters, D. Berg-Lyons, J. Huntley, N. Fierer, S. M. Owens, J. Betley, L. Fraser, M. Bauer, N. Gormley, J. A. Gilbert, G. Smith, and R. Knight. Ultra-high-throughput microbial community analysis on the Illumina Hiseq and Miseq platforms. *ISME J*, 6(8):1621–4, Mar 2012.

[16] S. W. Chan, C. J. Lim, Y. F. Chong, A. V. Pobbati, C. Huang, and W. Hong. Hippo pathway-independent restriction of TAZ and YAP by angiomotin. *J Biol Chem*, 286(9):7018–26, Mar 2011.

[17] A. Daemen, O. L. Griffith, L. M. Heiser, N. J. Wang, O. M. Enache, Z. Sanborn, F. Pepin, S. Durinck, J. E. Korkola, M. Griffith, J. S. Hur, N. Huh, J. Chung, L. Cope, M. J. Fackler, C. Umbricht, S. Sukumar, P. Seth, V. P. Sukhatme, L. R. Jakkula, Y. Lu, G. B. Mills, R. J. Cho, E. A. Collisson, L. J. van't Veer, P. T. Spellman, and J. W. Gray. Modeling precision treatment of breast cancer. *Genome Biol*, 14(10):R110, Oct 2013.

[18] P. Dalerba, T. Kalisky, D. Sahoo, P. S. Rajendran, M. E. Rothenberg, A. A. Leyrat, J. Sim, S. an d Okamoto, D. M. Johnston, D. Qian, M. Zabala, J. Bueno, N. F. Neff, J. Wang, A. A. Shelton, B. Visser, S. Hisamori, Y. Shimono, M. van de Wetering, H. Clevers, M. F. Clarke, and S. R. Quake. Single-cell dissection of transcriptional heterogeneity in human colon tumors. *Nat Biotechnol*, 29(12):1120–7, Nov 2011.

[19] A. Dammermann and A. Merdes. Assembly of centrosomal proteins and microtubule organization depends on PCM-1. *J Cell Biol*, 159(2):255–66, Oct 2002.

[20] N. Dephoure, C. Zhou, J. Villen, S. A. Beausoleil, C. E. Bakalarski, S. J. Elledge, and S. P. Gygi. A quantitative atlas of mitotic phosphorylation. *Proc Natl Acad Sci U S A*, 105(31):10762–7, Aug 2008.

[21] S. DiMauro and E. A. Schon. Mitochondrial respiratory-chain diseases. *N Engl J Med*, 348(26):2656–68, Jun 2003.

[22] F. Fernandez-Madrid, N. Tang, H. Alansari, J. L. Granda, L. Tait, K. C. Amirikia, M . Moroianu, X. Wang, and R. L. Karvonen. Autoantibodies to Annexin XI-A and Other Autoantigens in the Diagnosis of Breast Cancer. *Cancer Res*, 64(15):5089–96, Aug 2004.

[23] M. L. Flores, C. Castilla, R. Avila, M. Ruiz-Borrego, C. Saez, and M. A. Japon. Paclitaxel sensitivity of breast cancer cells requires efficient mitotic arrest and disruption of Bcl-xl/Bak interaction. *Breast Cancer Res Treat*, 133(3):917–28, Jun 2012.

[24] C. Friesen, A. Lubatschofski, G. Glatting, K. M. Debatin, and S. N. Reske. Activation of intrinsic apoptotic pathway by re-188 irradiation and paclitaxel in coronary artery smooth muscle cells. *Q J Nucl Med Mol Imaging*, 52(3):289–95, Sep 2008.

[25] X. Ge, C. L. Frank, F. Calderon de Anda, and L. H. Tsai. Hook3 interacts with PCM1 to regulate pericentriolar material assembly and the timing of neurogenesis. *Neuron*, 65(2):191–203, 2010.

[26] Consortium Genomes Project, G. R. Abecasis, D. Altshuler, A. Auton, L. D. Brooks, R. A. Durbin, R. M. a nd Gibbs, M. E. Hurles, and G. A. McVean. A map of human genome variation from population-scale sequencing. *Nature*, 467(7319):1061–73, Oct 2010.

[27] M. Gerlinger, A. J. Rowan, S. Horswell, J. Larkin, D. Endesfelder, E. Gronroos, P. Martinez, N. Matthews, A. Stewart, P. Tarpey, I. Varela, B. Phillimore, S. Begum, N. Q. McDonald, A. Butler, D. Jones, K. Raine, C. Latimer, C. R. Santos, M. Nohadani, A. C. Eklund, B. Spencer-Dene, G. Cla rk, L. Pickering, G. Stamp, M. Gore, Z. Szallasi, J. Downward, P. A. Futreal, and C. Swanton. Intratumor heterogeneity and branched evolution revealed by multiregion sequencing. *N Engl J Med*, 366(10), Mar 2012.

[28] M. M. Gottesman. Mechanisms of cancer drug resistance. *Annu Rev Med*, 53:615–27, Jan 2002.

[29] R. V. Grindberg, J. L. Yee-Greenbaum, M. J. McConnell, M. Novotny, A. L. O'Shaughnessy, G. M. Lambert, M. J. Arauzo-Bravo, J. Lee, M. Fishman, G. E. Robbins, X. Lin, P. Venepally, J. H. Badger, D. W. Galbraith, F. H. Gage, and R. S. Lasken. Rna-sequencing from single nuclei. *Proc Natl Acad Sci U S A*, 110(49):19802–7, Dec 2013.

[30] T. Gu, F. W. Buaas, A. K. Simons, C. L. Ackert-Bicknell, R. E. Braun, and M. A. Hibbs. Canonical A-to-I and C-to-U RNA editing is enriched at 3'UTRs and microRNA target sites in multiple mouse tissues. *PLoS One*, 7(3):e33720, Mar 2012.

[31] Guo, Y. and Li, J. and Li, C. I. and Long, J. and Samuels, D. C. and Shyr, Y. The effect of strand bias in Illumina short-read sequencing data. *BMC Genomics*, 13:666, Nov 2012.

[32] H. Harada, J. S. Andersen, M. Mann, N. Terada, and S. J. Korsmeyer. p70s6 kinase signals cell survival as well as growth, inactivating the pro-apoptotic molecule BAD. *Proc Natl Acad Sci U S A*, 98(17):9666–70, Aug 2001.

[33] T. Hashimshony, F. Wagner, N. Sher, and I. Yanai. CEL-Seq: single-cell RNA-Seq by multiplexed linear amplification. *Cell Rep*, 2(3):666–73, Sep 2012.

[34] K. Hishikawa, B. S. Oemar, F. C. Tanner, T. Nakaki, T. F. Luscher, and T. Fujii. Connective tissue growth factor induces apoptosis in human breast cancer cell line MCF-7. *J Biol Chem*, 274(52):37461–6, Dec 1999.

[35] S. Islam, U. Kjallquist, A. Moliner, P. Zajac, J. B. Fan, P. Lonnerberg, and S. Linnarsson. Characterization of the single-cell transcriptional landscape by highly multiplex RNA-seq. *Genome Res*, 21(7):1160–7, Jul 2011.

[36] S. Islam, A. Zeisel, S. Joost, G. La Manno, P. Zajac, M. Kasper, P. Lonnerberg, and S. Linnarsson. Quantitative single-cell RNA-seq with unique molecular identifiers. *Nat Methods*, 11(2):163–6, Feb 2014.

[37] Z. Kan, B. S. Jaiswal, J. Stinson, V. Janakiraman, D. Bhatt, H. M. Stern, P. Yue, P. M. Haverty, R. Bourgon, J. Zheng, M. Moorhead, S. Chaudhuri, L. P. Tomsho, B. A. Peters, K. Pujara, S. Cordes, D. P. Davis, V. E. Carlton, W. Yuan, L. Li, W. Wang, C. Eigenbrot, J. S. Kaminker, D. A. Eb erhard, P. Waring, S. C. Schuster, Z. Modrusan, Z. Zhang, D. Stokoe, F. J. de Sauvage, M. Faham, and S. Seshagiri. Diverse somatic mutation patterns and pathway alterations in human cancers. *Nature*, 466(7308):869–73, Aug 2010.

[38] D. Karolchik, A. S. Hinrichs, T. S. Furey, K. M. Roskin, C. W. Sugnet, D. Haussler, and W. J. Kent. The UCSC Table Browser data retrieval tool. *Nucleic Acids Res*, 32(Database issue):D493–6, Jan 2004.

[39] W. J. Kent. BLAT–the BLAST-like alignment tool. *Genome Res*, 12(4):656–64, Apr 2002.

[40] W. J. Kent, C. W. Sugnet, T. S. Furey, K. M. Roskin, T. H. Pringle, A. M. Zahler, and D. Haussler. The human genome browser at UCSC. *Genome Res*, 12(6):996–1006, Jun 2002.

[41] C. L. Kleinman, V. Adoue, and J. Majewski. RNA editing of protein sequences: a rare event in human transcriptomes. *RNA*, 18(9):1586–96, Sep 2012.

[42] A. Kloss-Brandstatter, G. Schafer, G. Erhart, A. Huttenhofer, S. Coassin, C. Seifarth, M. Summerer, J. Bektic, H. Klocker, and F. Kronenberg. Somatic mutations throughout the entire mitochondrial genome are associated with elevated PSA levels in prostate cancer patients. *Am J Hum Genet*, 87(6):802–12, Dec 2010.

[43] R. Kumar, K. Chaudhary, S. Gupta, H. Singh, S. Kumar, A. Gautam, P. Kapoor, and G. P. Raghava. CancerDR: cancer drug resistance database. *Sci Rep*, 3:1445, March 2013.

[44] N. Kurn, P. Chen, J. D. Heath, A. Kopf-Sill, K. M. Stephens, and S. Wang. Novel isothermal, linear nucleic acid amplification systems for highly multiplexed applications. *Clin Chem*, 51(10):1973–81, Oct 2005.

[45] O. Kutuk and A. Letai. Alteration of the mitochondrial apoptotic pathway is key to acquired paclitaxel resistance and can be reversed by ABT-737. *Cancer Res*, 68(19):7985–94, Oct 2008.

[46] D. Lai, K. C. Ho, Y. Hao, and X. Yang. Taxol resistance in breast cancer cells is mediated by the hippo pathway component TAZ and its downstream transcriptional targets Cyr61 and CTGF. *Cancer Res*, 71(7):2728–38, Apr 2011.

[47] B. Langmead and S. L. Salzberg. Fast gapped-read alignment with Bowtie 2. *Nat Methods*, 9(4):357–9, Mar 2012.

[48] B. Langmead, C. Trapnell, M. Pop, and S. L. Salzberg. Ultrafast and memory-efficient alignment of short DNA sequences to the human genome. *Genome Biol*, 10(3):R25, Mar 2009.

[49] K. Lao, N. L. Xu, and N. A. Straus. Whole genome amplification using single-primer PCR. *Biotechnol J*, 3(3):378–82, Mar 2008.

[50] D. E. Larson, C. C. Harris, K. Chen, D. C. Koboldt, T. E. Abbott, D. J. Dooling, T. J. Ley, E. R. Mardis, R. K. Wilson, and L. Ding. SomaticSniper: identification of somatic point mutations in whole genome sequencing data. *Bioinformatics*, 28(3):311–7, Feb 2012.

[51] A. Lauri, G. Lazzari, C. Galli, I. Lagutina, E. Genzini, F. Braga, P. Mariani, and J. L. Williams. Assessment of MDA efficiency for genotyping using cloned embryo biopsies. *Genomics*, 101(1):24–9, Jan 2013.

[52] S. Le, J. Josse, and F. Husson. FactoMineR: An R package for multivariate analysis. *J Stat Softw*, 25(1):1–18, Mar 2008.

[53] H. Li, B. Handsaker, A. Wysoker, T. Fennell, J. Ruan, N. Homer, G. Marth, G. Abecasis, R. Durbin, and Subgroup Genome Project Data Processing. The Sequence Alignment/Map format and SAMtools. *Bioinformatics*, 25(16):2078–9, Aug 2009.

[54] L. Lin, B. Hutzen, H. F. Lee, Z. Peng, W. Wang, C. Zhao, H. J. Lin, D. Sun, P. K. Li, C. Li, H. Korkaya, M. S. Wicha, and J. Lin. Evaluation of STAT3 signaling in ALDH+ and ALDH+/CD44+/CD24- Subpopulations of Breast Cancer Cells. *PLoS One*, 8(12):e82821, Dec 2013.

[55] M. T. Lin, C. C. Chang, S. T. Chen, H. L. Chang, J. L. Su, Y. P. Chau, and M. L. Kuo. Cyr61 expression confers resistance to apoptosis in breast cancer MCF-7 cells by a mechanism of NF-kappaB-dependent XIAP up-regulation. *J Biol Chem*, 279(23):24015–23, Jun 2004.

[56] W. L. Lingle, W. H. Lutz, J. N. Ingle, N. J. Maihle, and J. L. Salisbury. Centrosome hypertrophy in human breast tumors: implications for genomic stability and cell polarity. *Proc Natl Acad Sci U S A*, 95(6):2950–5, Mar 1998.

[57] Y. Liu, L. Chen, T. C. Ko, A. P. Fields, and E. A. Thompson. Evi1 is a survival factor which conveys resistance to both TGFbeta- and taxol-mediated cell death via PI3K/AKT. *Oncogene*, 25(25):3565–75, Feb 2006.

[58] F. J. Livesey. Strategies for microarray analysis of limiting amounts of RNA. *Brief Funct Genomic Proteomic*, 2(1):31–6, Apr 2003.

[59] M. M. Magiera, M. Gupta, C. J. Rundell, N. Satish, I. Ernens, and S. J. Yarwood. Exchange protein directly activated by cAMP (EPAC) interacts with the light chain (LC) 2 of MAP1A. *Biochem J*, 382(Pt 3):803–10, Sep 2004.

[60] C. M. Malboeuf, X. Yang, P. Charlebois, J. Qu, A. M. Berlin, M. Casali, K. N. Pesko, C. L. Bout well, J. P. DeVincenzo, G. D. Ebel, T. M. Allen, M. C. Zody, M. R. Henn, and J. Z. Levin. Complete viral RNA genome sequencing of ultra-low copy samples by sequence-independent amplification. *Nucleic Acids Res*, 41(1):e13, Jan 2013.

[61] E. R. Mardis. A decade's perspective on DNA sequencing technology. *Nature*, 470(7333):198–203, Feb 2011.

[62] Marinov, G. K. and Williams, B. A. and McCue, K. and Schroth, G. P. and Gertz, J. and Myers, R. M. and Wold, B. J. From single-cell to cell-pool transcriptomes: stochasticity in gene expression and RNA splicing. *Genome Res*, 24(3):496–510, Mar 2014.

[63] M. Matsushima, T. Fujiwara, E. Takahashi, T. Minaguchi, Y. Eguchi, Y. Tsujimoto, K. Suzumori, and Y. Nakamura. Isolation, mapping, and functional analysis of a

novel human cDNA (BNIP3L) encoding a protein homologous to human NIP3. *Genes Chromosomes Cancer*, 21(3):230–5, Mar 1998.

[64] A. M. McGee, D. L. Douglas, Y. Liang, S. M. Hyder, and C. P. Baines. The mitochondrial protein C1qbp promotes cell proliferation, migration and resistance to cell death. *Cell Cycle*, 10(23):4119–27, Dec 2011.

[65] B. T. McGrogan, B. Gilmartin, D. N. Carney, and A. McCann. Taxanes, microtubules and chemoresistant breast cancer. *Biochim Biophys Acta*, 1785(2):96–132, Nov 2008.

[66] A. Mortazavi, B. A. Williams, K. McCue, L. Schaeffer, and B. Wold. Mapping and quantifying mammalian transcriptomes by RNA-Seq. *Nat Methods*, 5(7):621–8, Jul 2008.

[67] L. Musumeci, J. W. Arthur, F. S. Cheung, A. Hoque, S. Lippman, and J. K. Reichardt. Single nucleotide differences (SNDs) in the dbSNP database may lead to errors in genotyping and haplotyping studies. *Hum Mutat*, 31(1):67–73, Jan 2010.

[68] S. Nakayama, Y. Torikoshi, T. Takahashi, T. Yoshida, T. Sudo, T. Matsushima, Y. Kawasaki, A. Katayama, K. Gohda, G. N. Hortobagyi, S. Noguchi, T. Sakai, H. Ishihara, and N. T. Ueno. Prediction of paclitaxel sensitivity by CDK1 and CDK2 activity in human breast cancer cells. *Breast Cancer Res*, 11(1):R12, Feb 2009.

[69] S. Neph, M. S. Kuehn, A. P. Reynolds, E. Haugen, R. E. Thurman, A. K. Johnson, E. Rynes, M. T. Maurano, J. Vierstra, S. Thomas, R. Sandstrom, R. Humbert, and J. A. Stamatoyannopoulos. BEDOPS: high-performance genomic feature operations. *Bioinformatics*, 28(14):1919–20, Jul 2012.

[70] K. Nishikura. Functions and regulation of RNA editing by ADAR deaminases. *Annu Rev Biochem*, 79:321–49, Mar 2010.

[71] J. V. Olsen, M. Vermeulen, A. Santamaria, C. Kumar, M. L. Miller, L. J. Jensen, F. Gnad, J. Cox, T. S. Jensen, E. A. Nigg, S. Brunak, and M. Mann. Quantitative phosphoproteomics reveals widespread full phosphorylation site occupancy during mitosis. *Sci Signal*, 3(104):ra3, Jan 2010.

[72] D. J. Pagliarini, S. E. Calvo, B. Chang, S. A. Sheth, S. B. Vafai, S. E. Ong, G. A. Walford, C. Sugiana, A. Boneh, W. K. Chen, D. E. Hill, M. Vidal, J. G. Evans, D. R. Thorburn, S. A. Carr, and V. K. Mootha. A mitochondrial protein compendium elucidates complex I disease biology. *Cell*, 134(1):112–23, Jul 2008.

[73] E. Park, B. Williams, B. J. Wold, and A. Mortazavi. RNA editing in the human ENCODE RNA-seq data. *Genome Res*, 22(9):1626–33, Sep 2012.

[74] B. Pedrotti and K. Islam. Purified native microtubule associated protein MAP1A: kinetics of microtubule assembly and MAP1A/tubulin stoichiometry. *Biochemistry*, 33(41):12463–70, Oct 1994.

[75] Z. Peng, Y. Cheng, B. C. Tan, L. Kang, Z. Tian, Y. Zhu, W. Zhang, Y. Liang, X. Hu, X. an d Tan, J. Guo, Z. Dong, Y. Liang, L. Bao, and J. Wang. Comprehensive analysis of RNA-Seq data reveals extensive RNA editing in a human transcriptome. *Nat Biotechnol*, 30(3):253–60, Feb 2012.

[76] Quail, M. A. and Smith, M. and Coupland, P. and Otto, T. D. and Harris, S. R. and Connor, T. R. and Bertoni, A. and Swerdlow, H. P. and Gu, Y. A tale of three next generation sequencing platforms: comparison of Ion Torrent, Pacific Biosciences and Illumina MiSeq sequencers. *BMC Genomics*, 13:341, Jul 2012.

[77] A. J. Radenbaugh, S. Ma, A. Ewing, J. Stuart, E.A. Collisson, J. Zhu, and D. Haussler. RADIA: RNA and DNA Integrated Analysis for Somatic Mutation Detection. *PLoS One*, Nov 2014. (Accepted: Oct 2014).

[78] G. Ramaswami, R. Zhang, R. Piskol, L. P. Keegan, P. Deng, M. A. O'Connell, and J. B. Li. Identifying RNA editing sites using RNA sequencing data alone. *Nat Methods*, 10(2):128–32, Jan 2013.

[79] D. Ramskold, S. Luo, Y. C. Wang, R. Li, Q. Deng, O. R. Faridani, G. A. Daniels, I. Khrebtuko va, J. F. Loring, L. C. Laurent, G. P. Schroth, and R. Sandberg. Full-length mRNA-Seq from single-cell levels of RNA and individual circulating tumor cells. *Nat Biotechnol*, 30(8):777–82, Aug 2012.

[80] E. Ruiz-Pesini, M. T. Lott, V. Procaccio, J. C. Poole, M. C. Brandon, D. Mishmar, C. Yi, J. Kreuziger, P. Baldi, and D. C. Wallace. An enhanced MITOMAP with a global mtDNA mutational phylogeny. *Nucleic Acids Res*, 35(Database issue):D823–8, Jan 2007.

[81] R. K. Saiki, S. Scharf, F. Faloona, K. B. Mullis, G. T. Horn, H. A. Erlich, and N. Arnheim. Enzymatic amplification of beta-globin genomic sequences and restriction site analysis for diagnosis of sickle cell anemia. *Science*, 230(4732):1350–4, Dec 1985.

[82] Saliba, A. E. and Westermann, A. J. and Gorski, S. A. and Vogel, J. Single-cell RNA-seq: advances and future challenges. *Nucleic Acids Res*, 42(14):8845–60, Jul 2014.

[83] N. Samadi, C. Gaetano, I. S. Goping, and D. N. Brindley. Autotaxin protects MCF-7 breast cancer and MDA-MB-435 melanoma cells against taxol-induced apoptosis. *Oncogene*, 28(7):1028–39, Dec 2009.

[84] J. Z. Sanborn. Tumor versus Matched-Normal Sequencing Analysis and Data Integration, 2012. PhD dissertation (California Digital Library, Santa Cruz, CA).

[85] Y. Sasagawa, I. Nikaido, T. Hayashi, H. Danno, K. D. Uno, T. Imai, and H. R. Ueda. Quartz-Seq: a highly reproducible and sensitive single-cell RNA sequencing method, reveals non-genetic gene-expression heterogeneity. *Genome Biol*, 14(4):R31, 2013.

[86] N. A. Saunders, F. Simpson, E. W. Thompson, M. M. Hill, L. Endo-Munoz, G. Leggatt, R . F. Minchin, and A. Guminski. Role of intratumoural heterogeneity in cancer drug resistance: molecular and clinical perspectives. *EMBO Mol Med*, 4(8):675–84, Aug 2012.

[87] Roberto Scatena, Patrizia Bottoni, and Bruno Giardina. *Advances in Mitochondrial Medicine*, volume 942 of *Advances in Experimental Medicine and Biology*. Springer, 2012.

[88] S. Sehrawat, X. Cullere, S. Patel, Jr. Italiano, J., and T. N. Mayadas. Role of Epac1, an exchange factor for Rap GTPases, in endothelial microtubule dynamics and barrier function. *Mol Biol Cell*, 19(3):1261–70, Mar 2008.

[89] A. K. Shalek, R. Satija, X. Adiconis, R. S. Gertner, J. T. Gaublomme, R. Raychowdhury, S. Schwartz, N. Yosef, C. Malboeuf, D. Lu, J. J. Trombetta, D. Gennert, A. Gnirke, A. Goren, N. Hacohen, J. Z. Levin, H. Park, and A. Regev. Single-cell transcriptomics reveals bimodality in expression and splicing in immune cells. *Nature*, 498(7453):236–40, Jun 2013.

[90] S. V. Sharma, D. Y. Lee, B. Li, M. P. Quinlan, F. Takahashi, S. Maheswaran, U. McDermott, N. Azizian, L. Zou, M. A. Fischbach, K. K. Wong, K. Brandstetter, B. Wittner, S. Ramaswamy, M. Classon, and J. Settleman. A chromatin-mediated reversible drug-tolerant state in cancer cell subpopulations. *Cell*, 141(1):69–80, Apr 2010.

[91] J. R. Shearstone, N. E. Allaire, J. Campos-Rivera, S. Rao, and S. Perrin. Accurate and precise transcriptional profiles from 50 pg of total RNA or 100 flow-sorted primary lymphocytes. *Genomics*, 88(1):111–21, Jul 2006.

[92] S. T. Sherry, M. Ward, and K. Sirotkin. dbSNP-database for single nucleotide polymorphisms and other classes of minor genetic variation. *Genome Res*, 9(8):677–9, Aug 1999.

[93] L. Shkreta, U. Froehlich, E. R. Paquet, J. Toutant, S. A. Elela, and B. Chabot. Anticancer drugs affect the alternative splicing of Bcl-x and other human apoptotic genes. *Mol Cancer Ther*, 7(6):1398–409, Jun 2008.

[94] R. Siegel, D. Naishadham, and A. Jemal. Cancer statistics, 2012. *CA Cancer J Clin*, 62(1):10–29, Jan 2012.

[95] A. H. Sillars-Hardebol, B. Carvalho, J. A. Belien, M. de Wit, P. M. Delis-van Diemen, M. Tijssen, M. A. van de Wiel, F. Ponten, R. J. Fijneman, and G. A. Meijer. BCL2L1 has a functional role in colorectal cancer and its protein expression is associated with chromosome 20q gain. *J Pathol*, 226(3):442–50, Feb 2012.

[96] D. Sims, I. Sudbery, N. E. Ilott, A. Heger, and C. P. Ponting. Sequencing depth and coverage: key considerations in genomic analyses. *Nat Rev Genet*, 15(2):121–32, Feb 2014.

[97] J. L. Sun, X. S. He, Y. H. Yu, and Z. C. Chen. Expression and structure of BNIP3L in lung cancer. *Ai Zheng*, 23(1):8–14, Jan 2004.

[98] R. Suzuki and H. Shimodaira. Pvclust: an R package for assessing the uncertainty in hierarchical clustering. *Bioinformatics*, 22(12):1540–2, Apr 2006.

[99] C. Swanton. Intratumor heterogeneity: evolution through space and time. *Cancer Res*, 72(19), Oct 2012.

[100] Y. Tabuchi, J. Matsuoka, M. Gunduz, T. Imada, R. Ono, M. Ito, T. Motoki, Y. Yamatsuji, T. an d Shirakawa, M. Takaoka, M. Haisa, N. Tanaka, J. Kurebayashi, V. C. Jordan, and Y. Naomoto. Resistance to paclitaxel therapy is related with Bcl-2 expression through an estrogen receptor mediated pathway in breast cancer. *Int J Oncol*, 34(2):313–9, Feb 2009.

[101] S. Tagami, Y. Eguchi, M. Kinoshita, M. Takeda, and Y. Tsujimoto. A novel protein, RTN-XS, interacts with both Bcl-XL and Bcl-2 on endoplasmic reticulum and reduces their anti-apoptotic activity. *Oncogene*, 19(50):5736–46, Nov 2000.

[102] F. Tang, C. Barbacioru, E. Nordman, B. Li, N. Xu, V. I. Bashkirov, K. Lao, and M. A. Surani. RNA-Seq analysis to capture the transcriptome landscape of a single cell. *Nat Protoc*, 5(3):516–35, Mar 2010.

[103] T. Tang, B. Zheng, S. H. Chen, A. N. Murphy, K. Kudlicka, H. Zhou, and M. G. Farquhar. hNOA1 interacts with complex I and DAP3 and regulates mitochondrial respiration and apoptosis. *J Biol Chem*, 284(8):5414–24, Feb 2009.

[104] M. A. Tariq, H. J. Kim, O. Jejelowo, and N. Pourmand. Whole-transcriptome RNAseq analysis from minute amount of total rna. *Nucleic Acids Res*, 39(18):e120, 2011.

[105] R Core Team. *R: A Language and Environment for Statistical Computing*. R Foundation for Statistical Computing, Vienna, Austria, 2012.

[106] P. D. Thomas, M. J. Campbell, A. Kejariwal, H. Mi, B. Karlak, R. Daverman, K. Diemer, A. Muruganujan, and A. Narechania. PANTHER: a library of protein families and subfamilies indexed by function. *Genome Res*, 13(9):2129–41, Sep 2003.

[107] Y. Tian, A. C. Tan, X. Sun, M. T. Olson, Z. Xie, N. Jinawath, D. W. Chan, M. Shih Ie, Z. Zhang, and H. Zhang. Quantitative proteomic analysis of ovarian cancer cells identified mitochondrial proteins associated with Paclitaxel resistance. *Proteomics Clin Appl*, 3(11):1288–95, Nov 2009.

[108] C. Trapnell, L. Pachter, and S. L. Salzberg. TopHat: discovering splice junctions with RNA-Seq. *Bioinformatics*, 25(9):1105–11, May 2009.

[109] S. Tugendreich, J. Tomkiel, W. Earnshaw, and P. Hieter. CDC27Hs colocalizes with CDC16Hs to the centrosome and mitotic spindle and is essential for the metaphase to anaphase transition. *Cell*, 81(2):261–8, Apr 1995.

[110] Tusher, V. G. and Tibshirani, R. and Chu, G. Significance analysis of microarrays applied to the ionizing radiation response. *Proc Natl Acad Sci U S A*, 98(9):5116–21, Apr 2001.

[111] L. Wang, Z. Feng, X. Wang, X. Wang, and X. Zhang. DEGseq: an R package for identifying differentially expressed genes from RNA-seq data. *Bioinformatics*, 26(1):136–8, Jan 2010.

[112] L. Wang, S. Wang, and W. Li. RSeQC: quality control of RNA-seq experiments. *Bioinformatics*, 28(16):2184–5, Aug 2012.

[113] B Ward and K Heuermann. Transplex™ whole transcriptome amplification of RNA from low cell-number samples. *Journal of biomolecular techniques: JBT*, 21(3 Suppl):S30, 2010.

[114] A. Watanabe, S. Yasuhira, T. Inoue, S. Kasai, M. Shibazaki, K. Takahashi, T. Akasaka, T. Mas uda, and C. Maesawa. BCL2 and BCLxL are key determinants of resistance to antitubulin chemotherapeutics in melanoma cells. *Exp Dermatol*, 22(8):518–23, Aug 2013.

[115] J. D. Watson, S. Wang, S. E. Von Stetina, W. C. Spencer, S. Levy, P. J. Dexheimer, J. D. Kurn, N. a nd Heath, and 3rd Miller, D. M. Complementary RNA amplification methods enhance microarray identification of transcripts expressed in the *C. elegans* n ervous system. *BMC Genomics*, 9:84, Feb 2008.

[116] S. Willimott, T. Merriam, and S. D. Wagner. Apoptosis induces Bcl-XS and cleaved Bcl-XL in chronic lymphocytic leukaemia. *Biochem Biophys Res Commun*, 405(3):480–5, Feb 2011.

[117] A. Wilm, P. P. Aw, D. Bertrand, G. H. Yeo, S. H. Ong, C. H. Wong, C. C. Khor, R. Petric, M. L. Hibberd, and N. Nagarajan. LoFreq: a sequence-quality aware, ultra-sensitive variant caller for uncovering cell-population heterogeneity from high-throughput sequencing datasets. *Nucleic Acids Res*, 40(22):11189–201, Dec 2012.

[118] A. R. Wu, N. F. Neff, T. Kalisky, P. Dalerba, B. Treutlein, M. E. Rothenberg, F. M. Mburu, G. L. Mantalas, S. Sim, M. F. Clarke, and S. R. Quake. Quantitative assessment of single-cell RNA-sequencing methods. *Nat Methods*, 11(1):41–6, Jan 2014.

[119] X. Xu, Y. Hou, X. Yin, L. Bao, A. Tang, L. Song, F. Li, S. Tsang, K. Wu, H. Wu, W. He, L. Zeng, M. Xing, R. Wu, H. Jiang, X. Liu, D. Cao, G. Guo, X. Hu, Y. Gui, Z. Li, W. Xie, X. Sun, M. Shi, Z. Cai, B. Wang, M. Zhong, J. Li, Z. Lu, N. Gu, X. Zhang, L. Goodman, L. Bolund, J. Wang, H. Yang, K. Kristiansen, M. Dean, and Y. Li. Single-cell exome sequencing reveals single-nucleotide mutation characteristics of a kidney tumor. *Cell*, 148(5):886–95, 2012.

[120] N. Yamakawa, K. Kaneda, Y. Saito, E. Ichihara, and K. Morishita. The increased expression of integrin alpha6 (ITGA6) enhances drug resistance in EVI1(high) leukemia. *PLoS One*, 7(1):e30706, Jan 2012.

[121] L. Yan, M. Yang, H. Guo, L. Yang, J. Wu, R. Li, P. Liu, Y. Lian, X. Zheng, J . Yan, J. Huang, M. Li, X. Wu, L. Wen, K. Lao, R. Li, J. Qiao, and F. Tang. Single-cell RNA-Seq profiling of human preimplantation embryos and embryonic stem cells. *Nat Struct Mol Biol*, 20(9):1131–9, Sep 2013.

[122] D. A. Yardley. Drug resistance and the role of combination chemotherapy in improving patient outcomes. *Int J Breast Cancer*, 2013:137414, June 2013.

[123] Ye, K. and Lu, J. and Ma, F. and Keinan, A. and Gu, Z. Extensive pathogenicity of mitochondrial heteroplasmy in healthy human individuals. *Proc Natl Acad Sci U S A*, 111(29):10654–9, Jul 2014.

[124] H. G. Zhou and C. Zhang. Study on application of the whole genome amplification in LCN. *Fa Yi Xue Za Zhi*, 22(1):43–4, 47, Feb 2006.

[125] L. Zhou, X. Cai, X. Han, N. Xu, and D. C. Chang. CDK1 switches mitotic arrest to apoptosis by phosphorylating Bcl-2/Bax family proteins during treatment with microtubule interfering agents. *Cell Biol Int*, Feb 2014.

[126] M. Zhou, Z. Liu, Y. Zhao, Y. Ding, H. Liu, Y. Xi, W. Xiong, G. Li, J. Lu, O. Fodstad, A. I. Riker, and M. Tan. MicroRNA-125b confers the resistance of breast cancer cells to paclitaxel through suppression of pro-apoptotic Bcl-2 antagonist killer 1 (Bak1) expression. *J Biol Chem*, 285(28):21496–507, Jul 2010.

[127] T. Zhou, J. P. Aumais, X. Liu, L. Y. Yu-Lee, and R. L. Erikson. A role for Plk1 phosphorylation of NudC in cytokinesis. *Dev Cell*, 5(1):127–38, Jul 2003.

[128] T. Zhou, W. Zimmerman, X. Liu, and R. L. Erikson. A mammalian NudC-like protein essential for dynein stability and cell viability. *Proc Natl Acad Sci U S A*, 103(24):9039–44, Jun 2006.